TAPHONOMIC CHARACTERISTICS OF FOSSILS ON THE BURGESS-SHALE-TYPE SPECTRUM

---

by

Jesse S. Broce

Prof. James D. Schiffbauer, Dissertation Supervisor

A dissertation

presented to

the faculty of the Graduate School

at the University of Missouri-Columbia

In partial fulfillment

of the requirements for the degree

Doctor of Philosophy

May 2018

The undersigned, appointed by the dean of the Graduate School, have examined the dissertation entitled

TAPHONOMIC CHARACTERISTICS OF FOSSILS ON THE BURGESS-SHALE TYPE SPECTRUM

presented by Jesse S. Broce, a candidate for the degree of doctor of philosophy and hereby certify that, in their opinion, it is worthy of acceptance.

_____

Professor James D. Schiffbauer

_____

Professor John W. Huntley

_____

Professor Peter I. Nabelek

_____

Professor Tommi A. White

ACKNOWLEDGEMENTS

This project would not be possible without the contributions of many of my colleagues. My advisor, James D. Schiffbauer was an excellent source of advice (practical and theoretical) and funding. My committee members were a bountiful source of information. The suggestions of Dr. Huntley were invaluable for the statistical methodologies employed in the research. Dr. Nabelek provided excellent mineralogical advice. Dr. White, being the director of the Electron Microscopy Core, where the majority of the research in this dissertation was conducted, was, of course, invaluable for the process. A former committee member, Dr. Judy Wall, provided the bacteria, advice on using an anoxic chamber, and a strong microbiology background that was indispensable for the experimental decay project. Many of the specimens were lent to me from the University of Kansas Biodiversity Institute, where Drs. Farrell, Casey, Kimmig and Lieberman were very helpful. Eric Schneider assisted with the chemical monitoring of the experimental decay project. I am greatly indebted to the University of Missouri Geological Sciences department for providing facilities and funding without which this research would be impossible.

TABLE OF CONTENTS

Table of Figures

Table of Tables

CHAPTER 1: INTRODUCTION TO RESEARCH OF BURGESS-SHALE-TYPE LAGERSTÄTTEN

1.1. The study of lagerstätten

1.1.1 Lagerstätten and taphonomy

Study of exceptional fossil preservation tends to yield exciting results. Since soft-bodied organisms and the soft tissues of biomineralizing organisms are usually not preserved in the fossil record, instances of soft-tissue preservation are of immense value to paleontology and biology. Anatomical details of soft tissues are invaluable for understanding the phylogenetic relationships between organisms, as well as interpreting their life modes. Soft-bodied organisms are not only valuable phylogenetically, but they also are important members of ecological community structure. Without soft-tissue preservation, the interpretation of past environments, ecologies, and evolutionary lineages becomes extremely limited. That soft-tissue preservation is relatively rare is an unfortunate phenomenon that not only decreases the amount of available information, but also imposes biases on our understanding of the past. Soft-bodied organisms represent the vast majority of diversity, but are the minority of diversity in the fossil record. In fact, only about 30% of modern marine benthic macroorganisms contain hard parts suitable for easy preservation (Johnson, 1964) and in the Phyllopod Bed of the Cambrian Burgess Shale, only about 14% of species or 2% of individuals have hard parts (Morris, 1986), and consequently would not be preserved in most fossiliferous deposits.

There is much to be gained by having a complete understanding of the processes that produce soft-tissue preservation, especially the conditions that control soft-tissue preservation in different environments. Such an understanding could eliminate some of the

biases that result from soft-tissue preservation, and could even improve the ability to find new localities of exceptional fossil preservation (*konservat-lagerstätten*). Further, taphonomic features can impose biases on the morphological interpretations of an organism, perhaps best exemplified by the stemward-slippage principle, which states that since decay often destroys diagnostic characters in an organism early on, soft-bodied organisms will be assigned more basal positions in a clade's phylogeny (Sansom et al, 2010).

Soft-tissue preservation generally only occurs in particular environments, some of which can be very small, temporally and geographically. The environments in which soft-tissue preservation typically occurs varies throughout Earth's history (Orr, 2014). Starting from Stage 2 (529 Ma, Cohen, Harper and Gibbard, 2017), the Cambrian period (541-485 Ma, Cohen, Harper and Gibbard, 2017) has a higher incidence of lagerstätten than any other time in Earth's history, even without correcting for the "pull of the recent," which usually skews geologic data towards younger ages due to greater sampling of younger rocks (Jablonski et al, 2003). Fossil preservation may have been more difficult in the lowest Cambrian and the Precambrian due to the scarcity of organisms that build recalcitrant tissues. In the Cambrian heyday of exceptional preservation, almost all lagerstätten were marine because animals and vascular plants would not colonize land until the Silurian (444-419 Ma, Cohen, Harper and Gibbard, 2017), and insects would not diversify until the Carboniferous (359-299 Ma, Cohen, Harper and Gibbard, 2017; Muscente et al, 2017).

The Cambrian exhibited a number of peculiar conditions that may have contributed to the enhanced marine preservation. The beginning of the Cambrian roughly coincided with an increase in mid-ocean ridge spreading rates. The greater interaction with

hydrothermal brines at mid-ocean ridges caused an increase in marine calcium concentration and an increase in atmospheric pCO_2. The resulting increase in temperature melted the permanent ice reserves of the planet, typical for a transition from icehouse to greenhouse conditions, which is commonly a result of increasing spreading rates (Hardie, 1996).

The melting ice and thermal expansion of water caused a sea level rise (the Sauk transgression), covering the continental margin, thus expanding the area of available shallow sea. The incredible erosive power of wave action (often called the "wave razor") scoured the continental areas. This famous erosive event (the "Great Unconformity") exposed vast quantities of crystalline basement rock, supplying the oceans with even more calcium, along with aluminum and silicon. As a result of the much higher calcium, inorganic carbon, aluminum and silicon concentrations, Cambrian marine environments exhibited anomalously high calcite cementation rates, and quantities of glauconite production. The ease of calcite precipitation during this time is considered a potential contributing factor for the concomitant advent of biomineralization across many phyla (Peters and Gaines, 2012). The increased calcium and carbonate concentrations coincided with a decrease in magnesium and sulfate concentrations (Horita, Zimmerman and Holland, 2002). This change in seawater chemistry was very extreme, one estimate (based on evaporite fluid inclusions) indicating that calcium had increased from 14 to 37 mM, but sulfate had decreased from 20.5 to 8 mM over the interval from 549-515 Ma (Breannan, Lowenstein and Horita, 2004). Magnesium concentrations dropped from over 70 mM to around 40 mM (Horita, Zimmerman and Holland, 2002).

Oxygen concentrations were increasing throughout the Cambrian, which may have contributed to the Cambrian Explosion (Sperling et al, 2011). Estimates for atmospheric oxygen concentration during this time are imprecise, but it was probably around 15% present atmospheric level (PAL) at the beginning of the Cambrian (Canfield, Poulton and Narbonne, 2007). During the Late Cambrian, roughly coinciding with the Steptoean Positive Carbon Isotope Excursion (SPICE), atmospheric oxygen concentrations could have increased from ~15 to 25% partial pressure (Saltzman et al, 2011). Though atmospheric oxygen concentrations may have reached modern values by the end of the Cambrian, this does not necessarily correspond to modern-like marine oxygen concentration. In the modern ocean, seawater cooling and freezing in contact with ice at high latitudes causes downwelling which injects surface oxygen into the deep ocean (Eby,2004). Without ice, like in the Cambrian greenhouse, vertical circulation would be inhibited, meaning that the oceans were highly stratified with anoxic, or even euxinic bottom-waters (Tucker, 1992). The low oxygen and sulfate concentrations of deep ocean settings could have contributed to the excellent preservation in this period.

By the middle-Ordovician (470 Ma, Cohen, Harper and Gibbard, 2017), however, the lagerstätten incidence had become anomalously low, and remained low until the Carboniferous. Marine lagerstätten were disappearing, and the dominant setting for lagerstätten formation during this time was transitional environments (read: estuaries, deltas, shoreface deposits, etc). It is unclear whether this is reflective of a global trend in favor of transitional environments, since the lagerstätten of the time were almost totally restricted to eastern North America and adjacent (at the time) parts of Europe (Muscente et al, 2017). This region, the “Appalachian Basin” consisted of a variable number of

intermittently-connected tropical seas, some of which had periods of hypersalinity (Vrazo, Brett and Ciurca, 2017). Even in the (fairly modest) peak of transitional lagerstätten during the Carboniferous, the localities were restricted to the same area. Authors have invoked many different reasons for why fossil preservation declined after the Cambrian, mainly focusing on changes in marine and atmospheric chemistry, but different taphonomic pathways have different chemical requirements. Increasing atmospheric oxygen concentrations is a popular explanation because it would improve preservation via numerous different pathways, and is well-established during this interval (Muscente et al, 2017).

By the Permian (299 Ma, Cohen, Harper and Gibbard, 2017), non-marine deposits had become the dominant environment for lagerstätten, as it would remain until the present day. Curiously, while the incidence of marine and transitional lagerstätten are poorly correlated to marine and transitional outcrop area and rock volume, non-marine lagerstätten are strongly correlated to non-marine outcrop area and rock volume. Non-marine lagerstätten may be less susceptible to the changes in marine and atmospheric chemistry than marine rocks are, potentially due to the tendency for non-marine lagerstätten to occur in restricted environments that may deviate from average global conditions (Muscente et al, 2017).

In fossils where soft tissues are preserved, the study of the organism should be inextricable from the study of its taphonomy (fossil preservation). An organism's soft-tissues are rarely preserved as their original tissues. There is usually some mineral that templates or replicates the tissues of the organism (Butterfield, 2003), and any soft tissues that remain become altered into other forms of carbon over geologic time scales (Musico

and Horsfield, 1996). Thus, any investigation into the original morphology of a fossil organism must involve differentiation between morphological features and mineralogical features. The methods used to study the morphology and taphonomy of exceptionally preserved fossils are similar (electron microscopy, micro-CT, etc.), and the same data can be used to both ends.

The study of fossil material has generated a tremendous amount of discussion and debate regarding the processes that control soft-tissue preservation. The understanding of these processes, as discerned from real fossil material, is only theoretical, but it consists of hypotheses that can be tested experimentally; causing fossilization by replicating the conditions of fossilization. This branch of research is known as "experimental" or "actualistic taphonomy" (or "*aktuopaläontologie"*) (Sansom, 2014). Without this empirical basis, the science of taphonomy would be entirely speculative, but the results that have been produced by experimental taphonomy are problematic. Even very successful taphonomic experiments do not perfectly replicate the patterns seen in the fossil record (Martin et al, 2005). Taphonomic experiments in laboratory settings can be criticized for not replicating natural environments, but in natural settings they can be criticized for not having good controls. In spite of its shortcomings, actualistic taphonomy is an essential part of our understanding of taphonomy. Only through continued work in actualistic taphonomy can researchers bridge the gap between theoretical and actual taphonomy.

1.1.2 Analytical methods

The processes used to study actual taphonomy include optical examination, but experience has shown that specimens that appear simple or similar to light microscopy can

display radically different patterns when examined with scanning electron microscopy (SEM). The importance of SEM cannot be overstated in taphonomy. Submicron-scale mineralogical features are readily visible with the magnification typical of SEM. Compositional differences are often readily apparent in images collected with a Backscattered Electron Detector (BSD). For more detailed compositional information, Energy-Dispersive X-ray Spectroscopy (EDS) is capable of determining the elemental composition of substances, even producing maps of occurrences of different elements (Goldstein et al, 2003).

Like all instruments, SEMs have limitations that must be borne in mind while interpreting data. The greatest caveat is differences in "interaction volume" between different methods. Secondary electrons are generated within the sample, but are so low-energy (below 50 eV) that they cannot escape the sample from any significant depth. As a result, secondary electrons are excellent for collecting topographic details. Another issue with secondary electron generation is sample charging. Nonconductive specimens, like shale, can accumulate a static charge in parts of the sample, which can produce secondary electrons, and even bend the path of beam electrons with the electric field. These problems can be mitigated by coating a sample with a conductive material, by collecting data in low vacuum (so that small quantities of water vapor can neutralize the surface charge), or by scanning with a lower voltage (which decreases the total amount of signal, and contrast) (Goldstein et al, 2003).

Backscattered electrons originate in the electron beam, and are elastically scattered (meaning no loss of kinetic energy) out of the sample by interactions with the nuclei and electron orbitals. Due to their high energy, backscattered electrons can escape the sample,

even if they penetrate deep into the sample. This can cause fine details like edges and corners of euhedra to appear rounded. Materials with light elements may appear semi-transparent to backscattered electrons, since electrons can more easily pass through them more easily. On the other hand, materials with heavy elements will only produce BSE signal close to the sample surface, but will produce more total signal due to the greater ability for heavy elements to bend the path of electrons. Interaction volume (read: penetration depth) increases with increasing voltage (Goldstein et al, 2003).

EDS detects the x-rays that are produced by interactions between beam electrons (like backscattered electrons) and atoms. Characteristic x-rays are produced at any part of the sample that beam electrons reach. This includes beam electrons that wander too deep into the sample and are unable to escape. Contrariwise, x-rays have a great capacity to pass through the sample, so they can reach the detector regardless of the depth at which they are generated. Thus, EDS signal is produced from a greater depth than is possible for BSE. Thus, EDS collects compositional data from parts of the sample that are undetectable to electron imagery. There are limits to the ability of x-rays to penetrate sample material. This becomes a problem because the EDS detector is oriented at an angle. Thus, areas that are perfectly visible to electron imagery can be blocked to EDS. These “shadowed” regions do not merely have lower signal; their compositional values are also skewed. Since elements are identified based on the energy of their characteristic x-rays, and low energy x-rays are not as capable of penetrating a sample, elements that produce low-energy x-rays will be disproportionately blocked (Goldstein et al, 2003).

The most catastrophic danger of using EDS is misidentification of elements. Similar peaks can be produced by different elements, so it is possible for elements to be

conflated, or multiple elements to contribute to the same peak. To some degree, *a priori* knowledge of sample composition is useful to interpret EDS data. Stoichiometry of compositions is somewhat subjective as well, since EDS cannot identify chemical bonds or oxidation states (Goldstein et al, 2003).

1.2. Burgess-Shale-type fossil preservation

The Burgess Shale is, without question, the most famous of lagerstätten. It was the first major invertebrate conservat-lagerstätten ever discovered, in 1909, by the famous paleontologist Charles Walcott (Walcott, 1911). The arthropods and other taxa recovered from the Burgess Shale became famous for their bizarre-seeming morphologies, but the discoveries had far-reaching implications for our understanding of phylogenetic relationships, and uncovered fossil representatives of numerous clades that had previously only been known in the modern, like priapulids. The Burgess Shale showed that diverse and complex arthropods once thrived within a vibrant ecosystem in the Middle Cambrian, a time that was previously regarded to contain only very rudimentary organisms in a simple ecosystem (Gould, 1989).

Many fossil lagerstätten similar to the Burgess Shale have been discovered since, and have been termed "Burgess-Shale-type" (BST). As defined by Butterfield (1995), BST preservation "includes all those exceptionally preserved fossils whose primary taphonomic mode is one of non-mineralizing organisms preserved as carbonaceous compressions (organic preservation) in fully marine sediments." The marine requirement for BST preservation seems unusual in light of numerous exceptionally preserved lacustrine carbonaceous compression lagerstätten (Clarkia, Green River, Florissant, etc.), but

Butterfield (1995) excludes these on the basis of their burial in volcanogenically-derived sediment. While the Butterfield definition is widely accepted (Butterfield 2003; Gaines et al, 2008; Cai et al, 2012), it is clear that the lacustrine and marine carbonaceous compressions not only appear similar, but are preserved through similar mechanisms. Whether a descriptive or a genetic category is being used, nonmarine carbonaceous compressions should be grouped with the marine, especially considering that some of these lakes were saline (e.g. Green River and Crato according to Downen, 2014). Due to the near identical mechanisms of preservation, most of what is said for BST taphonomy applies to carbonaceous compression fossils as well.

It is common for taphonomic classifications to be named after localities, like Fermuse, Nama, Bitter-springs, Orsten and Doushantuo, almost using the localities as holotypes. This tendency leads to unnecessary ambiguity in cases where the descriptive and genetic properties of the taphonomy of fossils at a locality are not unambiguously resolved, or if taphonomic characteristics have not been fully disentangled from later diagenetic or metamorphic ones. This is especially a problem for BST deposits, since use of analytical techniques only within the last twenty-one years have revealed that the fossils of the Burgess Shale are definitely both aluminosilicified and contain carbonaceous compressions (Butterfield, 1996; Butterfield et al, 1997; Orr et al, 1998) but this new information did little to clarify the taphonomy of the Burgess Shale, since some workers consider the clay minerals to be a result of low-grade metamorphism (Butterfield et. al, 1997). The classification of fossils based on taphonomic criteria should be strictly taphonomic, without taking into account late-stage processes which operate on a regional level, having little to do with biology or sedimentology, so unless the origin of the clay

minerals in the Burgess Shale fossils are unambiguously resolved, the Burgess Shale will remain problematic as a point of comparison. Regardless, the accepted definition (Butterfield, 1995), while perhaps imperfect, considers carbonaceous compression as the fundamental characteristic of the Burgess Shale and BST fossils, even though evidence of carbonaceous compression can be difficult to ascertain in some deposits.

One innovative scheme of BST classification identifies three main taphonomic modes that often co-occur within fine-grained, low-oxygen environments similar to the Burgess Shale: kerogenization (preservation as carbon), pyritization (preservation of pyrite), and aluminosilicification. This classification scheme still only considers fossils that are kerogenized to be BST (excluding fossils that are exclusively pyritized and aluminosilicified), but includes fossils that are predominantly pyritized or aluminosilicified (Cai et al, 2012).

1.3. Processes of kerogenization

Organic tissues have a very poor capacity to survive geologic timescales, largely due to their susceptibility to scavenging, decay, but also abiotic conversion to other forms of carbon, which can get mobilized (Butterfield, 1990). Resultantly, the majority of soft-tissue preservation in macroorganisms is facilitated by mineralization. The forms of carbon to which organic tissues convert via geologic processes are generally referred to as kerogen, hence instances where the original carbon of an organism remains in the fossil (sometimes preserving fine detail) are considered kerogenized fossils. The processes of kerogenization have been thoroughly studied because coal is considered kerogen, and kerogen is a source of petroleum and natural gas (Bernard et al, 2012).

1.3.1 Transport and burial-

The first hurdle that organic carbon must overcome in order to become kerogenized is the risk of scavengers. Corpses are basically a free meal that comes without the usual energetic costs of predation, and it is very likely that organisms like *Sidneyia* did scavenge as early as the Cambrian (Morris, 1986). It is possible that a corpse may escape notice of potential scavengers, if it is located in a sufficiently deserted area, which may occur if, say, geochemical conditions preclude intrusion by most animals (like anoxia, or toxicity), but a much more reliable means by which a corpse may avoid scavenging is rapid burial. BST deposits, however, occur in settings with fine-grained sediments. In the quiescent settings where fine-grained siliciclastics and carbonates accumulate, sedimentation rates are normally very low, due to the low settling rates of fine-grained particles through a fluid (Stokes' Law). The settling rate of a sedimentary particle is the velocity at which the force of gravity pulling it downward is equal to the viscous drag force pushing against it. Stokes' equation is: $v_s = \frac{2r^2 g(\rho - 1)}{9\eta}$ (Stokes, 1851; Faure, 1998) for spherical particles where v_s is the settling velocity, r is the radius, g is gravitational acceleration, ρ is the density of the particle, and η is the viscosity of water. Thus a clay-sized (radius < 1/512 mm) clay-density (*generously* 3 g/cc) particle will fall through water at a maximum of $1.7*10^{-11}$ cm/s, or 5.2 mm per century. More realistically, the motion of the clay particle will be dominated by any disturbance of the water, negating the settling motion. As a result, suspended clay particles can be considered colloids, and the mixture a "sol" (Faure, 1998)

Due to the negligible settling velocity of clay particles, it may seem unlikely that an organism could be rapidly interred by fine-grained sediment in order to be kerogenized,

but in such settings, it is commonly the case that the majority of the total sediment is a result of event deposition, such as turbidites and other density flows. Such density flows are underwater mudslides which can cause large quantities of clay and carbonate mud to be transported into settings which are ordinarily low-energy with gradual deposition. Due to the suspended clay load in a density flow, it acts as a higher density fluid than the surrounding seawater, and acts like a separate unit. Once the density flow reaches a flatter area and becomes slower or less turbulent, it loses its capacity to carry sediment, forcing a large portion of its clay load out of suspension (Arnott, 2010). While individual clay particles have low settling velocities, circumstances where clay particles occur in high concentrations can result in clay particles being forced out of suspension. In fact, by some measured observations, clay particle concentrations are proportional to clay settling velocity (Sutherland, 2014), so it is possible for rapid burial to occur in density flows. Many BST lagerstätten are obrution deposits (buried in rapid sedimentation events) (Zhang and Hou, 2007; Gabbot et al, 2008).

There are a few factors that facilitate greater net clay sedimentation in nearshore (uphill) settings. For instance, in deltaic settings, the deposition of clay sediments is greatly accelerated, due to the abrupt change in salinity between fluvial and marine systems. Clay particles generally have a positively-charged core, but their sides are negatively charged. For clays in suspension, this causes individual clay particles to repel each other, but the ions in salt water neutralize this charge, allowing clay particles to clump together into larger particles, called “flocs,” which precipitate out much more quickly than individual clay particles would from Stokes’ Law, alone (Sutherland et al, 2014). Another mechanism for accelerated nearshore clay deposition is the action of filter-feeding organisms, which, as

an incidental result of their feeding process, often ingest some suspended clay particles. The clay particles pass through their digestive systems and become part of the sediment as faecal material (Giresse et al, 1988; Wotton et al, 1998), which usually disintegrate rapidly (Jones, 2010), but can be a majority of the sediment in some environments (Wotton et al, 1998). Zooplankton are significant contributors to faecal clay deposition, not just via digestion, but their faeces can remove additional clays from suspension as they sink (Deuser et al 1983). The muds which accumulate in nearshore settings can get mobilized by earthquakes or sea level changes, but instead of settling out as discrete particles, they move as a high-density fluid and spread out across the seafloor, and are thus unaffected by the throttling effects of Stokes' Law (Arnott, 2010).

1.3.2 Microbial degradation

Having avoided destruction by hungry macroorganisms, the soon-to-be fossil is still vulnerable to hungry microorganisms. Bacteria dominate decay in marine sediments, but fungi, mainly yeasts, also degrade some organic carbon (Killops and Killops, 2005). Microbes that consume organic materials for use as an energy source are considered "heterotrophs." Their metabolism relies on redox reactions wherein forms of organic carbon (typically very reducing substances) react with oxidants (a.k.a. oxidizing agents, electron acceptors) to form new compounds. There are many different electron acceptors that microorganisms can utilize in their metabolism, each which produces a different by-product. The amount of energy that an organism receives through the metabolism of organic carbon is proportional to the difference in the "electrode potential" of the reactants.

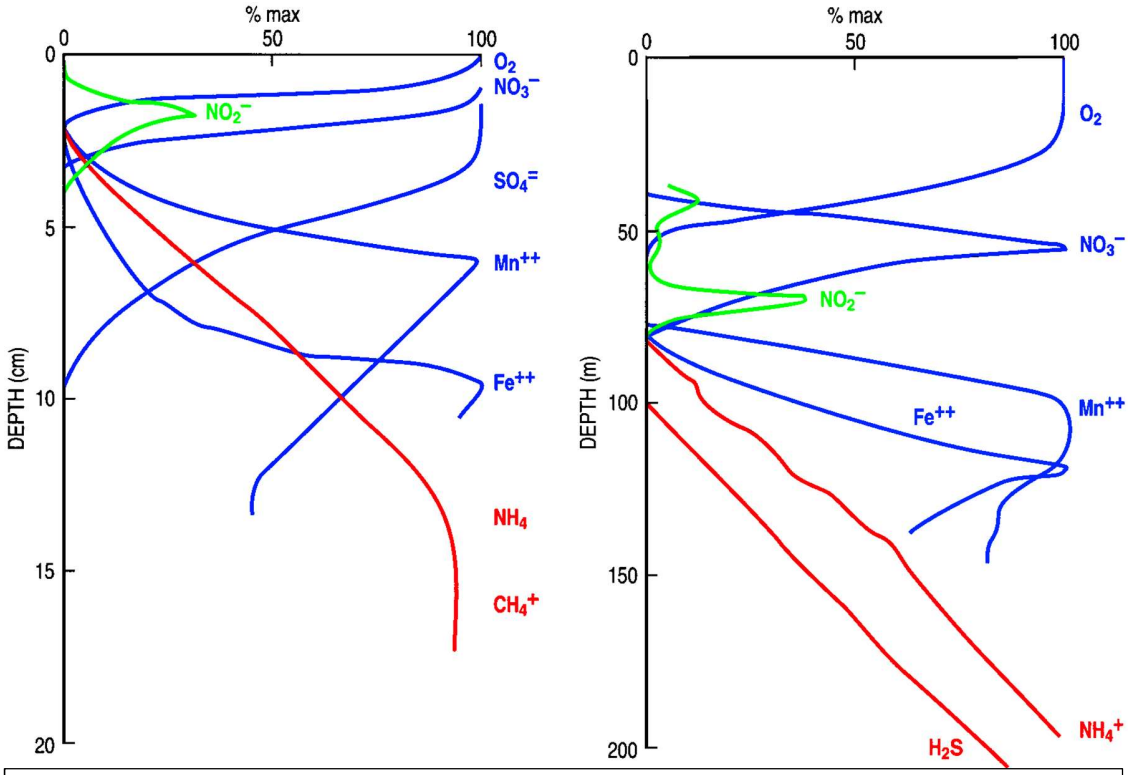

Figure 1.1 Concentration of dissolved constituents (relative to measured maximum) vs. sediment depth for Lake Michigan (left) and the Black Sea (right). Color coded by their relation to heterotrophic microbial metabolisms: blue = electron acceptor, red = electron donor, green = both. Modified pending permission from Nealson, 1997.

Many organisms, like ourselves, use oxygen gas as the oxidant, which is one of the most efficient metabolisms, but in many settings, oxygen is not available for such use. Due to the difference in availability and metabolic efficiency between different oxidizing agents, microorganisms in sediment columns will tend to form layers, with the most efficient metabolisms at top, and progressively less efficient metabolisms at greater depth, where the more favorable oxidizing agents are limited (Fig. 1.1). Complicating matters, there are also abundant "autotrophs" in the sediment microbiota, which reduce inorganic carbon to organic carbon by using dissolved constituents as reducing agents, driving the heterotrophic reaction in reverse, using heterotrophic products as their reactants (Nealson, 1997).

This hierarchy is well known from microbial mats, where photoautotrophs form the top layer, where sunlight enables photosynthesis to occur (Reid et al, 2000). These photoautotrophs are the source of carbon for heterotrophs, and a source of oxygen. The aerobes (oxygen-breathers) are just below, removing all oxygen and converting it to carbon dioxide. In successively deeper layers, the denitrifiers (consumes nitrate that is generated deeper in the sediment, often produces ammonium), manganese reducers (converts Mn^{4+} to Mn^{2+}), and iron reducers (Fe^{3+} to Fe^{2+}). Below that lives the sulfate-reducing microbes (SRBS), which produce bisulfide as a product of their respiration. Finally, at the bottom of the hierarchy live the methanogens, which use carbon dioxide (the by-product of oxic degradation) as the electron acceptor for their metabolism (Nealson, 1997). Methanogenesis can occur via $CO_2 + 4H_2 \rightarrow CH_4 + 2H_2O$, which is in direct competition with acetogens that use $2CO_2 + 4H_2 \rightarrow CH_3COOH + 2H_2O$. The methanogenic reaction is usually favored, since it produces more energy, but acetogens can tolerate lower-pH conditions (Killops and Killops, 2005).

If even carbon dioxide becomes limited, decay can only progress via fermentation. The term “fermentation” is sometimes used to refer to any anaerobic decay, but is here used to describe a heterotrophic redox reaction that uses organic carbon as electron donor and acceptor. Fermenters are capable of producing enzymes which break organic macromolecules down into sugars, amino acids and fatty acids, which are suitable substrates for fermentation. Their products (some of which can be fermented further) can include alcohols, methylated amines, carbon dioxide, water, and short-chain volatile acids like formate, propionate, butyrate, lactate, pyruvate and acetate (Killops and Killops, 2005).

Acetate is a useful substrate for other metabolic pathways (Killops and Killops, 2005). In fact, a study of sediment from a salt marsh mudflat indicated that 61% of the sulfate reduction required acetate as a substrate (Winfrey and Ward, 1983), however *Desulfovibrio,* an important genus of SRBs, cannot utilize acetate since it cannot perform the Krebs cycle, For the same reason, *Desulfovibrio* cannot break down glucose (Killops and Killops, 2005). Some archaea can ferment acetate via $CH_3COOH \rightarrow CH_4 + CO_2$ (Ferry, 1992). Acetate continues to be a very important substrate long after burial. Inorganic thermal maturation of organic carbon can produce acetate (Wellsbury et al, 1997), resulting in active communities of bacteria at depths greater than 500 m (Parkes et al, 1994). This is not the limit of depth at which sediment-dwelling marine microbial communities can survive. For instance, living sulfate-reducing archaea and bacteria have been recovered from 1670 m below an Alaskan oil field (at about 70°C and 180 bar). These microorganisms are very similar to marine sulfate-reducers, which raises the possibility that they are the descendants of the original sediment microbes (L'Haridon et al, 1995).

There are numerous factors that can inhibit microbial degradation. First, since each pathway is totally reliant on some oxidizing agent or other diffusing in, anything that restricts diffusion will slow microbial degradation. Dissolved constituents diffuse more slowly through fine-grained sediment, and so having fine grained sediment slows degradation. Early cementation, as occurs in concretion formation, is capable of stopping diffusion, and therefore microbial decay, entirely. There are some kinds of fossil lagerstätten which rely on concretion formation. Some, like the Mazon Creek and the Santana Formation, rely on some decay in order to produce the constituents to create the concretions (McCoy, 2014). In others, fossils are trapped incidentally. The Burgess Shale

does not rely on concretions for preservation, but there is some possibility that in the Burgess Shale and other BST deposits, early cementation by carbonates (Gaines et al, 2005) or other minerals could have occurred, which would have severely limited the amount of decay that microorganisms would be capable of accomplishing. Any conditions that would inhibit or kill microorganisms would arrest decay, including toxic waters like those found in peat bogs (Allison and Briggs, 1991). Peat bogs form more easily in cold climates because bacterial decay is inhibited more by cold temperatures than plant growth is, resulting in greater net carbon burial (Killops and Killops, 2005). Extremely cold climates are capable of preserving soft tissues indefinitely via freezing (Boeskorov, 2014).

This microbial hierarchy is established and maintained by continual microbial action. Thus, in sediments where supply of organics is high relative to sedimentation rate, then the availability of electron acceptors is the limiting factor, and the microbial hierarchy and its corresponding stratification of dissolved ions will be well-established. In sediments with slow deposition of organics, diffusion will predominate, and the available electron acceptors will not vary much with sediment depth. In carbon-poor marine sediments, oxygen can penetrate to appx. 0.5 m sediment depth, whereas in fine-grained shelf sediments, anoxia is established within the top few millimeters (Killops and Killops, 2005). In deep ocean settings (Fig 1.2 B & C), the rates of microbial metabolism are orders of magnitude slower than in ocean margin settings (Fig 1.2 A), so sulfate may never become limiting (D'Hondt et al, 2002). For a corpse buried in such a circumstance, the amount of organic carbon may be the limiting factor, and none of its labile tissues may survive decay (see chap. 2.1 on pyritization). Microbial biofilms are ubiquitous in marine sediments, but

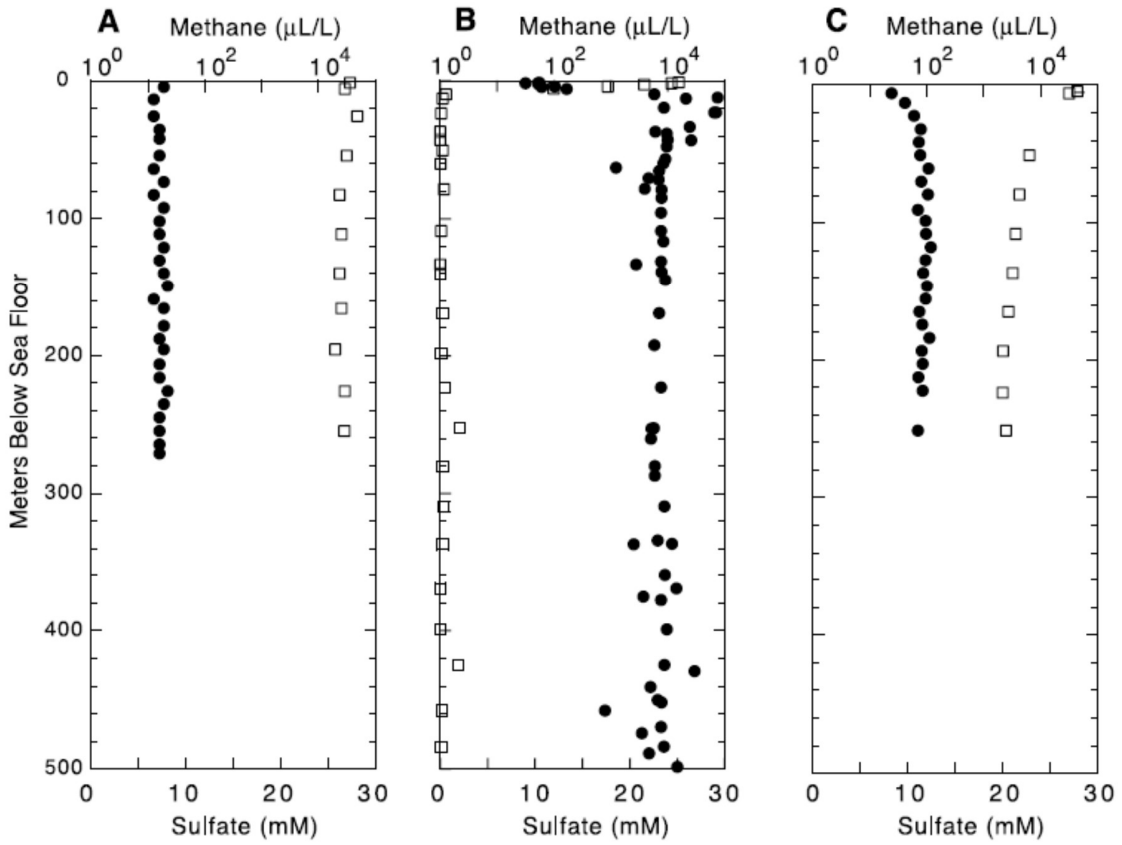

Figure 1.2 Concentration of dissolved constituents vs. sediment depth for the Japan Sea (A) and two deep-ocean cores (B and C). Sulfate is represented as squares and methane is represented as circles. From D'Hondt et al, 2002. Reprinted with permission from AAAS.

well-developed microbial hierarchies, though useful generalizations, are uncommon in natural settings (Briggs, 2003).

In settings with sulfidic bottom-waters, the microbial hierarchy is somewhat different. Aqueous sulfide is reactive with oxygen (and more reactive with oxidized metal species), making it difficult for oxic conditions to be reestablished (Rickard, 2012). Sulfide also reacts with cytochromes, which are necessary for oxygen transport in aerobes, thereby rendering them useless. Specialized anaerobic photosynthesizers utilize sulfides in their metabolism. Anaerobes typically decay organic matter more slowly than aerobes, but this is largely because they only have access to more recalcitrant tissues. Anoxic settings may not have substantially slower rates of decay (Killops and Killops, 2005).

Some organic tissues are more resistant to microbial decay than others. Proteins are generally very easy to break down, but insoluble proteins, like keratin, fibrinogen and collagen are more difficult for enzymes to access. Similarly, less soluble lipids are less susceptible for decay, making waxes extremely robust. Waxes are aromatic compounds, cyclic carbon polymers that are tougher to break apart. The presence of waxes on plant leaves and in arthopod cuticle contributes to their recalcitrance. Algae commonly contain aliphatic (chains) carbon compounds like fatty acids and alkanes, which are somewhat robust, but are inferior to aromatic compounds (Killops and Killops, 2005). Plants are known to have cell walls that are decay-resistant, in part due to the compounds algaenan, cutan and suberan (Allison and Briggs, 1991) and lignin (Nelsen et al, 2016). The cuticle of animals can have various compositions and structures (abundance of chitin and collagen, for instance), but for most animals, the cuticle is one of the most decay-resistant parts of their anatomy. Arthropods in particular have a robust exoskeleton, and are well represented in BST deposits. An arthropod exoskeleton contains several robust organic compounds, including cuticulin, chitin and sclerotin (Butterfield, 1990). Annelid cuticle contains collagen, which is regarded a decay-resistant compound (Butterfield, 1990), but the best-preserved worms in BST deposits are priapulids, which have both chitin and collagen in their cuticle (Schmidt-Rhaesa, 2013). Biopolymers, like algaenan, cellulose, chitin, cutan, lignin, polyesters, and suberin are difficult for microorganisms to digest, in part due to their size, which necessitates that they must be broken down with enzymes before they can be consumed (Briggs et al, 2000). Hydrolytic enzymes can break down many biopolymers by reversing the dehydration step that is important in forming bonds between smaller organic molecules (Killops and Killops, 2005)

1.3.3 Spontaneous degradation

Even when microbial degradation is prevented, deceased organisms can still decay via autolysis. Autolitic enzymes are useful for recycling cellular components during a cell's life. (Killops and Killops, 2005). After death, autolitic and digestive enzymes continue to beak down organic materials, eventually destroying the cell and causing organic tissues to be converted into a slurry that cannot easily be fossilized. Molted exoskeletons, or "exuviae," contain very little labile materials and no digestive tract, so they are protected from autolytic enzymes (Butterfield, 1990). Sediments with abundant organic detritus are likely to have more autolitic enzymes, and consequently poorer fossil preservation. The Burgess Shale has very low carbon concentrations (Butterfield, 1996). These enzymes require liquid water to function, so they are inhibited in settings that lack liquid water, such as arid conditions (Worthy, 1989), permafrost (Boeskorov, 2014), amber (although resin contains some water, it dehydrates entombed organisms) (Labandeira, 2014), interstellar space, etc. Some chemicals have properties that inhibit autolytic decay. Tannins and humic acids can neutralize autolytic enzymes, but are only produced in environments containing vascular plant matter (restricting their effects temporally and geographically). Dissolved silica and iron can also hamper enzymatic activity. Clay minerals have numerous effects that inhibit autolytic decay. Some clay minerals can absorb or adsorb organic molecules, including enzymes (Butterfield, 1990). This property makes certain clay minerals commercially useful in cat litter to absorb the most fragrant components of cat urine, and in absorbing oil and grease spills (Murray, 1999). Clays can also denature some enzymes (Butterfield, 1990).

Even in the absence of autolytic enzymes, some organic substances spontaneously degrade. Lipids are especially robust over geologic time spans, especially when they are polymerized. Some lipids are organism-specific, allowing for geologists to identify the presence of certain organisms in an environment based on lipid characterization, even where no fossils of those organisms are preserved. A lipid called TEX_{86} can be used to reconstruct sea surface temperature. Aerobes, oxidizing compounds and ionizing radiation are highly destructive to organic compounds. Unfortunately, DNA, though it would be very useful to paleontologists, degrades very easily (Summons, 2014).

1.3.4 Carbon maturation

Organic materials that survive the decay process become subject to geological alteration, e.g. diagenesis and metamorphism. These processes have been thoroughly studied due to their relevance to the oil, gas and coal industries. Progressive heat and pressure alter buried organic carbon in a predictable manner, commonly producing fossil fuels. First, the organic matter is converted to kerogen, which is a variety of carbonaceous substances. For oil and gas production, there are three main categories of kerogen, which are compositionally distinct and are derived from different source material. Conditions for the production of petroleum occur under lower temperatures than that of the production of natural gas (methane). Both have higher H/C ratios than kerogen, so kerogen becomes hydrogen-depleted as hydrocarbons are produced (Tissot et al, 1974). Kerogen Type I is mainly derived from marine algae; Type II from various marine plankton; and Type III from vascular plant material (Jacobsen, 1991). Of these, Type I has the highest H/C ratio

and the lowest O/C ratio, whereas Type III has the lowest H/C and highest O/C. Type II is intermediate.

Early stages of carbon alteration can occur at very low temperatures and pressures. Humic substances (fulvic acid and humic acid) are produced during the degradation of organic carbon compounds. Fulvic acid may be formed via oxidation of humic acid. They are the main source of dissolved organic matter in seawater. Though they commonly form in soils, where they are leached out and transported to the ocean, the majority of marine humic substances are not derived from terrestrial environments. Humic acid is insoluble in acidic conditions. Humic substances are difficult for microorganisms to degrade, even in oxic environments, and so their formation represents a conversion of labile to recalcitrant organic matter. Another kind of organic polymers, called melanoidins form via "Maillard reactions," which are abiotic polymerization reactions between dissolved sugars and amino acids, such as those released via autolysis and microbial decay produce soluble compounds. Melanoidins and humic substances can condense to an insoluble, solid form of carbon called humin or brown coal, which is a brown, hydrated gel. It is considered a form of kerogen. Humin is the main component of peats. (Killops and Killops, 2005).

The first stage of thermal maturation of kerogen is oxygen lost mainly through the production of carbon dioxide and water. Petroleum production can begin when the O/C ratio is sufficiently low, and conditions are sufficiently hot, which is usually at about 1 km of burial (Tissot et al, 1974). Thermal alteration that is high enough to produce petroleum is considered "catagenesis." Petroleum, and any other kerogen that is soluble in an organic solvent, is considered "bitumen." Solid forms of bitumen are fusible (Killops and Killops, 2005). Type III kerogen has a poor capacity to produce petroleum due to its high initial

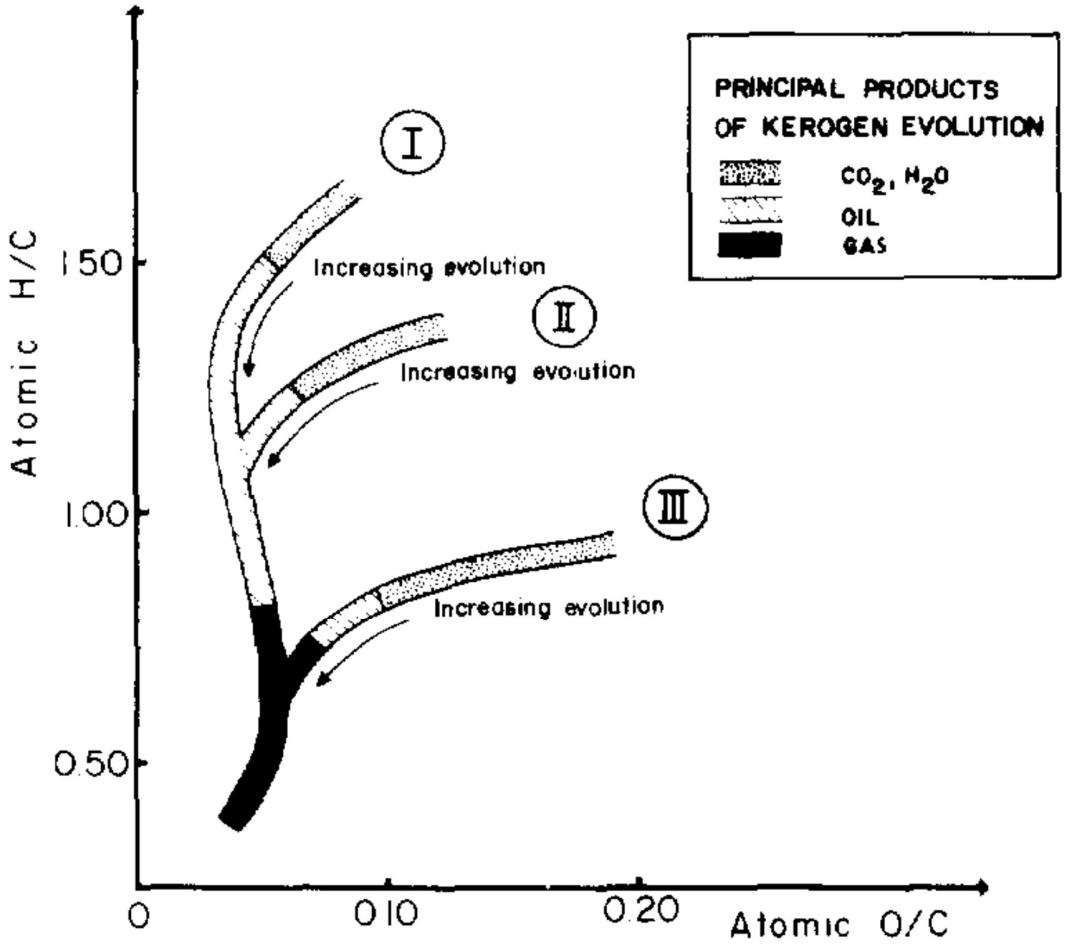

Figure 1.3 The maturation path of kerogen types. Early diagenesis involves oxygen loss, then oil then gas production. From Tissot et al, 1974, used with permission.

oxygen concentration, and low hydrogen content (Jacobsen, 1991). By the time temperatures are high enough to produce natural gas, all kerogen types are very depleted in both oxygen and hydrogen (Fig 1.3) (Tissot et al, 1974). Natural gas is methane, but other gaseous hydrocarbons can form concurrently (Killops and Killops, 2005). With the final production of natural gas, the kerogen that is left behind is a very pure carbon residue that forms strong aromatic chains, rendering it almost inert due to the strength of the covalent carbon-carbon bonds (Tissot et al, 1974). This last stage in kerogen maturation is called “inert kerogen” or “pyrobitumen.” Though pyrobitumen is insoluble, infusible, and scarcely reactive, it can produce bitumen with further thermal alteration. With even higher

temperatures, pyrobitumen can also be produced through the "cracking" of oil, where oil converts to natural gas (which has a higher hydrogen index than oil), leaving excess carbon behind in solid form. After the oil has "cracked," a rock is considered "overmature," and no more hydrocarbon production will occur because virtually all carbon is contained within aromatic groups, rendering them almost inert (Bernard and Horsfield, 2014). This is similar to the polymerization process that makes biotic organic polymers virtually inert. The aromatic groups, consisting of hexagons, can condense into a flat-lying preferred orientation, forming a precursor to graphite (Killops and Killops, 2005).

Solid forms of kerogen are also an important fuel source, as coal. Coals are almost entirely produced from Type III kerogen (vascular land plants), and the typical grades of coal (from lignite to bituminous coal to anthracite) is based on the kerogen maturity (from Type III Kerogen to bitumen to pyrobitumen). A small constituent in coals is "inertnite," Type IV kerogen, which is characterized by having already been oxidized, thus making it unsuitable for hydrocarbon generation. Inertinite can be sourced from charcoal (Jacobsen, 1991).

Carbonaceous fossils can be preserved as any solid form of kerogen, bitumen and pyrobitumen. Coals are, of course, wonderful sources of fossil material, especially of plants. In shales, BST fossils are known from every grade of carbon maturation. Cambrian rocks, from the heyday of BST preservation, are all fairly mature. The Burgess Shale, itself, is metamorphic (Butterfield et al, 2007). A perspective on BST preservation in less-mature shales can be gained from examination of Cenozoic lacustrine basins of the American West and the oil shales and stinkstones of Mesozoic European lagoons. One of the least mature carbonaceous-compression fossil deposits is the Clarkia lagerstätte of northern Idaho,

which, in spite of being at least 17 million years old (Smiley et al, 1975), contains fossil leaves that are still green (Lockheart et al, 2000) and preserve cellular resolution (Smiley et al, 1975) as well as insect carapaces that still retain original pigments and metallic lustre (McNamara et al, 2012). The Clarkia fossils are thought to have never been subjected to burial depths exceeding 100 m or temperatures exceeding 40°C (McNamara et al, 2012). In more mature shales, such details are lost, and more of the original carbon has been removed or microscopically altered. There is a histological bias regarding which tissues will preferentially become mobilized as hydrocarbons. Lipids derived from algae and bacteria (and some from vascular plants) are generally predisposed to becoming oil early, like 100-150°C (Pepper, 1991). Some lipids can polymerize in diagenesis, essentially becoming more resistant. This is observed in arthropod chitin and plant cuticles (Briggs, 1999). As a result, chitinous organisms may be preferentially preserved in mature shales even when microbial degradation is very minor.

From pyrobitumen, alteration can continue, but is mainly a result of changes in chemical structure, rather than composition. Pyrobitumen can become the mineral graphite, in a process that begins with ordering the flat, hexagonal aromatic groups into a layered structure (Killops and Killops, 2005). Since the metamorphic conditions necessary to form true graphite are fairly extreme, it may damage the morphological integrity of the fossil. Controversial microfossils are reported from rocks with a high grade of metamorphism, including chitinozoans and acritarchs from a mylonite formed under 0.2-0.6 GPa and 580-710°C (Hanel et al, 1999).

Diamonds tend to have low $\delta^{13}C$ values, (~ -5‰ vs. PDB), which may seem to suggest a biogenic origin (phototrophs fix ^{12}C more readily than ^{13}C, causing them and all

that eats them to be isotopically light compared to atmospheric values), but a solid-state conversion directly from graphite to diamond is probably not feasible. Some diamonds do contain graphite inclusions, however, and in eclogitic diamonds can bear a strongly negative (down to -23‰ $\delta^{13}C_{PDB}$) carbon isotopic signature, which could plausibly be due to trapped organic-derived carbon (Stachel et al, 2009). Like diamonds, zircons might also be able to trap biogenic graphite. The low (-24‰ $\delta^{13}C_{PDB}$) carbon isotopic signature of the graphite included in a 4.1 billion-year-old diamond is purported to be the oldest evidence of life on Earth (Bell, 2016).

REFERENCES

Allison, Peter A. and Derek E. G. Briggs (1991) "Taphonomy of Nonmineralized Tissues" *Taphonomy: Releasing the Data Locked in the Fossil Record* pp. 25-70 Eds. Peter A. Allison and Derek E. G. Briggs. Plenum Press, NY

Arnott, R. William C. (2010) "Deep-marine sediments and sedimentary systems" *Facies Models 4* pp. 295-322 Eds. Noel P. James and Robert W. Dalrymple. Geological Association of Canada, Canada.

Bell, Elizabeth A., Patrick Boehnke, T. Mark Harrison and Wendy L. Mao (2016) "Potentially biogenic carbon preserved in a 4.1 billion-year-old zircon" *Proceedings of the National Academy of Science* 112:14518-14521

Bernard, Sylvain and Brian Horsfield (2014) "Thermal Maturation of Gas Shale Systems" *Annual Review of Earth and Planetary Science* 42:635-651

Bernard, Sylvain, Brian Horsfield, Hans-Martin Schulz, Richard Wirth, Anja Schreiber and Neil Sherwood (2012) "Geochemical evolution of organic-rich shales with increasing maturity: A STXM and TEM study of the Posidonia Shale (Lower Toarcian, northern Germany)" *Marine and Petroleum Geology* 31:70-89

Boeskorov, Gennady G., Olga R. Potapova, Eugeny N. Mashchenko, Albert V. Protopopov, Tatyana V. Kunznetsova, Larry Agenbroad and Alexy N. Tikhonov (2014) "Preliminary analyses of the frozen mummies of mammoth (*Mammuthus primigenius*), bison (*Bison priscus*), and horse (*Equus* sp.) from the Yana-Indigirka Lowland, Yakutia, Russia" *Integrative Zoology* 9:471-480

Breannan, Sean T., Tim K. Lowenstein and Juske Horita (2004) "Seawater chemistry and the advent of biocalcification" *Geology* 32:473-476

Briggs, Derek E. G., (1999) "Molecular taphonomy of animal and plant cuticles: selective preservation and diagenesis" *Philosophical Transactions of the Royal Society of London B* 354:7-17

Briggs, Derek E. G., (2003) "The Role of Decay and Mineralization in the Preservation of Soft Bodies" *Annual Review of Earth and Planetary Science* 31:275-301

Butterfield, Nicholas J. (1990) "Organic preservation of non-mineralizing organisms and the taphonomy of the Burgess Shale" *Paleobiology* 16:272-286

Butterfield, Nicholas J. (1995) "Secular distribution of Burgess-Shale-type preservation" *Lethaia* 28:1-12

Butterfield, Nicholas J. (1996) "Fossil preservation in the Burgess Shale: Reply" *Lethaia* 29:109-112

Butterfield, Nicholas J. (2003) "Exceptional Fossil Preservation and the Cambrian Explosion" *Integrative and Comparative Biology* 43:166-177

Butterfield, Nicholas J., Uwe Balthasar and Lucy A. Wilson (2007) "Fossil diagenesis in the Burgess Shale" *Palaeontology* 50:537-543

Cai, Yaoping, James D. Schiffbauer, Hong Hua and Shuhai Xiao (2012) "Preservational modes in the Ediacaran Gaojiashan Lagerstätte: Pyritization, aluminosilicification and carbonaceous compression" *Palaeogeography, Palaeoclimatology, Palaeoecology* 326-328:109-117

Canfield, Don E., Simon W. Poulton and Guy M. Narbonne (2007) "Late-Neoproterozoic Deep-Ocean Oxygenation and the Rise of Animal Life" *Science* 315:92-95

Cohen, K.M., D. A. T. Harper, P. L. Gibbard (2017) ICS International Chronostratigraphic Chart 2017/02. International Commission on Stratigraphy, IUGS. www.stratigraphy.org

Deuser, W. G., P. G. Brewer, T. D. Jickells and R. F. Commeau (1983) "Biological Control of the Removal of Abiogenic Particles from the Surface Ocean" *Science* 219:388-391

D'Hondt, Steven, Scott Rutherford and Arthur J. Spivack (2002) "Metabolic Activity of Subsurface Life in Deep-Sea Sediments" *Science* 295:2067-2070

Downen, Matthew Ross (2014) "The taxonomy and taphonomy of fossil spiders from the Crato Formation of Brazil" M.S. Thesis, Department of Geology, University of Kansas

Eby, G. Nelson (2004) *Principles of Environmental Chemistry* Brooks/Cole, Belmont, CA

Faure, Gunter (1998) "Principles and applications of geochemistry: a comprehensive textbook for geology students" 2nd ed. Prentice Hall, NJ.

Ferry, James G. (1992) "Methane from Acetate" *Journal of Bacteriology* 174:5489-5495

Gabbot, S. E., J. Zalasiewicz and D. Collins (2008) "Sedimentation of the Phyllopod Bed within the Cambrian Burgess Shale Formation of British Columbia" *Journal of the Geological Society, London* 165:307-318

Gaines, Robert R. (2005) "A new hypothesis for organic preservation of Burgess Shale taxa in the middle Cambrian Wheeler Formation, House Range, Utah" *Palaeogeography, Palaeoclimatology, Palaeoecology* 220:193-205

Giresse, P., A. Wiewiora and B. Lacka (1988) "Mineral phases and processes within green peloids from two Recent deposits near the Congo River mouth" *Clay Minerals* 23:447-458

Goldstein, Joseph, Dale Newbury, David Joy, Charles Lyman, Patrick Echlin, Eric Lifshin, Linda Sawyer and Joseph Michael (2003) *Scanning Electron Microscopy and X-ray Microanalysis 3rd edition*, Springer Science, NY

Gould, Stephen Jay (1989) *Wonderful Life* .W. W. and Norton Company, NY

Hanel, M., M. Montenari and A. Kalt (1999) "Determining sedimentation ages of high-grade metamorphic gneisses by their palynological record: a case study in the northern Schwarzwald (Variscan Belt, Germany) *Journal of Earth Sciences* 88:49-59

Hardie, Lawrence A. (1996) "Secular variation in seawater chemistry: An explanation for the coupled secular variation in the mineralogies of marine limestones and potash evaporites over the past 600 m.y." *Geology* 24:297-283

Horita, Juske, Heide Zimmermann and Heinrich D. Holland (2002) "Chemical evolution of seawater during the Phanerozoic: Implications from the record of marine evaporites" *Geochimica et Cosmochimica Acta* 66:3733-3756

Jablonski, David, Kaustuv Roy, James W. Valentine, Rebecca M. Price, Philip S. Anderson (2003) "The Impact of the Pull of the Recent on the History of Marine Diversity" *Science* 300:1133-1135

Jacobsen, S. R. (1991) "Petroleum Source Rocks and Organic Facies" *TR: Source and Migration Processes and Evaluation Techniques* pp. 3-11 Eds. Robert K. Merrill, Norman H. Foster, Edward A. Beaumont. American Association of Petroleum Geologists

Johnson, Ralph Gordon (1964) "The Community Approach to Paleoecology" *Approaches to Paleoecology* (Eds. John Imbrie and Normal Newell) 107-134

Killops, Stephen and Vanessa Killops (2005) *Introduction to Organic Geochemistry* 2nd Ed. Blackwell Publishing, Malden, MA.

Labandeira, Conrad C. (2014) "Amber" *Reading and Writing of the Fossil Record: Preservation Pathways to Exceptional Fossilization*. pp. 163-216 Eds. Marc Laflamme, James D. Schiffbauer and Simon A. F. Darroch. The Paleontological Society Papers v. 20.

L'Haridon, S., A.-L. Reysenbach, P. Glénat, D. Prieur and C. Jeanthon (1995) "Hot subterranean biosphere in a continental oil reservoir" *Nature* 377:223-224

Lockheart, Matthew J., Pim F. van Bergen and Richard P. Evershed (2000) "Chemotaxonomic classification of fossil leaves from the Miocene Clarkia lake deposit, Idaho, USA based on *n*-alkyl lipid distributions and principal component analyses" *Organic Geochemistry* 31:1233-1246

Martin, Derek, Derek E. G. Briggs and R. John Parkes (2005) "Decay and Mineralization of Invertebrate Eggs" *Palaios* 20:562-572

McCoy, Victoria E. (2014) "Concretions as agents of soft-tissue preservation: A review" *Reading and Writing of the Fossil Record: Preservation Pathways to Exceptional Fossilization*. pp. 147-162 Eds. Marc Laflamme, James D. Schiffbauer and Simon A. F. Darroch. The Paleontological Society Papers v. 20.

McNamara, Maria E., Derek E. G. Briggs and Patrick J. Orr (2012) "The controls on the preservation of structural color in fossil insects" *Palaios* 27:443-454

Morris, S. Conway (1986) "The Community Structure of the Middle Cambrian Phyllopod Bed (Burgess Shale)" *Palaeontology* 29:423-467

Muscente, A. D., James D. Schiffbauer, Jesse Broce, Marc Laflamme, Kenneth O' Donnell, Thomas H. Boag, Michael Meyer, Andrew D. Hawkins, John Warren Huntley, Maria McNamara, Lindsay A. MacKenzie, George D. Stanley Jr., Nancy W. Hinman, Michael H. Hofmann, and Shuhai Xiao (2017) "Exceptionally preserved fossil assemblages through geologic time and space" *Gondwana Research* 48:164-188

Musico, Gary P. A. and Brian Horsfield (1996) Neoformation of Inert Carbon during the Natural Maturation of a Marine Source Rock: Bakken Shale, Williston Basin. Energy and Fuels 10, 10-18

Nealson, Kenneth H. (1997) "Sediment Bacteria: Who's There What Are They Doing, and What's New?" *Annual Review of Earth and Planetary Sciences* 25:403-34

Nelsen, Matthew P., William A. DiMichele, Shanan E. Peters and C. Kevin Boyce (2016) "Delayed fungal evolution did not cause the Paleozoic peak in coal production" *Proceedings of the National Academy of Science* 113:2442-2447

Orr, Patrick J., Derek E. G. Briggs, Stuart L. Kearns (1998) "Cambrian Burgess Shale Animals Replicated in Clay Minerals" *Science* 281:1173-1175

Orr, Patrick J. (2014) "Late Proterozoic-Early Phanerozoic 'taphonomic windows': The environmental and temporal distribution of recurrent modes of exceptional preservation" *Reading and Writing of the Fossil Record: Preservation Pathways to Exceptional Fossilization.* Eds. Marc Laflamme, James D. Schiffbauer and Simon A. F. Darroch. The Paleontological Society Papers v. 20.

Parkes, R. J., B. A. Cragg, S. J. Bale, J. M. Getliff, K. Goodman, P. A. Rochelle, J. C. Fry, A. J. Weightman and S. M. Harvey (1994) "Deep bacterial biosphere in Pacific Ocean sediments" *Nature* 371:410-413

Peters, Shanan E. and Robert R. Gaines (2012) "Formation of the 'Great Unconformity' as a trigger for the Cambrian explosion" *Nature* 484:363-366

Reid, R. P., P. T. Visscher, A. W. Decho, J. F. Stolz, B. M. Bebout, C. Dupraz, I. G. Macintyre, H. W. Paerl, J. L. Pinckney, L. Prufert-Bebout, T. F. Steppe and D. J. DesMarais (2000) "The role of microbes in accretion, lamination and early lithification of modern marine stromatolites" *Nature* 406:989-992

Rickard, David (2012) "Sulfidic Sediments and Sedimentary Rocks" Developments in Sedimentology 65. NLD:Elsevier Science and Technology, Amsterdam

Saltzman, Matthew R., Seth A. Young, Lee R. Kump, Benjamin C. Gill, Timothy W. Lyons and Bruce Runnegar (2011) "Pulse of atmospheric oxygen during the late Cambrian" *Proceedings of the National Academy of Science* 108:3876-3881

Sansom, Robert S., Sarah E. Gabbott and Mark A. Purnell (2010) "Non-random decay of chordate characters causes bias in fossil interpretation" *Nature* 463:797-800

Sansom, Robert S. (2014) "Experimental Decay of Soft Tissues" in Reading and Writing of the Fossil Record: *Preservation Pathways to Exceptional Fossilization*. Eds. Marc Laflamme, James D. Schiffbauer and Simon A. F. Darroch. The Paleontological Society Papers v. 20.

Satchel, Thomas, Jeff W. Harris, Karlis Muehlenbachs (2009) "Sources of carbon in inclusion bearing diamonds" *Lithos* 112S:625-637

Schmidt-Rhaesa, Andreas (2013) "Priapulida" In Ed. Schmidt-Rhaesa *Handbook of Zoology: Gastrotricha, Cycloneuralia and Gnathifera: Volume 1: Nematomorpha, Priapulida, Kinorhyncha, Lorcifera*, DeGruyter, Germany. 147-180

Smiley, Charles J., Jane Gray and L. Maurice Huggins (1975) "Preservation of Miocene fossils in unoxidized lake deposits, Clarkia, Idaho; with a section on fossil Insecta by W. F. Barr and J. M. Gillespie" *Journal of Paleontology* 49:833-844

Sperling, Erik A., Christina A. Frieder, Akkur V. Raman, Peter R. Girguis, Lisa A. Levin and Andrew H. Knoll (2013) "Oxygen, ecology, and the Cambrian radiation of animals" *Proceedings of the National Academy of Science* 110:13446-13451

Stokes, George Gabriel (1851) "On the effect of the internal friction of fluids on the motion of pendulums" *Transactions of the Cambridge Philosophical Society* 9:8

Summons, Roger E. (2014) "The exceptional preservation of interesting and informative biomolecules" *Reading and Writing of the Fossil Record: Preservation Pathways to Exceptional Fossilization*. pp. 217-236 Eds. Marc Laflamme, James D. Schiffbauer and Simon A. F. Darroch. The Paleontological Society Papers v. 20.

Tissot, B., B. Durand, J. Epistalié and A. Combaz (1974) "Influence of Nature and Diagenesis of Organic Matter in Formation of Petroleum" *The American Association of Petroleum Geologists Bulletin* 58:499-506

Tucker, Maruice E. (1992) "The Precambrian-Cambrian boundary: seawater chemistry, ocean circulation and nutrient supply in metazoan evolution, extinction and biomineralization" *Journal of the Geological Society* 149:655-668

Vrazo, Matthew B., Carlton E. Brett and Samuel J. Ciurca Jr. (2017) "Paleoecological and stratigraphic controls on eurypterid Lagerstätten: a model for preservation in the mid-Paleozoic" *Paleobiology* 43:383-406

Walcott, Charles D. (1911) "Middle Cambrian Holothurians and Medusae" *Smithsonian miscellaneous collections* 57:41-68

Wellsbury, Peter, Kim Goodman, Tanja Barth, Barry A. Cragg, Stephen P. Barnes and R. John Parkes (1997) "Deep marine biosphere fueled by increasing organic matter availability during burial and heating" *Nature* 388:573-576

Winfrey, Michael R. and David M. Ward (1983) "Substrates for Sulfate Reduction and Methane Production in Intertidal Sediments" *Applied and Environmental Microbiology* 45:193-199

Worthy, T. H. (1989) "Mummified moa remains from M. Owen, northwest Nelson" *Notornis* 36:36-38

Wotton, Roger S., Björn Malmqvist, Timo Muotka and Kristina Larsson (1998) "Fecal pellets from a dense aggregation of suspension-feeders in a stream: An example of ecosystem engineering" *Limnology and Oceanography* 43:719-725

Zhang, Xi-Guang and Xian-Guang Hou (2007) "Gravitational constraints on the burial of Chengjiang fossils" *Palaios* 22:448-453

CHAPTER 2: INTRODUCTION TO ACCESSORY MINERALIZATION OF BURGESS SHALE-TYPE FOSSILS

2.1. Processes of Pyritization

2.1.1- Sulfur sources

In ordinary seawater, sulfate is highly abundant (appx 28 mM), but sulfide, which is necessary to produce pyrite, is largely absent, due to the propensity for sulfides to convert to sulfates in oxic conditions. Though sulfide oxidation can occur via reaction with oxygen, it is a slow reaction, so reactions with oxidized metal species are a more important mechanism for sulfide oxidation. (Rickard, 2012). In freshwater, even sulfate is generally found in low concentrations, around 0.12 mM (Faure, 1998), but is subject to local variation. Sulfur concentrations in aqueous reservoirs have varied through time, as well. Early Earth atmospheres and oceans were heavily sulfide-dominated, but transitioned towards more sulfate-rich circumstances during and after the ~2.3 Ga Great Oxidation Event. Since then, sulfides are largely restricted to porewaters in the sediment, except in stratified basins where anoxic conditions extend to the bottom-waters. The main source of sulfide in modern oceans is the action of SRBs (Rickard, 2012). Sulfide is produced as a by-product of their metabolism, so as a corpse is decayed by SRBs, pyrite will form in its immediate vicinity, enabling the replication of the corpse via pyrite association. This process is easily disrupted in settings where the sediment contains a large quantity of organic carbon. In such settings, SRBs produce sulfide, and therefore pyrite, throughout the sediment, rather than just in fossil association. Consequently, pyritization is best known from deposits where the sediment is organic-poor (Farrell, 2014).

There are different metabolic pathways for the degradation of different organic compounds by SRBs. Many compounds (like lactate, formate and pyruvate) are degraded via a two-step process. The first stage of decay oxidizes them to acetate (incomplete oxidation). The second stage oxidizes acetate to bicarbonate, completing the oxidation, but it produces less energy than the first stage (-80 kJ/mol from lactate to acetate and bicarbonate, -47.6 from acetate to bicarbonate), and requires more sulfate (0.5 moles sulfate per 1 mole lactate to acetate, 1 mole sulfate to finish the job). Because of this, stopping at the first stage is more favorable to SRBs unless organic carbon becomes limited, but also, a sulfate limitation may inhibit complete oxidation from occurring (Postgate, 1984).

Most forms of metabolism have some influence on the pH of a fluid (Fig. 2.1). For instance, oxic metabolism like our own produces carbon dioxide gas. When CO_2 becomes dissolved in water, it becomes carbonic acid first, which can then dissociate to bicarbonate and finally carbonate (in high pHs), producing two hydrogen ions (acidity). Sulfur-reducing metabolisms have a different effect on pH, since bicarbonate is produced, rather than CO_2. Hydrogen ions are also produced directly, but the bicarbonate and bisulfide have a buffering effect on pH. Essentially, bicarbonate (HCO_3^-) and bisulfide (HS^-) may react with free H^+ ions to produce carbonic acid (H_2CO_3) and sulfidic acid (H_2S). In fact, at STP (standard temperature and pressure), the diprotic (containing two hydrogen atoms) forms of these ions are dominant at pH below 6.35 for carbonate species and 7.03 for sulfide

Figure 2.1 (next page) Computer model (PHREEQC) of pH changes resulting from microbial decay in seawater with sediment that contains 5 millionths of a wt. % Fe at 20 °C. Both complete (orange) and incomplete (red) sulfate reduction of lactate are modeled, and methanogenic fermentation of the acetate produced from incomplete SR. Supersaturation of 10^{10} is necessary for pyrite nucleation in this model. Events are numbered as onset of dissolution of (1) haematite, (2) dolomite, (3) pyrite, (4) calcite; disappearance of (5) dolomite, (6) haematite, (7) greigite; onset of precipitation of (8) haematite, (9) dolomite, (10) greigite, (11) pyrite, (12) calcite; and establishment of (13) euxinic conditions.

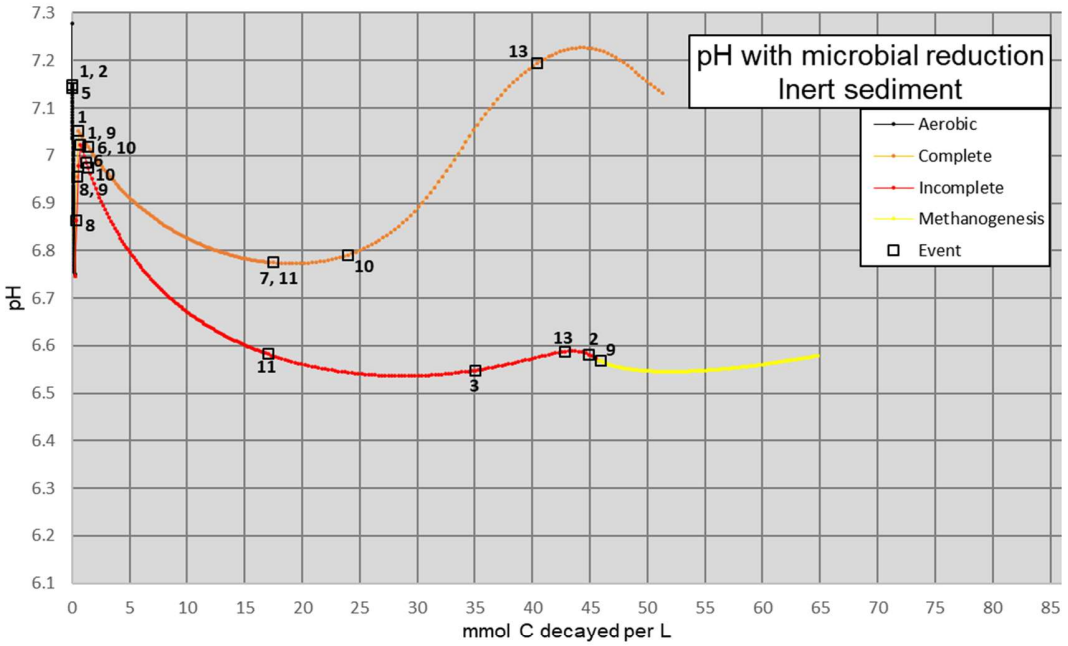

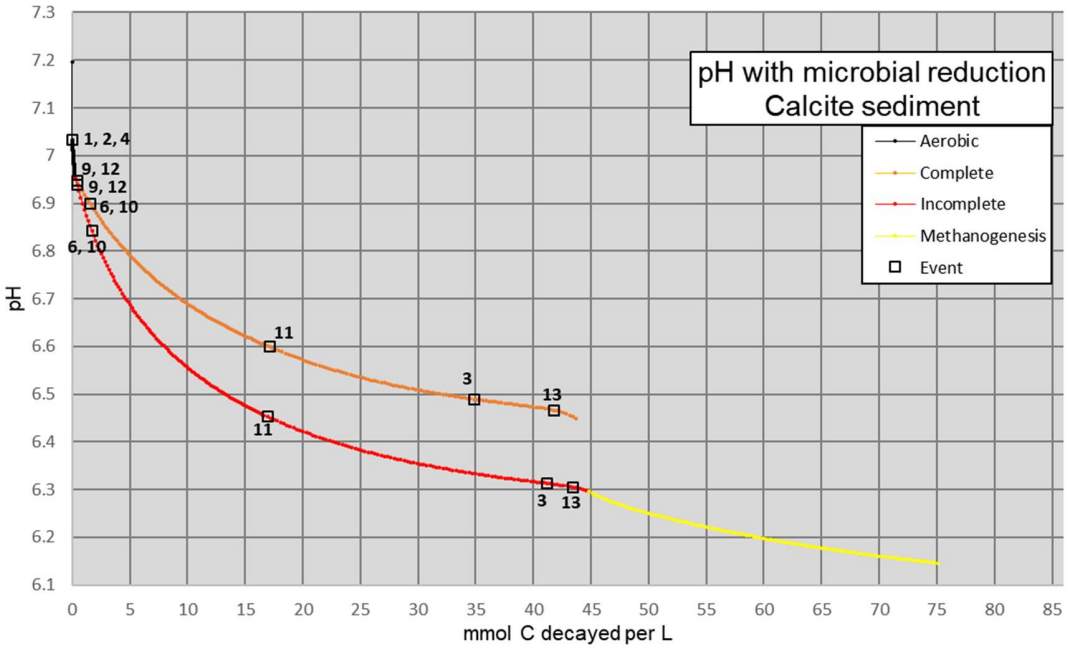

species (Eby, 2004). Since the various types of sulfate reduction produce more sulfide than H^+ ions, the added sulfide should inhibit pH decline from SRB metabolism. In addition, the sulfidic acid which is produced can nucleate as a bubble of hydrogen sulfide and escape the system, effectively removing acidity from the solution permanently (Postgate, 1984).

Sulfides are sometimes produced during hydrocarbon maturation, and this process is known to produce pyrites (Killops and Killops, 2005).

2.1.2 Iron sources

Ferrous iron is another requirement for pyritization. Iron concentrations are generally very low in seawater (1-5 nM), partly because iron is an important nutrient that is scavenged by organisms (Rickard, 2012). Fresh water can achieve much higher concentrations of iron, due to their lower pH and ionic strength (Odin and Gupta, 1988), resulting in an average concentration of dissolved iron in streams to be ~700nM (Faure, 1991), most of which precipitates out in deltaic environments. Much of the iron content in seawater is not dissolved. Some microorganisms release chelating agents called "siderophores" to scavenge iron from seawater. Thus, dissolved iron can get trapped in siderophores, where they are available for biological use, but not for inorganic reactions. Much of the iron in seawater is nanoparticulate hæmatite or goethite (iron oxide and oxy-hydroxide minerals which do not transition to pyrite). The miniscule dissolved fraction of iron in seawater readily adsorbs to organic compounds and the surfaces of mineral grains. Most of the dissolved iron in seawater is not ferrous iron ($Fe^{2+}_{(aq)}$), as is required for pyrite precipitation (Rickard, 2012). Since ferrous iron readily reacts with dissolved oxygen to form $Fe(OH)_{3}^{-}{}_{(aq)}$, ferrous iron essentially will not be found outside of anoxic conditions (Lyons and Severmann, 2006). Dissolved iron was likely less severely limited in the Precambrian, especially before the Great Oxygenation Event (Rickard, 2012).

The problem of low dissolved iron concentrations is somewhat circumvented by iron storage in sediment. Nanoparticulate iron oxyhydroxides readily adsorb to mineral

surfaces, which is why beach sand is typically yellow-colored at the surface, despite being composed of (usually) colorless quartz. Quartzose sands are generally very low in iron content, as compared to other marine sediments which are usually a few wt% (Rickard, 2012). The coloration of sediment is often a function of the redox conditions, because the chemical changes which iron and manganese species rapidly undergo with changing redox conditions (Lyle, 1983). A few centimeters below the surface of the beach, it is common to find that the sand is of a black coloration, which is usually related to the appearance of iron sulfides at that depth (Bossellmann, 2007), but there is at least one case where the black layer was a result of tetrahedral elemental sulfur (Rickard, 2012). There is sometimes an intermediate layer, often described as grey (Bossellmann, 2007), but sometimes referred to as the "blue mud," which also usually receives its coloration from iron sulfide particles (Rickard, 2012). The sand surrounding animal burrows within the gray sand often turns a reddish color because of the redox state of iron. In argillaceous deeper marine conditions, the sediment-depth color gradient is largely controlled by the color of the clay minerals in the sediment. When incorporated into smectite interlayers, Fe (III) imparts a brownish color to the sediment, whereas Fe (II) imparts a greenish hue (Lyle, 1983). It should be noted that in waterlogged soils, a greenish tint is due to a different suite of Fe (II) minerals (the green rusts, of which only fougerite has been characterized), but are reflective of similar redox conditions (Rickard, 2012). The redox state of the iron ions can change in response to the surrounding porewaters, even whilst they are bound to clays. There can also be an intermediate tan layer where reduced manganese is present. The thickness of these layers is thought to be smaller in areas of higher primary productivity, in addition to numerous other factors (Lyle, 1983).

Though iron may have extremely low solubility, iron storage in sediment may serve to replenish the supply of dissolved iron when iron concentrations decline, due to pyrite precipitation, for instance. Supporting example for this relationship include Beecher's Trilobite Bed (Briggs et al, 1991; Farrell et al, 2013) and the Hunsrück Slate (Briggs et al, 1996), two of the best pyritization lagerstätte in the world. The positive relationship between sedimentary iron content and pyritization only applies to areas with anoxic bottom waters because high concentrations of sedimentary iron oxides, as can occur in oxic settings, will re-oxidize sulfides to sulfates (Lyons and Severmann, 2006), or as aqueous elemental sulfur (Rickard, 2012). One source of dissolved ferrous iron is the use of ferric iron as an electron donor in microbial metabolisms, but since sulfate is so much more abundant in marine settings, reaction with sulfides is likely a greater source of ferrous iron than microbial iron reduction (Bossellmann, 2007). Provided an adequate supply of sulfide, iron oxides and hydroxides are a readily available source of dissolved iron, due to being highly reactive with sulfides, so much so that sedimentary particles of iron oxides are commonly partly replaced by pyrite during diagenesis. Another sedimentary source of available iron is the iron in certain reactive silicate minerals (chlorite and biotite, possibly others), which are also reactive with sulfide and can generate localized pyrite. Both iron in the interlayers and in the silicate layer seem to be susceptible to reaction with sulfide, but these reactions are very gradual even in high concentrations of sulfide. Canfield, Raiswell and Bottrell (1992) estimated that the iron in sheet silicates reacts with sulfides with a half-life of approximately 100,000 years, and postulated that other iron-bearing silicates, like garnets, augite and amphiboles, may be reactive with sulfides over even longer timescales. Whereas iron oxides are so reactive that they can inhibit high concentrations of sulfide

from accumulating, iron-bearing silicate minerals react too gradually to act as a significant sulfide sink in microbially-active sediments (Canfield, Raiswell and Bottrell, 1992).

2.1.3 Chemistry of pyrite nucleation and growth

Once both sulfides and ferrous iron are present in solution, pyrite precipitation can commence. Unfortunately, pyrite is kinetically inhibited from nucleation. Once pyrite has nucleated, pyrite growth can occur rapidly, but that first nucleation site is a difficult initial requirement that may require a supersaturation greater than 10^{14} (Rickard, 2012). Mackinawite, elemental sulfur and biological surfaces are favorable nucleation sites (Schoonen, 2004), though the supersaturation limit is still above 10^{10} (Rickard, 2012). Before concentrations are high enough to cause pyrite to nucleate, metastable iron sulfides may precipitate. The iron monosulfide, mackinawite, is easy to form in sulfidic, ferrous fluids, since one Fe^{2+} and one S^{2-} have a perfect charge balance. Usually, the most available sulfide species for this reaction will be HS^- or H_2S, in which case acidity will be produced as iron monosulfides form. The common sedimentary iron sulfide minerals, namely greigite, mackinawite and marcasite, are not stable on geologic timescales, due to their solubility. They may, however, play an important role in pyrite formation. As monosulfides dissolve, they contribute to supersaturation that might create pyrite. Pyrite growth commences rapidly once nucleation happens, and as pyrite removes dissolved iron and sulfide from the porewaters, iron monosulfides suffer from increased solubility, supplying new ions for pyrite growth. Thus, pyrite growth can prompt iron monosulfide dissolution, which prompts further pyrite growth. Of the iron monosulfide minerals, mackinawite most

easily precipitates from seawater, although others have been observed naturally and under experimental conditions (Rickard, 2012).

Some authors have proposed that iron monosulfides can convert to pyrite via a solid-state transformation. Such a change would require the addition of one extra sulfide ion per iron atom. Additionally, since iron monosulfides bear a neutral charge (Fe^{2+} and S^{2-} cancelling out), the extra sulfide requires an electron acceptor. Since pyrite is a semiconductor, the electron acceptor for pyrite growth reactions could be located anywhere on the surface of the pyrite crystal (Schoonen, 2004). However, a conversion from iron monosulfide to pyrite is not mechanistically plausible as a solid state, and it more likely occurs as an aqueous phase. Pyrite-forming reactions between iron monosulfides and sulfide species are technically possible ($FeSH^{+}+HS^{-}$, $FeS+H_2S$), but would produce hydrogen gas, which is not observed experimentally. Sources of S(0) for pyrite-forming reactions include elemental sulfur and polysulfide, both of which exist in small concentrations, especially near the S(VI)/S(-II) redox boundary (the S-redox-cline). Elemental sulfur is produced via various redox reactions between sulfide species and metal oxides, most relevantly goethite/limonite (FeOOH) and pyrolusite (MnO_2). It is most stable in acidic conditions. Polysulfides are a group of aqueous sulfide species consisting of chains of sulfur atoms which bear a -2 charge (total), and up to two hydrogen atoms. Disulfide forms via a catenation reaction between a sulfide and elemental sulfur. Larger polysulfides form via reactions between smaller polysulfides and elemental sulfur. HS_2^{-} is the most stable polysulfide species under most conditions. Polysulfides are highly susceptible to reaction with oxygen, so they will not be found in oxic settings, but otherwise, they exist in all sulfidic solutions. The reaction to form pyrite from iron

monosulfide using polysulfides is actually a replacement of the sulfur atom in iron monosulfide with two sulfur atoms from a polysulfide. While the formation of iron monosulfide produces acidity (1-2 moles H^+ per mole FeS), the conversion of iron monosulfide to pyrite does not (Rickard, 2012).

2.1.4 Framboidal pyrite

Pyrite has many different crystal forms, including, of course, the "pyritohedron," (Fig. 2.2 a) which is merely a dodecahedron with slightly different angles. A highly abundant crystal form of sedimentary pyrite is the pyrite "framboid," *sensu* Rust, 1930 (Fig. 2.2 b & c) after the French word for raspberry, framboise, which consists of a spheroidal-to-icosahedral cluster of pyrite euhedra of consistent size. While the framboidal texture is almost exclusively known from sedimentary pyrite, there are exceptions, including pyrite framboids in igneous rocks and meteorites, and framboids composed of other metal sulfides (Rickard, 2012). Framboids typically range from ~5 μm to ~30 μm in diameter, but are known to grow up to 250 μm, though this is an extreme case (Farrell, 2014). One mysterious phenomenon in pyrite framboids is the rare "ordered framboids," in which the individual euhedra are arranged in a geometric pattern (Fig. 2.2 c). Ordered framboids, though their interior arrangement varies, achieve the overall shape of an icosahedron. It is possible that all framboids would naturally grow to become ordered, but that most framboids were perturbed at some point in their development, disrupting the internal structure (Rickard, 2012).

Measurements of pyrite framboids have been used as a proxy for environmental conditions, like euxinia. Pyrite framboids which are found in sediments of euxinic basins

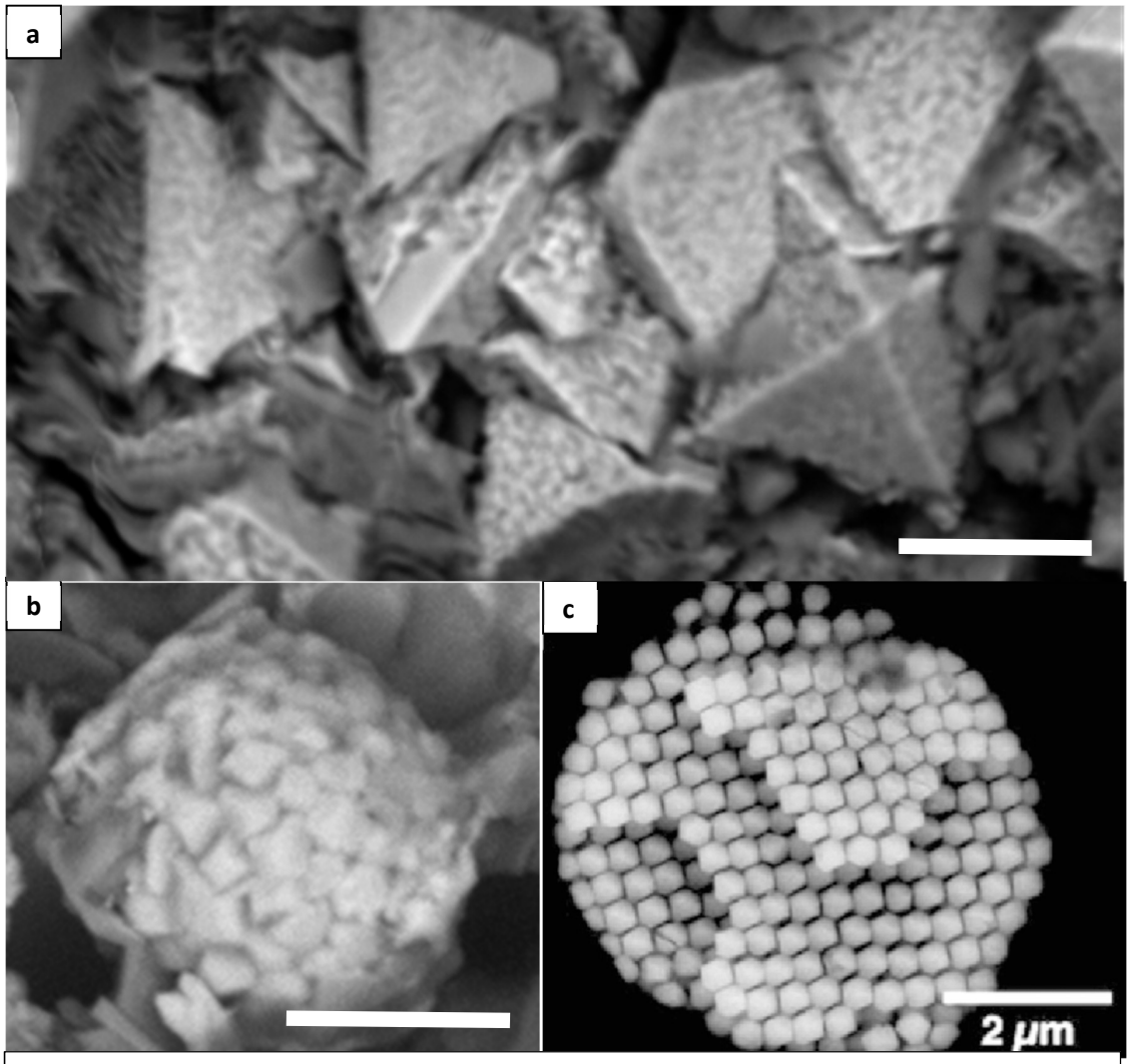

Figure 2.2 Backscattered electron images (BSE) of sedimentary pyrite varieties. (a) Intergrowing pyrite octahedra, KUMIP 293598, Cambrian of Utah. Scale bar is 10 µm. (b) Pyrite "cluster" from KUMIP 314248. Scale bar is 5 µm. (c) Ordered framboid from the Chattanooga Shale, from Rickard, 2012, used with permission.

have a smaller average size, which is attributed to a large proportion of the pyrite framboids having formed in the water column (syngenetic/detrital framboids). Diagenetic framboids (framboids that form within the sediment) do tend to be larger (Wilkin, Barnes and Brantley, 1996; Wilkin and Arthur, 2001). The ratio between the size of the microcrysts (individual euhedra) to the total framboid size is larger for detrital than diagenetic framboids (Wilkin, Barnes and Brantley, 1996), but since there is no known correlation between microcryst size and euxinia, this trend could be wholly driven by total framboid

size (which is easier to measure). Thus, euxinic basins are predominated by the smaller, detrital framboids and oxic-to-hypoxic basins will mainly contain the larger, diagenetic framboids and isolated pyrite euhedra. One might expect that, over time, the production of diagenetic framboids would cause the average pyrite framboid size to increase over time, but this trend is not observed, perhaps because framboid production is preferred at the S-redox-cline (perhaps due to the greater concentration of polysulfides, elemental sulfur or thiosulfate), which is located in the water column of euxinic basins, but in the sediment column in all other environments (Wilkin, Barnes and Brantley, 1996). It is important to remember that pyrite framboids *are not* concretions and *cannot* grow like concretions. Individual framboids are thought to form rapidly, and once they form, growth is not known to occur. Later pyrite precipitation can occur in framboids, but this does not cause growth of the framboid, and only serves to fill in the pore spaces. Where this secondary pyritization causes the microcrysts to overgrow, it is called a "cluster" (Canfield and Raiswell, 1991, see Fig 2.2 b), but where the secondary pyrite is void-filling, the framboid is considered "filled" (Wilkin and Arthur, 2001) Pyrite framboids can, however, shrink due to oxidative weathering, which would not occur under euxinic conditions (Gaudin et al, 2005).

While the close correspondence between framboid size and euxinia is well established in the Wilkin papers, the given explanation for this phenomenon is inadequate. Wilkin, Barnes and Brantley (1996) explain pyrite framboid formation because of the microcrysts growing independently in different places, and then aggregating into almost spherical framboids and somehow having every microcryst of equal size, a process which is estimated to take 0.4 years or less. This does not seem a sensible explanation, especially for diagenetic framboids. Granted, the mechanics of the growth of framboids is still

something of a mystery. The microcrysts are separate, with little, if any intergrowth, and are evenly spaced. The size of the microcrysts does not vary, even between the outside and center of a framboid. How do so many separately nucleated crystals manage to grow while maintaining an even spacing and size? If the consistent microcryst size is indicative of the same duration of crystal growth, they must nucleate almost simultaneously. Some authors invoke greigite as an intermediate solid phase, which, since it is magnetic, may cause a clustering of individual crystals like this. Some pyrite framboids do have greigite at the cores of their microcrysts, indicating pyrite replacement of greigite, but this is uncommon. Even in cases of greigite framboids, the magnetic aggregation process does not seem adequate to explain such regularly shaped objects with such evenly-sized microcrysts. Is the magnetic attraction of greigite particles adequate to pull microcrysts through the sediment towards one another? Pyrite framboids preferentially form in enclosed areas, and the consistent microcryst size indicates almost simultaneous nucleation and duration of growth. Therefore, constituents must have achieved a great supersaturation of pyrite, until numerous crystals nucleated, causing the rest of the constituents to rapidly come out of solution via crystal growth, quickly dropping the concentration of constituents beneath saturation, via a process called “burst nucleation”. In order for the concentration to rapidly drop beneath saturation, the framboid must form in a diffusion-restricted environment, and, in fact, most framboids are found in diffusion-restricted environments, like within fine sediment or microfossils (Rickard, 2012).

The burst-nucleation hypothesis seems rational, but has a few shortcomings. In open-water settings, where detrital framboids form, it would be difficult for a 10^{14} supersaturation of pyrite to rapidly drop to saturation as a result of the precipitation of

framboids, which is necessary for burst nucleation to occur. Honestly, the existence of detrital framboids seems to defy common-sense altogether, but there is compelling evidence that they are, indeed, formed in the open-water redox-cline of euxinic basins. Small pyrite framboids in the water column were first observed in a euxinic African rift lake (Degens et al, 1972), and have subsequently been found in several euxinic basins. These framboids are sometimes associated with organic particles (Wilkin, Barnes and Brantley, 1996). Framboids in the water of two euxinic Canadian lakes, though present in throughout the anoxic zone, are most abundant some distance beneath the anoxic boundary. Further, the maximum framboid abundance was found just beneath the S-redox-cline, and close to where pyrite supersaturation also reached a maximum ($> 10^{13}$ in both lakes). This is taken to mean that detrital framboids were precipitated in the water column, and did not enter the water column via resuspension (Perry and Pedersen, 1993). The trouble with framboids growing at the S-redox-cline and raining out once they are too large to remain suspended is that pyrite framboids are supposed to form rapidly.

Analysis of pyrite sulfur isotopes provides additional support for detrital framboids. Porewater sulfide $\delta^{34}S$ is a result of SRBs more readily utilizing ^{32}S, which makes typical porewater sulfide sulfur isotopically lighter than the sulfate sulfur which produced it. There are exceptions to this rule, such as extremely rapid reactions, where the effects of fractionation are of lesser extent, and in cases of "Rayleigh distillation," where the supply of sulfate decreases from sulfide production, which causes the sulfide $\delta^{34}S$ values to approach the sulfate $\delta^{34}S$ values as sulfate becomes progressively limited. Precipitation of pyrite only causes minor fractionation in marine settings (Böttcher, Smock and Cypionka, 1998), so pyrite $\delta^{34}S$ values can be considered reflective of sulfide $\delta^{34}S$ values.. Modern

seawater sulfate is typically appx. +20‰ $\delta^{34}S$ vs. the CDT standard, and the sulfide $\delta^{34}S$ values near the redox-cline tend to be appx. -20‰ due to the sulfur isotope fractionation via SRBs. Deeper in the sediment column, sulfate becomes more and more limited, since more sulfate has been consumed by SRBs, so the $\delta^{34}S$ values are susceptible to Rayleigh distillation. Sulfide $\delta^{34}S$ values approach +20‰ with progressive sediment depth (Rickard, 2012). In typical marine settings, pyrite $\delta^{34}S$ values reflect this trend, with the earliest framboids to form being isotopically much lighter than the later framboids (for example, Canfield, Raiswell and Bottrell, 1992). In fact, detrital framboids, both found in the sediment and recovered from the water column, closely match the $\delta^{34}S$ values of sulfide at the S-redox-cline, but not sulfide at the water-sediment interface, which adds credence to their formation in the S-redox-cline (Wilkin, Barnes and Brantley, 1996).

Detrital pyrite framboids are, of course, subject to Stokes' Law. The Wilkin model, as mentioned previously, suggests that detrital framboids grow in the S-redox-cline until they reach a particular size, and then settle out of the water column (considering that framboids aren't supposed to grow gradually, this should be incorrect, but since no existing model of framboid formation is satisfactory, I will suspend disbelief for now). Wilkin, Barnes and Brantley (1996) provide some analysis of framboid settling rates via Stokes' Law. A Stokes' Law calculation is dependent on a density calculation, which is tricky with framboids, since only some of their volume is occupied by microcrysts. As the authors correctly surmised, the density of the interstices of the framboid should be approximated as the same density of the surrounding fluid. For the density calculation, assumptions must be made for the shape of microcrysts and their packing arrangement. Wilkin, Barnes and Brantley (1996) assumed spheres packed in a cubic arrangement. This is a reasonable

assumption, but there is a great deal of variation with the packing of framboid microcrysts. Some framboids have such perfect packing that there is very little interstitial space (Fig. 2.2 c). On the other end of the spectrum, Rickard (1970) estimated the minimum volumetric concentration of pyrite in framboids to be 9%. This is based on a hypothetical framboid where the distance between the centres of microcrysts is four times greater than the radius of spherical microcrysts, with a cubic packing arrangement. I have never observed, nor seen figured, any framboid with such loosely-packed microcrysts, and I consider a 9% volume framboid to be impossible.

One of the ramifications of a loose-packed framboid, as Rickard (1970) discussed, is that if the interstices were filled with a low-density organic substance, the framboid could be buoyant. The potentially low density of framboids was relevant to Rickard's (1970) work because he postulated that framboids might be forming within oil droplets (emulsion), an idea which I have not seen addressed in later works. Since framboids in the rock record are commonly found with the interstices filled with organic carbon, they were believed to be related to the formation of framboids (Love, 1957). This idea was elaborated by Maclean et. al. (2008), with pyrite "framboids" forming within spheres of bacterial EPS (exopolysaccharides, read: mucous). The Maclean framboids formed within a 1.4 km deep borehole. These "framboids" consisted of irregularly-shaped, rounded microcrysts. More typical framboids were also found in the same environment. Maclean et al. (2008) suggested that the round-grained "microcrysts" represented a precursor to the equant, polyhedral microcrysts typical of framboids. The rounded grains would rapidly precipitate in an acicular habit, then mature to euhedral grains via slow overgrowth (Maclean et al, 2008). Of course, it would be very difficult for acicular pyrite to become euhedral via

overgrowth. There must be some other explanation for the presence of EPS in the interstices of a rounded-grained framboid (see section 2.1.5). While it may be possible for framboids to form within a globule of organic-carbon compounds, many modern framboids and all framboids synthesized under laboratory conditions form without organic carbon in the interstices. Today, most of the organic carbon found within ancient framboids is considered to be secondary (Rickard, 2012).

Another factor affecting the ultimate size of detrital framboids is salinity. Since density of the fluid is an important part of Stokes' Law, differences in salinity may impact the size of framboids that are deposited, and Wilkin and Arthur (1996) offered this phenomenon as an explanation as to why the size distribution varied in the sediment column (Perry and Pedersen, 1993). Testing this hypothesis is simple with Stokes' equation. To take one example, Wilkin and Arthur's (1996) GC59 core from the Black Sea has a median framboid diameter of ~4.6 µm in the uppermost sediment, whereas framboids sampled from 150 cm depth show a median diameter of ~3.6 µm. Assuming close-packed cubic arrangement of spherical microcrysts, and a Black Seawater density of 1.024, the settling rate of a 4.6 µm framboid is 0.12 mm/s. Then, we can calculate what density of Black Seawater would cause a 3.6 µm framboid to have a 0.12 mm/s settling rate. In this case, the density would actually need to be -1.49 g/cc, an absurd result. The density changes necessary to cause even small differences in settling velocities between framboids is too great to be plausible in the Black Sea.

As previously discussed, the greatest hurdle for pyrite precipitation is the kinetic barrier for nucleation, which is more easily overcome by nucleating on certain substances. This raises the question of nucleation sites in framboids. Perhaps they are nucleating within

the open water, but the nucleation would be greatly facilitated by some organic compound or iron monosulfide. Some credence to this hypothesis is that some pyrite framboids do appear to have something at the centre of their microcrysts. If the nucleation site of microcrysts could be ascertained, it may offer clues for the mechanism of pyrite framboid formation. Some microcrysts are hollow, though this is possibly due to the dissolution of a different mineral phase (for example, greigite, which is metastable) after having been broken open (Rickard, 2012).

The idea of pyrite framboid formation via an iron monosulfide precursor is the oldest hypothesis for pyrite framboid formation, from a paper published by Doss in 1912. It was initially suggested to be a result of hydrotroilite (at the time believed to be a hydrous combination of iron oxides, hydroxides and sulfides) converting to pyrite via an iron sulfide gel called "melnikovite." Unfortunately, later researchers were not consistently able to confirm the existence of melnikovite (Vallentyne, 1963). Since then, there has been a great deal of confusion about the properties and usage of the term "melnikovite," but it is most commonly used as an unofficial synonym of greigite in the Russian literature (Rickard, 2012).

2.1.5 Pyritized bacterial pseudoframboids

The interpretation of pyrite framboids as microfossils dates to a paper by Naumann in 1919, but is also described in a 1920 paper by Thiessen that was based on a 1919 meeting. Since the Thiessen paper, written in English, did not mention the Doss paper, which was in German, it is reasonable to think that the discovery was independent and virtually contemporaneous (Thiessen, 1920; Vallentyne, 1963). Thiessen's microfossil

interpretation was based on petrographic observations of modern peats. The peats contained coccoidal bacteria, as well as pyrite framboids. Both the bacteria and the framboids had similar size and shape. Whereas the bacteria exhibited a range of opacities, the framboids were opaque. This led Thiessen to the conclusion that the framboids were pyritized bacteria, and the various opacities of the bacteria showed a sequence of progressive pyritization (Thiessen, 1920). Pyrite does prefer precipitation on organic substances, including gram-positive bacteria due to the ability of their negatively charged external surfaces to attract metal cations (Ferris, Fyfe and Beveridge, 1987), so bacteria should be a favorable target for pyritization. Such a phenomenon would be similar to the "substrate microfabric" in phosphatization, where organisms can be preserved by the phosphatization of the microbial biofilm that is decaying it (Wilby and Briggs, 1997).

The interpretation of framboids as bacterial fossils was developed further by Love (1957), who suggested that the microcrysts were individual bacteria cells within a spherical colony. This interpretation was based on the dissolution of pyrite framboids from Carboniferous oil shales of Scotland in nitric acid, leaving behind an aggregate of hollow, organic carbon spheres (Love, 1957). The organic carbon associated with pyrite framboids is now considered to be secondary, due to their absence in modern framboids (Rickard, 2012). The status of framboids as potential bacterial fossils was disputed until Sweeny and Kaplan (1973) synthesized framboids abiotically, laying to rest a 54-year-long controversy…

…which was reawakened 29 years later by Schieber (2002a), who used a Transmission Electron Microscope (TEM) to identify carbonaceous bacterial fossils within a pyrite nodule. In addition to numerous other fossils, Scheiber (2002a) found a colony of

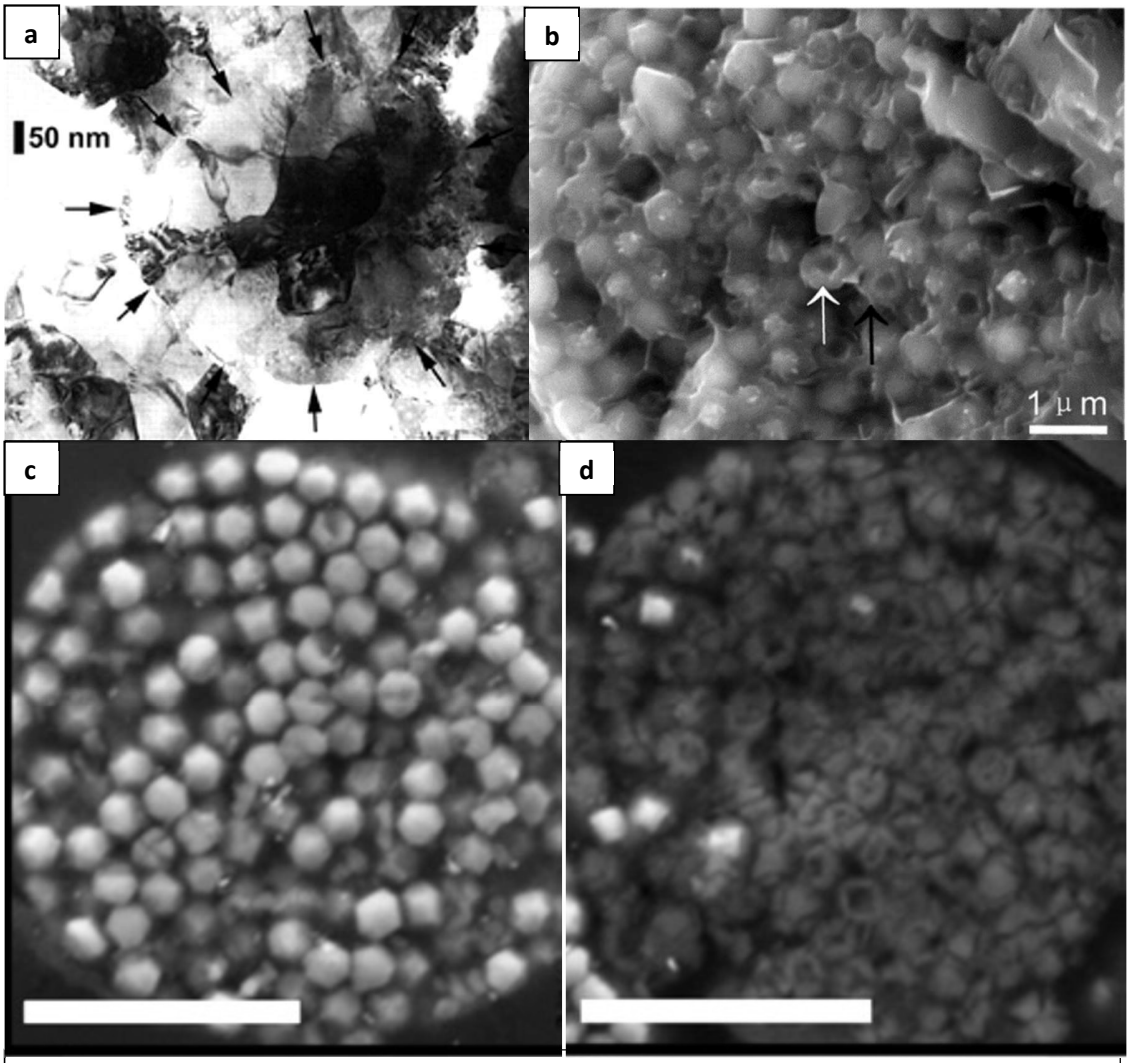

Figure 2.3 Framboids or pseudoframboids. (a) Transmission Electron Microscope (TEM) image of single, round microcryst of a "framboid" from the inside of a pyrite concretion from the Devonian. Note that it is comprised of several crystals. From Shieber, 2002a, used with permission. (b) A hollow-microcrysted framboid from the Broughton Formation, from Gong, 2008, used with permission. (c) Greigite framboid from methane seep near California (d) Pseudofossil formed by oxidation of greigite framboid near the same methane seep. Note irregular shape of some microcryst molds. From Bailey, et al., 2010, used with permission.

spherical bacterial fossils that closely resembled a pyrite framboid in size and arrangement. Scheiber (2002a) did not consider this to be a true framboid because the "microcrysts" were polycrystalline (Fig. 2.3 a), instead of being single crystals, like true framboidal microcrysts. Had the Scheiber (2002a) fossil been found outside of a pyrite nodule, it would be scarcely distinguishable from a true framboid. This raises the possibility that some

objects that were assumed to be pyrite framboids might actually be bacterial fossils. A method of distinguishing between ordinary framboids and pyritized bacterial colonies (termed here *bacterial pseudoframboids*) without resorting to TEM, which requires meticulous, destructive sample preparation, is desirable so that valuable bacterial fossils don't go unnoticed.

Gong et al. (2008) interpreted some hollow-microcrysted framboids as pyritized SRB colonies (Fig 2.3 b). Gong et al. (2008), however, claims that their framboids are morphologically distinct (esp. spherical microcrysts) and could have formed through different processes. Bailey et al. (2010) criticize the Gong interpretation based on similar structures that they found in a methane seep near California. They found greigite framboids that had been pseudomorphed as iron oxides (Fig. 2.3 c & d). The oxides formed a coating around the dissolving greigite microcrysts, and some became infilled by a distinct iron oxide growth. The resulting pseudomorphs had rounded edges, and only preserved flat crystal planes in a few places, such that they resembled bacterial colonies, like the Gong framboids. A crucial difference between the two is that, while the Bailey framboids were found to be composed of iron oxides (at% Fe=51, O=36 S=5.4; Fe= 50, O=36, S=2.7), the Gong framboids retained much of their sulfide (Fe=29, O=17 S=23; Fe=21, O=28, S=22), therefore must not have been altered in a similar way.

Although the Bailey framboids are not bacterial fossils, methane seep environments are known to produce pyritized bacterial fossils, including external molds of bacterial sheaths (Shapiro and Fricke, 2002). Spherical pyritized bacterial clusters have been recovered from a modern methane seep environment in the South China Sea. The individual bacteria in the clusters bear no resemblance to microcrysts, so their biogenicity

is plausible (Chen et al, 2005). Methane seeps that contain probable bacterial fossils with a strong resemblance to framboids include Chen et al, 2007 near Louisiana and Calvalazzi et al, 2012 from the Devonian of Morocco.

There are several other bacterial pseudoframboid candidates in the literature. Kremer and Kaźmierczak (2005) found some non-oxidized pyrite pseudoframboids with very rounded "microcrysts" in Silurian cherts from Poland. Tomescu, Rothwell and Honegger (2006) and Wilson and Taylor (2017) (from a Silurian sandstone in Virginia and an Ordovician microbial mat from Ohio, respectively) both discovered oxidized pseudoframboids arranged in linear features, like the cells in a bacterial filament.

It is important for geologists to be aware of potential bacterial fossils so that they are not overlooked. A system of criteria to distinguish between framboids and pseudoframboids would be useful. An examination of the literature suggests that there is already something of a consensus regarding the distinguishing features of framboids and pseudoframboids, though it is not fully described anywhere. The correct criteria is: (I) The pseudoframboid hypothesis is refuted when the microcrysts are polygonal (II) the pseudoframboid hypothesis is unlikely if there are alteration intermediates between unambiguous framboids and the framboids in question, as in Bailey, 2010 (III) the framboid/pseudoframboid status is uncertain when (1) the pyrite is pseudomorphed by oxides, but the original microcryst shape cannot be discerned or (2) the available data is insufficient to distinguish between the two, for instance, due to low resolution (IV) the framboid hypothesis is unlikely if (1) the pseudoframboids are arranged like a bacterium as in Tomescu, Rothwell and Honegger (2006) and Wilson and Taylor (2017) or (2) the microcrysts are of inconsistent (a) size or (b) shape (V) the framboid hypothesis is refuted

if the original microcrysts are visible, but they are (1) round or (2) polycrystalline. With this system of criteria, it seems certain that the Maclean et al. (2008) "framboids" are most likely bacterial pseudoframboids on the basis of their irregular, rounded microcrysts of inconsistent size and their primary pyrite composition (Satisfying criteria V1 and IV 2 a & b).

2.1.6 Concretionary pyrite

Acicular pyrite also occurs, encrusting surfaces or forming nodules. These occur in settings with sparse nucleation, but where supersaturation is sustained. Pyrite nodules can grow quite large in soft sediment, up to 10 cm in diameter, which Rickard (2012) estimates to have taken at least 10 years to grow.

In order to determine the distance from the surface of an organism that pyrite will form, some authors use mathematical models for diffusion partly borrowed from concretionary formation. There are many ways for concretions to form, but the two most important genetic categories: centrifugal and centripetal, a.k.a. excretions and incretions (Gardner, 1908), or even concentric and inverse-concentric (Cotroneo et al, 2016). In order to understand their causes, consider the following system of with two reactants: Reactant A (analogous to Fe^{2+}) is at a homogenous concentration throughout the system, but reactant B (analogous to sulfides) is generated at some location in the system. When A and B meet, they form the solid precipitate C (pyrite). The highest concentration of B will be right where B is generated, so it is easy to imagine that the initial precipitation of C will occur near the source of B, and that C will grow outward from that point. This is one way that centrifugal (away from center) concretions form. If reactant A has a fairly low concentration, then the

reaction with B will quickly remove all A from the vicinity. B continues to diffuse outward from its source, and A diffuses inward. This forms a "reaction front," a surface where A and B meet. Initially, the reaction front will expand outward, but this increases the surface area of the reaction front. Beyond a certain size, the production of B will be inadequate to supply the whole reaction front, and it will cease expanding outward. C precipitation will predominantly occur at this equilibrium state of the reaction front. The reaction front will ultimately define the outermost boundary of the concretion, and infilling can occur later. This is the process that produces centripetal (towards center) concretions. The radius of the reaction front can be calculated from the concentration of A, the rate of B generation and the permeability of the sediment.

A centripetal concretionary model is sometimes applied to exceptional fossil pyritization, even in fossils that are not contained within concretions. There are a few complications to applying such a concretionary model to pyrite formation, and fossil pyritization specifically. First, in order for fine details to be preserved through pyritization, the reaction front would need to be in very close vicinity to the organism, itself. In submillimetric proximity to the surface of an organism, the system can actually be simplified as a one-dimensional model. The corpse has an approximately flat surface with an extent much greater than the distance of the reaction, so every point on the surface of the corpse can have the same linear diffusion gradient as every other. In this system, sulfate diffuses inward to a corpse, where it is converted to sulfides. If ferrous iron is abundant, then it merely diffuses inward, but if only ferric iron is present, it must first be converted, either by bacteria or via a reaction with sulfides. The latter would keep the reaction front closer to the organism because it removes sulfide from the outer parts of the reaction before

even forming iron sulfides. Every different pyrite-producing pathway would take place approximately at the iron-sulfide reaction front, though there are more than twenty known sulfide species and several elemental sulfur species, each of which is pH and redox sensitive and can be part of pyrite formation. Of course, pyrite usually forms through an $FeS_{(aq)}$ intermediate, which would require a second reaction with S(0), potentially at a different part of the gradient. Solid phases complicate the problem further, since (1) solid iron oxides are an important source of dissolved iron, but will become locally depleted due to reaction with sulfides and (2) mackinawite may precipitate, effectively causing temporary storage of solid iron monosulfides, followed by a radical change in the local chemistry once they start to dissolve. Precipitation and diffusion of solid phases would also result in changes in porosity, affecting diffusion rates.

Of course, existing models of pyritization in published literature are much simpler than what's described above. A highly-successful, one-dimensional model of pyritization was published by Canfield and Raiswell (1991), using the Helfferich and Katchalsky (1970) generalized model of "interdiffusion with precipitation," which models a diffusion gradient between two reservoirs of set concentrations of reactants, which precipitate where they exceed saturation. The Helfferich and Katchalsky model is useful because it can predict the concentration of reactants and rate of precipitation at any point in the system, and at any time. There are a few limitations for applying Helfferich and Katchalsky to pyritization. Namely, (1) it cannot solve systems where intermediate reactions are necessary prior to precipitation, which leaves only the $Fe^{2+}+S_2^{2-}$ pyritization pathway (2) it assumes that the precipitate will precipitate at any supersaturation, and nucleate

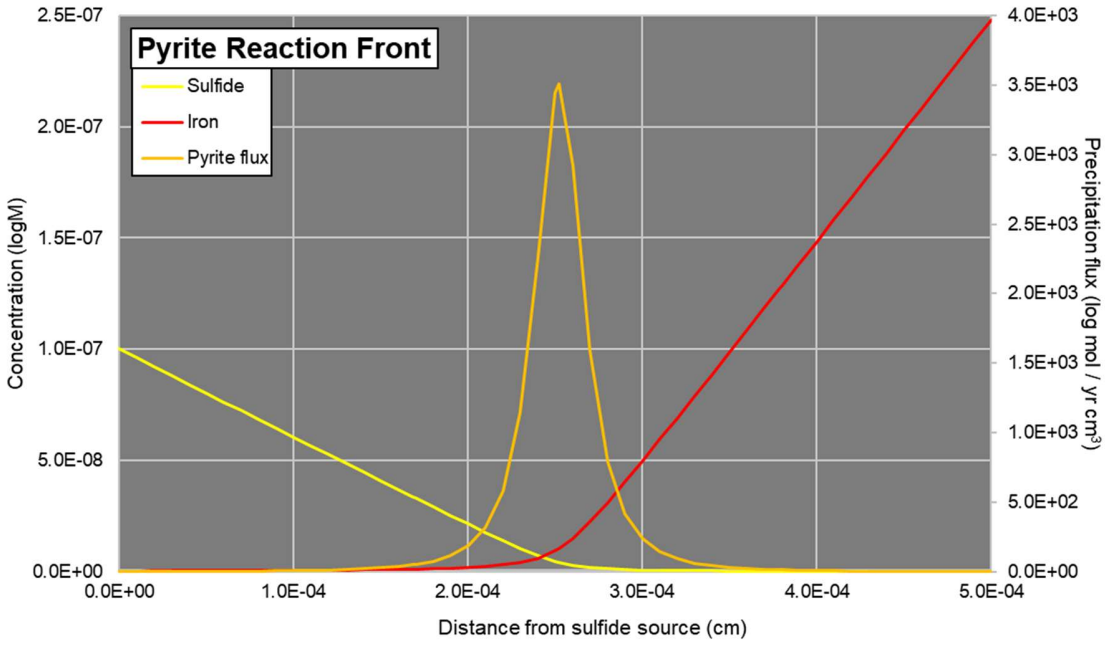

Figure 2.4 The Raiswell et al. (1993) model of pyritization, calculated for sulfide concentration 10^{-8} M, diffusion coefficient 376 cm^2/yr, iron concentration 10^{-4} M, diffusion coefficient 149 cm^2/yr, reaction equilibrium constant $10^{16.35}$ and sulfide source radius 1 cm. Note that this plot is calculated for the system at equilibrium. Initial pyritization is always favored at the sulfide source in this model.

anywhere. Canfield and Raiswell (1991) only applied the Helfferich and Katchalsky model to mackinawite.

Raiswell et al. (1993) developed a three-dimensional variant of the Helfferich and Katchalsky model specifically suited for pyritization of organic matter (Fig. 2.4). Instead of two infinite reservoirs, separated by a diffusion gradient, like in the Helfferich and Katchalsky model, the Raiswell model uses one inexhaustible reservoir of sulfide with finite, spherical dimensions, surrounded by an infinitely large infinite reservoir of iron, which is also the diffusion gradient. The spherical infinite reservoir is the organic carbon in this model. If the organic carbon produces sulfide at a particular rate, then the sulfide concentration next to the organic carbon can be estimated, and that sulfide concentration can be used for the spherical infinite reservoir. Applying their equations to pyritization systems, Raiswell et al. (1993) use the $Fe^{2+}+S^0+HS^- \rightarrow FeS_2+H^+$ pyritization pathway, but

only model concentrations of Fe^{2+} and HS^-. One interesting consequence of using this pathway is that it produces acidity, so the solubility product of the reaction (and, consequently, the precipitation flux) is pH dependent (though pH changes are not modeled). The Raiswell model retains the same pyrite-specific problems from the Helfferich and Katchalsky model, with regard to multiple reactions and nucleation. Raiswell et al. (1993) applied their model to the problem of framboidal pyrite formation by assuming that framboids were spheres of organic carbon, that were then replaced by pyrite. They found that for organic carbon spheres > ~50 μm, sulfide production would be so rapid that the reaction front would not remain close to the organic carbon sphere, unless iron concentrations were unusually high, and they posit this mechanism as a limiting factor for framboid size. Of course, this defies conventional explanations of pyrite framboid formation.

Regardless of the various complicating factors in pyritization reaction front, the concretionary model enables some specific predictions about conditions (Fig. 2.5) that would favor high-fidelity pyritization (by keeping the reaction front closer to the surface of the fossil). High iron concentrations would keep iron availability close to the surface of the fossil. High rate of decay would push the reaction front outward due to the increased supply of sulfides. Low sediment permeability would slow diffusion, thereby keeping the reaction front near the fossil and also slowing decay by limiting sulfate availability (Canfield and Raiswell, 1991). Low organic carbon concentrations in the sediment are also cited as important for the preservation of fine details, since that would cause production of sulfides, and, consequently, iron sulfides throughout the sediment, acting as an iron sink (Briggs, Bottrell and Raiswell, 1991; Briggs et al, 1996), but this is not necessarily true.

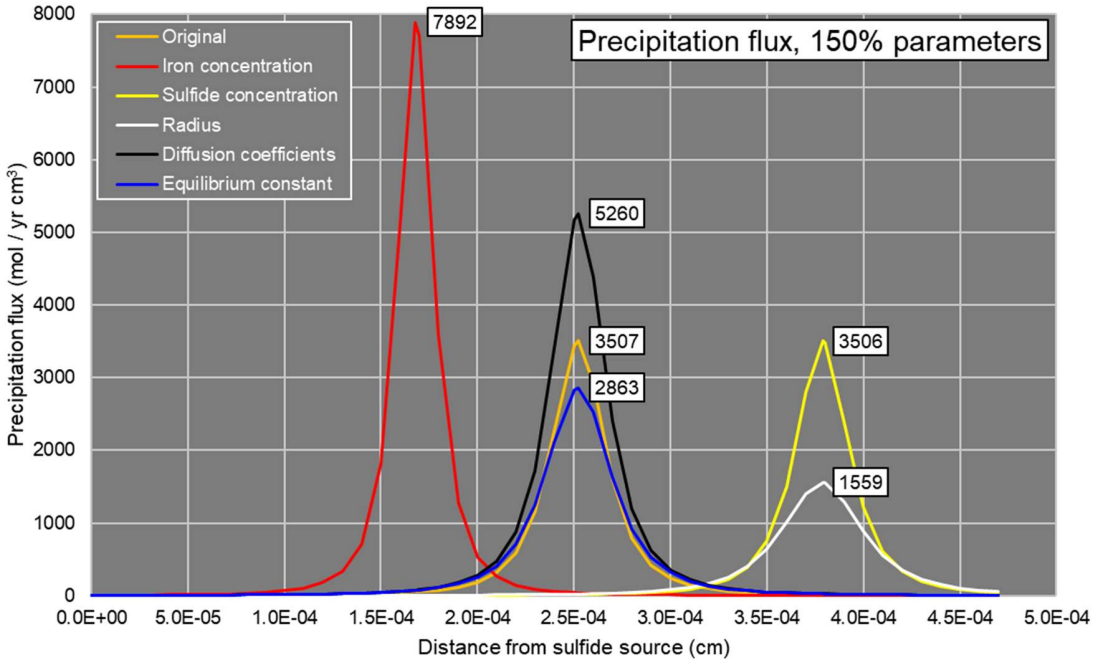

Figure 2.5 Precipitation flux calculated from the Raiswell et al. (1993) model, using the same parameters as fig. 4.5 (orange) or a specific parameter increased by 50% (other colors). Maximum precipitation fluxes are labelled for each.

Since pyrite requires such high supersaturation to nucleate, close proximity to the fossil would still have a higher sulfide concentration, and would still be the preferred location for pyrite production, even if there was sulfide produced from other sources. Precipitation of other iron sulfides, though, could still act as an iron sink, as described.

For preservation of fine details of a corpse, the reaction front should remain very close to the surface of the corpse, but in Beecher's trilobite beds, one of the best pyritization lagerstätte, the $\delta^{34}S$ values of pyrite from the body of trilobites is consistently lower than $\delta^{34}S$ values in the pyrite of the legs of each fossil. This is taken to mean that pyritization of the legs occurred later, when the effects of Rayleigh distillation had altered the sulfide $\delta^{34}S$ values (Briggs, Bottrell and Raiswell, 1991). Via this model, the sulfur isotopes could only be reflective of later timing on extremities if the body of the organism was the centre of decay and the reaction front extended centimeters away from the body, which would

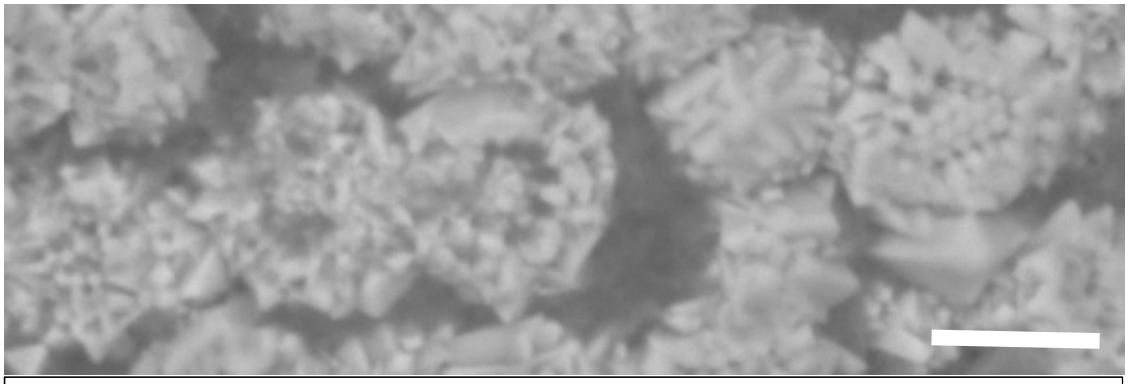

Figure 2.6 BSE texture of pyrite encrustation on trilobite eggs from the Beecher's trilobite beds lagerstätte. Note the framboidal texture and acicular overgrowth. For more information, see Hegna, Martin and Darroch, 2017. Image taken by D. R. Clark, used with permission from Thomas Hegna and D. R. Clark.

completely negate the submillimetric reaction front that was purported to be necessary for fine-scale preservation.

The pyrite growth in the Beechers' Trilobite Beds is not merely a result of encrustation during the decay stage. Microanalysis of textures on trilobite eggs and legs reveal what appears to be an acicular encrustation of pyrite (~2-15 μm in diameter), so extensive that it is almost a continuous coating (Hegna, Martin and Darroch, 2017; Fig 2.6). Some of these acicular features are broken, revealing pyrite framboids on the inside, which, though partially obscured, appear to be only a few microns in diameter at the most. There are also a few isolated euhedra. This indicates two periods of pyritization: (1) an initial period of decay-related pyrite framboid production, which produced a sparse distribution of small framboids across the surface of the sample, and (2) extensive overgrowth of the framboids via allochthonous sulfide. Images of the cephalon of a trilobite show a different texture entirely, and it is unclear whether this is a void-filling, encrustation or replacement texture.

2.1.7 Pervasive pyritization

Mass-balance issues cause problems many pyritization scenarios. Some pervasively pyritized fossils have soft-tissues or large cavities which are replaced by pyrite. The trouble is that any quantity of organic carbon is not capable of producing enough sulfide to replace its entire volume. Assuming a best-case scenario of homofermentive glucose reduction to lactate (Reddy et al, 2008) followed by complete SRB oxidation of lactate to carbon dioxide (Postgate, 1984), 2 mol glucose → 4 mol lactic acid → 6 mol sulfide → 3 mol pyrite. Due to the density difference between pyrite and glucose, the pyrite obviously takes up much less space than the original organic carbon. The beginnings of pervasive pyritization is decay, but there must be an outside source of sulfide to finish pyritization.

Another limitation in pyrite precipitation is availability of dissolved constituents. Sulfate is necessary for sulfate reduction to progress. For 1 g of pyrite, SRBs must reduce the quantity of sulfate contained within 600 mL of ordinary seawater (28 mM according to Eby, 2004). Diffusion through soft sediment can make this happen in relatively small timescales. For dissolved iron, this is a much more serious problem. That 1 g of pyrite would need the dissolved iron from 1.7 million litres of ordinary seawater (5 nM according to Rickard, 2012). The low concentration of dissolved iron represents a serious problem for the timescale necessary for diffusion. This problem is alleviated by the greater abundance of iron in sediment. Particles of iron minerals can go in and out of solution as a part of kinetic equilibrium, so if dissolved iron becomes incorporated in pyrite, this has little effect on the total iron concentration or its distribution. It doesn't take much typical

marine sediment to supply all the iron necessary for pyritization. Assuming 3 wt. % iron, a modest 15.5 grams of sediment is necessary—barely a handful.

Marine burrows are often pyrite-infilled, which is usually attributed to decay of the mucus in the walls of the burrow. Mucus is a colloidal mixture of polysaccharides and proteins, which is commonly used for its antimicrobial properties (Stabili et al, 2009; Naughton et al, 2014), but the mucus used to stabilize burrow walls, and facilitate transport through sediment is reportedly easily degraded by microbes (Scheiber, 2002b; Zorn, Gingras and Pemberton, 2010, see Fig. 2.7). Because mucus is mostly water, Scheiber (2002b) estimated that the sulfide from 50 cm^3 of decaying mucus would be sufficient to produce merely 1 cm^3 of pyrite. Even if the burrowing organism is rotting in its own burrow, it is an inconceivable prospect for a burrow to infill itself with its own SRB-produced sulfides. In pervasively pyritized burrows, it is common for pyrite framboids to be the first stage of mineralization, followed by centripetal burrow infill of pyrite. In some cases, the early framboids tend to have higher $\delta^{34}S$ values than later infill, a reversal of what is expected to occur via Rayleigh distillation. Virtasalo et al. (2010) explains this phenomenon by invoking changes in the source of the porewater. A similar trend was found

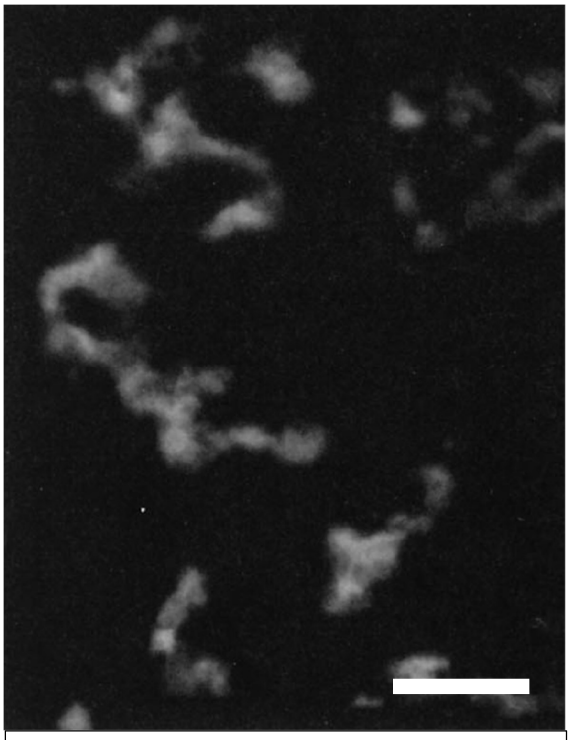

Fig. 2.7 X-radiograph of pyritized burrows of the Winnipeg Formation, likely mucus trails from mud-swimming polychaetes. Scale bar 1 cm. From Schieber, 2002b, used with permission from SEPM.

in one of the tube worm fossils studied in Schiffbauer et al. (2014), but with an alternate explanation. Initial pyritization would have occurred while decay was fairly rapid, causing sulfate limitation and Rayleigh distillation, but once nutrient supply becomes the limiting factor, sulfate limitation would cease, causing a drop in $\delta^{34}S$ values (Schiffbauer et al, 2014). In cases of large amounts of pyritization, some initial pyritization was the result of local decay, but the majority of pyrite growth must have occurred much later.

Supply of constituents is a difficulty for pyrite framboids, as well. Since pyrite framboids supposedly form rapidly, all of the constituents necessary for the formation of a framboid must be within quick access via diffusion, but by the numbers estimated above, a cubic close-packed pyrite framboid would require 3,000 times its own volume in sulfate-bearing seawater and 8.5 billion times its volume in iron-bearing seawater, or ~50 times its volume in marine sediment. If a framboid is considered the product of the decay of a small organic particle, like in Raiswell et al, 1993, it would require 7.5 times its own volume in organic carbon, too.

2.1.8 Late-stage diagenesis and weathering

Decay-related pyritization will commence after anoxic conditions develop around the organism, and will continue as long as there is digestible carbon available for SRBs to consume, or until sulfate or iron limitations force pyritization to cease. These ions can become limited through a reduction of sediment permeability, which typically results from sediment compaction and cementation. Sulfate can also become limited at depths where the diagenetic brines are sulfide-dominant. If the organism is converted to kerogen, the remaining carbon will become much more difficult for micoorganisms to process, and so

decay-related pyritization will cease. Post-decay pyritization can then commence, which is necessary in all cases of pervasive pyritization. If the availability of dissolved iron and sulfides from hydrothermal sources or from decay of other sources of organic carbon is sufficient, pyritization can continue, especially in areas where nucleation has already occurred (e.g. the fossil). Though post-decay pyritization can produce a large quantity of pyrite, it cannot pyritize a fossil unless some taphonomic pyrite had already nucleated. There is no limit to how long a fossil is subject to post-decay pyritization, provided available pore space.

Pyrite can be altered by oxidative weathering. Though it is a slow process, pyrite can become oxidized through a reaction with oxygen and water. Iron oxidizing bacteria can facilitate the oxidation of pyrite, some even releasing enzymes that oxidize iron. The oxidation of one mole of pyrite produces two moles of acidity, and a Fe^{2+} ion. Oxygen, of course, converts Fe^{2+} to Fe^{3+}. The Fe^{3+} can then oxidize pyrite via a reaction that is much quicker than the reaction between pyrite and oxygen, but results in an astonishing 16 moles of acidity per mole pyrite. The Fe^{3+} which is produced through pyrite oxidation is ultimately converted to iron hydroxides, producing an additional two moles of acidity per mole pyrite (Faure, 1998). This is a common form of "acid mine drainage," which famously produced a record-setting pH of -3.6 in the Iron Mountain Superfund site in California (Nordstrom and Alpers, 1999). The iron oxides/hydroxides left behind by pyrite oxidation sometimes retain very fine detail of pyrite crystallography. This is especially evident in pyrite framboids which have been oxidized, yet preserve the original shape of the microcrysts (Rickard, 2012). Oxidative weathering like this is common in terrestrial settings post-uplift, in contact with oxic groundwater or meteoric water in the vadose zone,

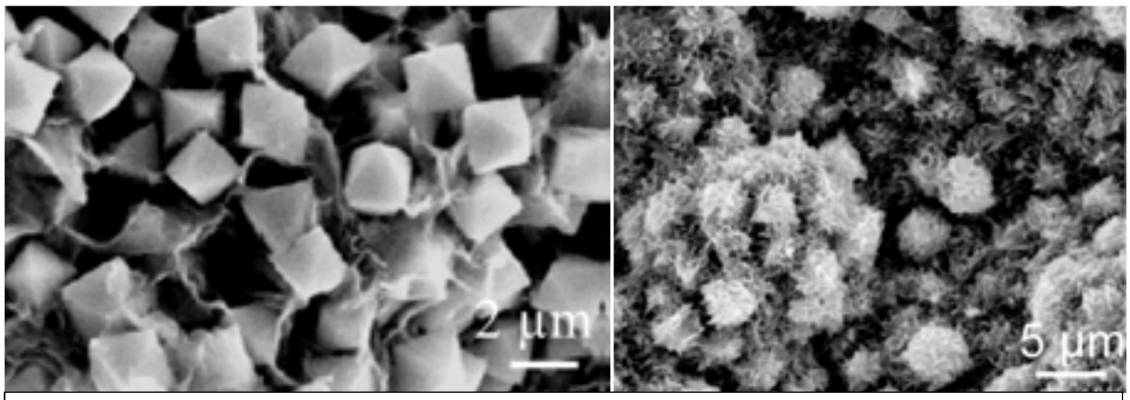

Fig. 2.8 Fossil-associated pyrite euhedra before (left) and after (right) oxidative alteration to Fe-smectites. From (Gaudin et al., [2005, Figures 4 a and e]). Reproduced with kind permission of The Clay Minerals Society, publisher of *Clays and Clay Minerals*.

but can also occur in marine settings in early diagenesis. In some cases of pyritization, the reducing conditions produced by decay are extremely localized. Once decay and pyritization ceases, oxic waters can infiltrate and oxidize the pyrite (Gaudin et al, 2005, see Fig. 2.8).

2.2. Processes of aluminosilicification

The role of clay minerals in BST preservation is hotly contested. First, the source of the clay minerals that are associated with BST fossils is arguably detrital, taphonomic or later diagenetic. The role of clay minerals in BST preservation is also contested, perhaps serving in a templating capacity, or improving kerogenization by inhibiting decay. The question of aluminosilicification is further compounded by the difficulty in identifying extremely small quantities of clay minerals, the numerous drivers of clay compositional alteration, and the rather minute quantity of clays produced in aluminosilicification experiments.

Clay minerals have a layered crystal structure, which alternates between layers of silica tetrahedra and aluminum or magnesium hydroxide octahedral layers. “Two-layered

clays" are simply an alternation between the tetrahedral and octahedral layers. "Three-layered clays" consist of one octahedral layer sandwiched between two tetrahedral layers. The adjacent tetrahedral layers in a three-layer clay do not form molecular bonds. The tetrahedral layers have a net negative charge, and adsorb cations and water molecules into the space between the tetrahedral layers (the interlayers). These positively charged ions are the force that holds three-layered clays together. Calcium, sodium and magnesium are common cations in the interlayer, and, since they aren't truly bonded, can be readily substituted by other ions. Potassium is not readily substituted because it is small enough to fit neatly between the silica tetrahedra. Larger ions open space between the clay layers, allowing for ion interchange. The silicon and aluminum in the tetrahedral and octahedral layers are also susceptible to substitution, but not as readily as in the interlayers. The silicon (IV) in the tetrahedral layers can be substituted with aluminum (III). The aluminum (III) in the octahedral layers can be substituted with many different ions with a +1 to +3 charge, commonly Fe (II) and (III), and Mg (II). Note that many of the substitutions in the octahedral and tetrahedral layers cause a net decrease in the charge of the clay mineral. This charge imbalance must be compensated by cations in the interlayers (Faure, 1998).

2.2.1 Detrital clays

There are many properties of clay minerals which have been proposed to have a positive effect on the preservation of organic tissues. Some of these properties are likely to be as effective for detrital clays as authigenic ones. For instance, detrital clay minerals are very small, and consequently are effective at decreasing the rate of diffusion around an organism, thus slowing decay. Likewise, growth of clays on an organisms' surface would

disrupt diffusion. Enzymes used in microbial degradation and in autolysis can adsorb to clay particles, or even be denatured, rendering them ineffective. Proteins, too, can adsorb to clay particles, which prevents them from breaking down. Three-layer clays may be more effective for adsorbing proteins, due to the extra space in their interlayers (Butterfield, 1996). Clays may also enhance preservation of organics by facilitating tanning, which causes some organic molecules to become cross-linked (Wilson and Butterfield, 2014).

In addition to the clays with which an organism is buried, clay particles in suspension often adhere to organic tissues. It is common for biological tissues to carry a negative charge on the cell membrane, and clay particles inherently have negatively-charged surfaces as a result of their structure, so one would expect them to repel each other. Instead, cations are attracted to both biological surfaces and clay particles, so when they adsorb to one, they adhere to the other (Butterfield, 1996; Petrovich, 2001). The cations between a clay particle and an organic tissue hold them together for the same reason the cations in a clay interlayer hold the layers together. To see evidence of this phenomenon, one merely needs to observe vegetation within a pond, or even leaves in a puddle. A fluffy, grey coating is commonly evident, and this is clay particles which have adhered to the vegetable matter due to electrostatic attraction. Cations are more abundant in saline fluids, so the effect is greater in marine or saline lacustrine settings, but this also causes clay particles to adhere together, which can cause them to rain out of suspension, a process known as flocculation (Sutherland et al, 2014). Petrovich (2001) speculated that interactions between detrital clay particles and organic substrates in a way that can improve the preservation potential of soft tissues would be a highly unlikely phenomenon, but it has been demonstrated experimentally (Wilson and Butterfield, 2014).

2.2.2 Aluminosilicate weathering

Clay minerals can be reactive at all stages of diagenesis. Clay minerals that precipitate from dissolved aluminum and silica (authigenic clays) have been suggested as a potential driver of BST preservation. They should have similar properties to detrital clays, and, consequently, the same effects on fossil preservation (Orr, Briggs and Kearns, 1998). There are numerous natural sources for dissolved silica and aluminum. Chemical weathering of continental rock is the most obvious source for both. After oxygen, silicon and aluminum (respectively) are the second and third most abundant elements in the Earth's crust. Though the most silicate-rich and aluminum-rich minerals (quartz and gibbsite) are nigh-insoluble in surficial waters, other aluminosilicate minerals readily undergo chemical weathering in surficial environments. Some silicates, like olivine (Mg_2SiO_4) will undergo congruent dissolution, reacting with acidity to form silicic acid (H_4SiO_4), but aluminosilicates, like the feldspars, typically leave solid products behind (that is, incongruent dissolution). The solid products are somewhat dependent on the conditions of the alteration, and can undergo a series of different reactions. For instance, in cases where the fluid has low silicic acid concentrations (e.g. rainwater, modern seawater), the following reaction will occur: $NaAlSi_3O_8 + H^+ + 7H_2O \rightarrow Al(OH)_3 + 3H_2SiO_4 + Na^+$, leaving gibbsite as the solid product, but if the solution has a higher concentration of silicic acid, then instead $2NaAlSi_3O_8 + 2H^+ + 9H_2O \rightarrow Al_2Si_2O_5(OH)_4 + 4H_4SiO_4 + 2Na^+$ will occur, leaving kaolinite as the solid product. Similar reactions occur hydrothermally at mid-ocean ridges, the other main source of silicic acid (Eby, 2004).

The concentrations of silicic acid and dissolved aluminum remain very low in surface waters. Partly, this is due to the low solubility of these constituents at normal pHs

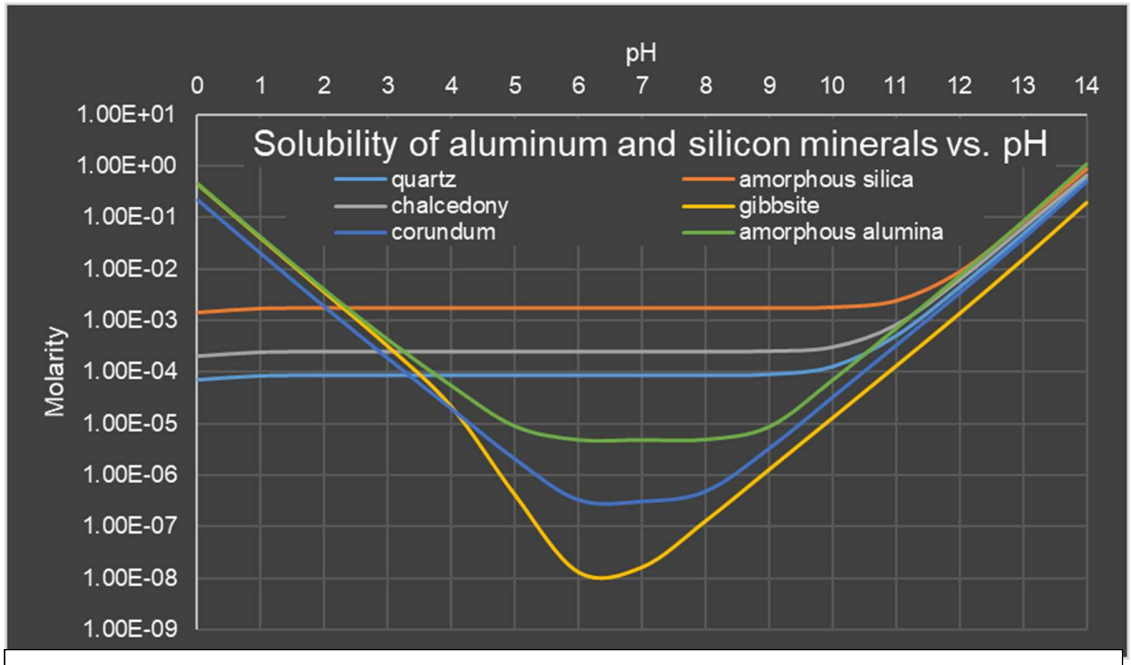

Fig. 2.9 Solubility of various aluminum and silicon minerals when exposed to fluids of a range of pH values. Calculated with PHREEQC at 20°C.

and temperatures (Fig. 2.9). One might expect concentrations of silicon to increase in marine settings, due to evaporative concentration of ions, but silicic acid is scavenged by organisms like diatoms, radiolarians and sponges to form opaline silica for use as structural elements, resulting in a net loss of 6 billion tons of silica per year (Iler, 1979). This produces a circumstance where silicic acid concentrations are actually lower in marine settings than in rivers (6.5 and 2.5 parts per million, respectively, from Faure, 1998). In the early Cambrian and the Precambrian, biological consumption of silicate was negligible, so silicate was commonly supersaturated (Pufahl, 2010). Volcanic ash is very effective at generating dissolved silica and alumina, not only because it is a fine powder of alumiosilicic glass, but also because the weathering reaction increases pH, conveniently increasing solubility of silica and alumina (Ballhaus et al., 2012).

Silicic acid is polyprotic, but has a low tendency to dissociate under natural pH conditions (<9). It most commonly exists as H_4SiO_4, “monosilicic” or “orthosilicic” acid,

but due to its neutral charge, it can polymerize, forming polysilicic acids. When these silicic acid polymers exceed a certain size (usually around 50 angstroms), they become stable colloidal particles. These silica colloids are a common form of suspended silica under conditions of silicic acid saturation (Iler, 1979).

Aluminum concentrations are also much lower in marine settings than in rivers ($5*10^{-2}$ and $8*10^{-4}$ parts per million, from Faure, 1998), likely because aluminum is "scavenged" from the water, that is, consumed by organisms as a nutrient or adsorbed to the surfaces of particles like sedimentary grains or organic compounds (Andrews, et al, 2005). There is no evidence for marine aluminum concentrations ever being much different.

2.2.3 Clay precipitation

Dissolved aluminum and silicon can precipitate to form authigenic clays (Fig. 2.10). In some environments, authigenic clays are so common that they form characteristic sedimentary facies. The high iron content typical in these clays imparts them with a green coloration, so the term for authigenic iron clay precipitation in sediment is termed *verdissement*, French for turning green. Oolitic ironstone facies are a form of oolite where the ooids are at least partially comprised of a green ferrous clay mineral, the original identity of which was likely berthierine or chamosite, but is commonly metamorphosed to other chlorites. One difficulty of the study of oolitic ironstone facies is the absence of any modern analogues. Ooids are essentially concentric concretions that precipitate from a fluid, but exhibit little intergrowth. Thus, they usually form chemically supersaturated environments where the ooids are jostled around enough to prevent intergrowth. Ooids can

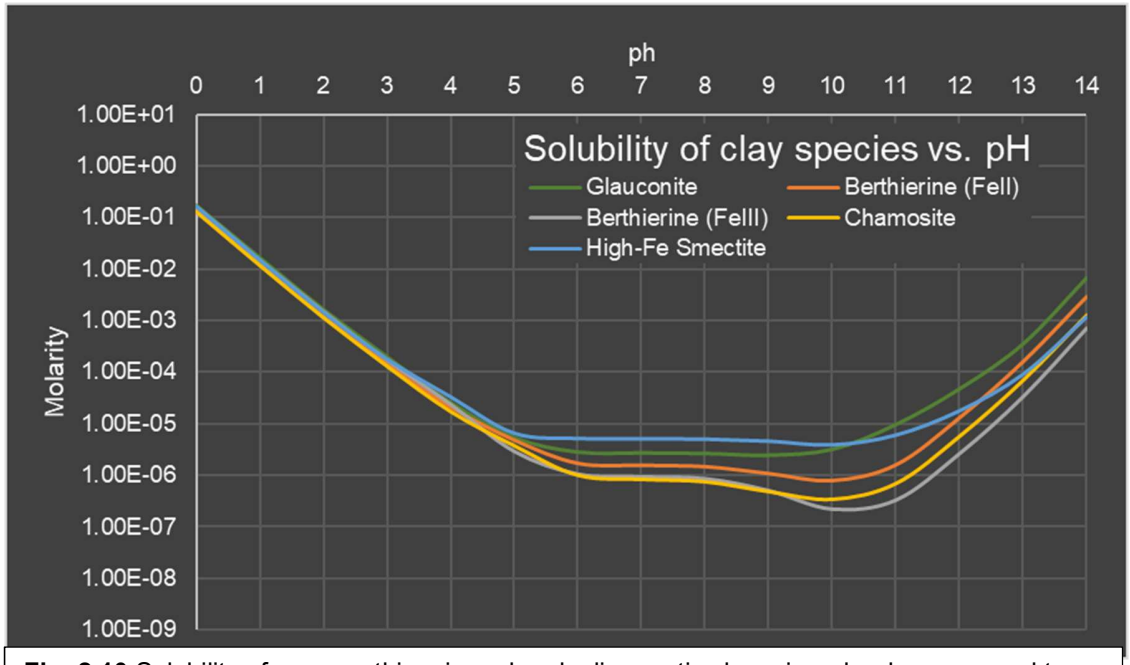

Fig. 2.10 Solubility of some authigenic and early diagenetic clay minerals when exposed to fluids of a range of pH values. Calculated with PHREEQC at 20°C.

be formed by many different minerals, including clays, iron oxides and (most commonly) calcite. The difficulty is that settings that form ooids are generally high energy, oxidizing environments, which would preclude the presence of dissolved ferrous iron. This seeming paradox can be resolved by considering the clays to have replaced the primary mineral composition, by suggesting that the environment may have fluctuated between a high-energy oxidizing environment and a quiescent reducing environment, or by suggesting that ooids can form in reducing environments. There is some credibility for the replacement reaction, since calcitic shelly fossils are often replaced by ferrous clays in oolitic ironstones, but the ooids retain such good interior structure that they are not likely replaced. Since ironstone ooids often contain an alternating pattern of goethite (a ferric iron oxide) and clays, it seems most likely that there were redox fluctuations in the environment, with ferric iron precipitating in the high-energy, oxidizing phase, and clays either precipitating on or forming an alteration rind on the ooid in the reducing phase (Odin, et al., 1988).

Verdine facies are characterized by sand-sized sediment where berthierine, chamosite and phyllite precipitate in nearshore envrionments. Reducing conditions in the sediment are not necessary for the *verdissement* in verdine facies. It is common for shells to become infilled with clay minerals in these environments, but when the shells dissolve, the exterior of the green clay cast alters to a reddish goethite (iron oxide), indicating that the pore waters are still oxidizing, and the reducing microenvironment within the shells facilitates the *verdissement*. Other substrates for green clays in verdine environments include fecal pellets, and biotite flakes. Due to the scarce availability of iron in typical seawater, verdine facies are only known in shallow water near river deltas and volcanic rock. (Odin and Gupta, 1988).

Glaucony facies are caused by a *verdissement* of sediment at greater water depths (>~60 m) but usually within the first centimeter of sediment. It progresses first by precipitation of glauconite within a porous substrate or particle. Later, other sediment grains may dissolve, giving more room for glauconite precipitation. Glauconitization is facilitated by grains remaining on or near the surface of the sediment for long periods of time. The water is not necessarily enriched in iron, but strong ocean currents can improve the exposure of sediment grains to dissolved iron. Glauconization usually occurs near the boundary between oxidizing and reducing conditions. Glaucony facies are especially common during a marine transgression (sea level rise). Normally, settings that accumulate large grains also have rapid sedimentation rates, but during a transgression, settings with coarse sediment may be cut off from sediment supply, allowing glauconitization to occur. A regression (sea level fall) can have the opposite effect, since it exposes glauconite to oxidizing conditions, converting it to goethite. Glaucony facies are often interbedded with

phosphorites, since they can form in similar conditions (Odin and Fullagar, 1988). Iron-rich, green smectites have been observed forming under similar conditions in very deep-water environments (Giresse and Wiewióra, 2001), and it is possible that they may convert to glauconite in diagenesis (Gaudin et al, 2005). In at least one tropical, carbonate, deep-water setting, Fe-smectites formed via replacement of pervasively pyritized burrows. The burrows had become pyritized in the reducing local conditions brought on by the decay of organic carbon, but the pyrite began to dissolve once oxidizing conditions resumed, resulting in the precipitation of iron clays (Gaudin et al, 2005)

Iron-rich green clays are, of course, not the only clays which can precipitate authigenically in marine sediments, but they have a special significance due to the iron-enrichment of many BST fossils. Other authigenic clay minerals are not as well-known for BST association, but are still informative for how clay minerals behave in sedimentary environments. For instance, authigenic smectite lath overgrowths on pre-existing smectites have been observed in many sedimentary envirionments (potentially related to alteration of the original smectites), leading to estimates of growth rates of between a few cm/kyr and 20 cm/kyr (Deconinck and Chamley, 1995). Lath-shaped crystals are a result of the tendency of sheet-silicates to preferentially grow along sheets, rather than orthogonal to the sheets. Thus, if clays nucleate on a surface in many random orientations, those crystals with sheets parallel to a surface will soon run into other crystals and stop growing, whereas those oriented perpendicular to the surface can grow indefinitely (Petrovich, 2001). In at least some basins, the overgrowths have higher iron content than the original smectites. Volcanogenic ash particles have also been altered to smectites in similar environments (Deconinck and Chamley, 1995).

Clays can also form and be altered during diagenesis. Chlorite is a common diagenetic mineral, which forms at a minimum temperature of 150° C, and is sometimes interstratified with smectite and vermiculite. At temperatures above 120° C, kaolinite can react with feldspar to form "hairy" illite, or can convert to dickite. Diagenetic processes can vary between basins, not only due to sediment composition, but also the temperature and composition of the fluids that migrate through the pore spaces, which vary with depth (Środoń, 1999).

2.2.4 Bacterial aluminosilicification

One potential mechanism that may facilitate authigenic clay mineralization on organic tissues is heavy-metal adsorption (Petrovich, 2001). One important effect of the adsorption of heavy metals to bacterial cell walls is the inhibition of autolytic decay, a pronounced effect for iron, copper and zinc (Beveridge et al, 1983). This effect is attributed to the metal ions complexing with sites that would normally be attacked by autolytic enzymes, enabling the cell wall to remain intact for long enough to become mineralized (Ferris, Fyfe and Beveridge, 1988). Silica, being an anion, would not normally associate with negatively-charged organic surfaces, but the adsorbed metal cations can theoretically form a "bridge," allowing silicate to complex with them, eventually leading to the precipitation of silicate minerals (Mera and Beveridge, 1993), but experimental results show that high iron concentrations actually inhibit silicification rates, yet still have a net positive impact on taphonomic fidelity due to its disruption of autolysis (Ferris, Fyfe and Beveridge, 1988). This phenomenon is best-known in bacteria, especially species of *Bacillus* (Beveridge et al, 1983), largely through complexation with teichoic acids and

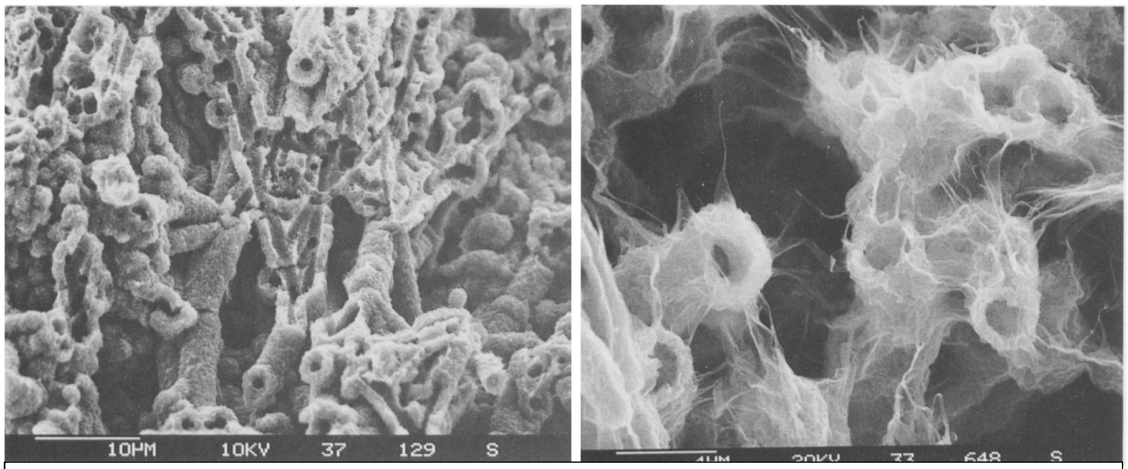

Fig. 2.11 nontronite molds of iron-reducing bacteria, formed at a mid-ocean ridge. From (Kohler, Singer and Stoffers, 1994 [Figures 1 c and e]). Reproduced with kind permission of The Clay Minerals Society, publisher of *Clays and Clay Minerals*.

peptidoglycan (Beveridge and Murray, 1980), which are external features for gram-positive bacteria only. The metal ions often form crystals of sulfides or clumps of oxides, but also form "(Fe, Al)-silicate phases," that evolve from (1) metastable iron and aluminum hydroxides that cannot convert to stable forms due to interaction with orthosilicate ions to (2) a gel-like accumulation of amorphous iron and aluminum silicate hydrates, which progressively becomes stratified into aluminum and iron layers to (3) a limonitic clay mineral like chamosite (Ferris, Fyfe and Beveridge, 1987). A similar process produces spectacular Fe-smectite molds of sheath-forming bacterial filaments in mid-ocean ridge microbial mats (Kohler, Singer and Stoffers, 1994; Fig. 2.11).

2.2.5 Silicification

The process of silica precipitation is pertinent to bacterial aluminosilicification due to its role in forming the alternating layers of the precursor to clay minerals. Silicification is a well-documented process which produced fantastic Precambrian microbial fossils in

lagerstätten like the Bitter Springs Formation (Schopf, 1968), Gunflint Chert (Barghoorn and Tyler, 1965) and the 3.4 Ma Strelley Pool Formation (Wacey et al, 2011).

The most stable and least soluble SiO_2 mineral at low temperatures is quartz, yet there are kinetic factors that inhibit the direct precipitation of quartz from a fluid. Silica dissolves via hydrolysis, producing orthosilicic acid, H_4SiO_4, in which the silicon atom is completely surrounded by hydroxyl groups. Thus, the growth of a quartz crystal in a solution requires a dehydration reaction. Complicating matters further, orthosilicic acid adsorbs to the surface of quartz particles, thereby inhibiting crystal growth. The same adsorbtion phenomenon inhibits the dissolution of quartz, resulting in experimental solubilities (at neutral pH) as low as 6 ppm. Curiously, this results in a phenomenon where higher concentrations of dissolved silica *decrease* the rate of growth for quartz crystals. This limitation can be overcome by producing fresh surfaces of quartz, for instance, by pulverizing quartz within the fluid. This method yields the true solubility of quartz of 70 ppm: nearly as soluble as amorphous silica (Iler, 1979).

The more usual method for silica precipitation is via the polymerization of orthosilicic acid to form polysilicic acids. While polymerization can occur for H_4SiO_4, the electrostatic repulsion of $H_3SiO_4^-$ makes polymerization unfeasible. This makes silica precipitation unfeasible in basic fluids (Iler, 1979). Polymerization is also uncommon at concentrations lower than 2 mM. Beyond a certain size (usu >50 Å in diameter), the silica polymers are so large that they become increasingly stable, and are considered colloids (Iler, 1979). Precipitation of amorphous silica occurs via a "gelling" process, as silicic acids and colloids continue to combine until they form a gel. This can occur in minutes at pH 6-9, or on the order of 1 day at pH 3 (Konhauser, 2004). Silica gel then undergoes a

dehydration reaction to form amorphous silica, which can eventually crystallize to chalcedony (Iler, 1979).

Microbes are favorable substrates for silicification. Part of this is the tendency for microbial metabolisms to acidify their environments, thereby reducing silica solubility, forcing some silica out of solution (Butts, 2014). Colloidal silica is more reactive with organic substrates than silicic acid is, so are a better mechanism for silica association (Konhauser, 2004). Precipitation can also begin with silicic acid association. Microbes and other forms of organic matter are commonly covered in hydroxyl groups, which are effective for binding silicic acids, essentially nucleating amorphous silica (Butts, 2014). Silica association is inhibited at higher pH because the negatively-charged $H^3SiO_4^-$ repels organic surfaces, but can still occur via a cation bridge (Amores and Warren, 2007), *á la* microbial aluminosilicification (Mera and Beveridge, 1993). Silicification of microbes can occur *in vivo*. Cells have been cultured in silicification environments, and have developed silica crusts 5 μm, without any apparent detriment to the cell's functions. The experimenters speculate that the silicification serves a practical purpose to the microbe, such as (1) preventing cytoplasmic mineralization by providing a more favorable site of silicification (2) filtering out colloidal silica (3) enhancing the cohesion of stromatolites or (4) protecting the cell from ultraviolet radiation, which is a serious hazard for cyanobacteria. It also provides a useful function to microbial fossilization, since it can preserve an organism prior to its death and autolysis (Phoenix, 2000).

Macroorganisms also silicify, most notably plants. Silicification of wood is well-understood, partly due to its industrial applications. People have been purposely silicifying wood since the 16th century, by dehydrating a beer cask. The siliceous phytoliths in grains

partially dissolve and infiltrate the wood during the brewing process. The silicification from this process is so thorough that the resulting wood is reportedly suitable for use as whetstone or flintstone (Butts, 2014). Wood is an acidic environment, and so is great for silicification (Ballhaus et al, 2012). Cellular permineralization of wood requires intracellular silicification. Colloidal silica may not be useful in this process, since it would have difficulty entering the cell (Butts, 2014).

Silicification of macroorganisms may also be responsible for "death-mask" Ediacaran preservation, almost exclusive to Ediacaran microbial mats, which consists of the top or bottom surface of an organism being preserved as a mould. It has been unclear whether pyrite, silica, or clay minerals have been responsible for death-mask preservation (Gehling, 1999). Recent evidence of early silica cementation provides support for silica death-masks. Silica precipitation would be favorable in these Ediacaran matgrounds because Precambrian marine silica concentrations were higher (Tarhan et al., 2016). In some death-mask localities, there is abundant volcanic ash ("Conception-style" preservation), which could provide a source of silica (Kenchington and Wilby, 2014; Ballhaus et al., 2012)

2.2.6 Burgess-Shale-type aluminosilicification

Petrovich (2001) proposed that dissolved iron could adsorb to chitin in the same way that it does to bacterial cell walls, thus preventing chitinase enzymes from being able to damage the chitin (as an example for structural biopolymers in general), but this is an as-yet unproven phenomenon. Iron is noted as being able to improve the preservation potential of collagen, but this is known to be accomplished via a tanning process that

improves cross-linking, but Petrovich theorized that the inhibition of enzymes would also occur.

Fossil evidence of a relationship between Burgess Shale fossils and authigenic clay minerals was proposed by Orr, Briggs and Kearns, 1998. Elemental maps generated from energy-dispersive X-ray spectroscopy demonstrated a clear difference between the composition of Burgess Shale fossils and their host rock other than carbon composition. Not only was a fossil/rock difference present, but different anatomical features displayed different compositions. In *Marrella*, a chitinous arthropod, the exoskeleton exhibited high silica, but the gut showed high aluminum, potassium and carbon. *Alalcomenaeus*, another arthropod, showed differences in composition between the eyes, cephalon, segments and gut wall. These anatomically-specific compositions must be reflective of initial tissue selectivity (Orr, Briggs, Kearns, 1998). An alternate explanation for the compositional differences is metamorphic. Butterfield, Balthasar and Wilson (2007) suggested that the differential composition between the *Marella* gut and exoskeleton was a result of clay replacement occurring at different stages of diagenesis. Since labile tissues volatilize at lower temperatures than recalcitrant tissues, labile tissues will be replaced by clay minerals from relatively early diagenesis, and recalcitrant tissues will be replaced by late-diagenetic clays.

To answer the question of Burgess Shale aluminosilicification, Petrovich (2001) proposed a theory of chlorite replacement of chitin in *Olenoides* (a trilobite) from the Burgess Shale, in which iron-rich clay minerals (namely the chlorite berthierine or the smectite ferroan saponate) precipitated upon the chitin and filled the void space while it decayed. The platy crystals infilled the entire void space, reminiscent of the lath-shaped

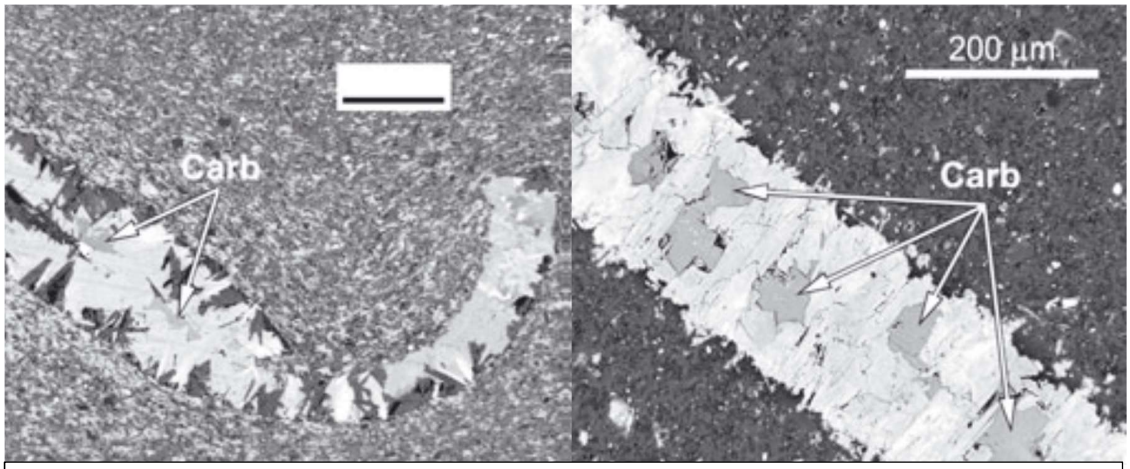

Fig. 2.12 BSE images of thin sections from the Burgess Shale. Left: An Olenoides trilobite from the Burgess Shale in cross section, showing chlorite infill (bright material) and grains of calcium carbonate. Scale bar = 200 µm Right: A Burgess Shale chlorite veinlet (bright) and grains of calcium carbonate. From Butterfield, Balthasar and Wilson, 2007, used pending permission.

clay overgrowths which result from randomly oriented nucleation of clay minerals. The crystals are considered to have originated as iron ions adsorbed to the chitin surface, which prompted nucleation of the clay minerals. Then the chitin began to decay, and the associated calcite began to dissolve, indicating that the iron and clay precipitation did not successfully protect the chitin from enzymatic degradation. Meanwhile, the clay nuclei (which remained in their initial position) began to grow inward from all sides, without running into remnants of the exoskeleton. Eventually the whole exoskeleton was replaced by clays, which were later replaced by chlorite without altering their original texture (Petrovich, 2001).

The alternate hypothesis that the chlorite nucleated on the walls of the void left behind by the decay (or volumetric reduction due to kerogenization) of the exoskeleton is not addressed in Petrovich's 2001 paper, but was suggested by later authors (Butterfield, Balthasar and Wilson, 2007), who noticed very similar textures and compositions between the *Olenoides* fossil and the abundant veinlets which permeate the Burgess Shale (Fig. 2.12). Their interpretation suggested that both the veinlets and fossil were originally

calcitic, and were susceptible to identical chlorite replacement. Support for this hypothesis includes calcite particles which are lodged within the *Olenoides* exoskeletons and veinlets, presumed to be remnants of the original calcite (Butterfield, Balthasar and Wilson, 2007; Fig. 2.12).

Preservation of macrofossils may be possible via aluminosilicification of bacteria. In phosphatization pathway of exceptional fossil preservation, macrofossils are sometimes preserved via the phosphatization of the bacteria on the surface of the corpse, producing what is known as a "microbial microfabric" (Wilby and Briggs, 1997). This phenomenon has been demonstrated by Martin, Briggs and Parkes (2004) in an experiment where kaolinite particles (and quartz) associated only with decaying invertebrate eggs that were inoculated with bacteria. Presumably the bacterial cell walls were a more favorable substrate for detrital clay association. It is possible that authigenic aluminosilicification of bacteria could produce a similar effect. This phenomenon was recently tested by Locatelli et al. (2017), in a decay experiment using leaves in closed containers. EDS analysis of the resulting leaves revealed elevated concentrations of aluminum, silicon and clay cations on the microbial biofilms on the leaves, indicating that bacterial decay might play a role in the aluminosilicification of macrofossils (Locatelli et al., 2017). Even if the biofilm-associated aluminosilicates do not result in greater carbon preservation, it may still capture the fossil as a region of differential clay composition.

Ultimately, the difficulty of assessing the role of authigenic aluminosilicification in BST taphonomy is a result of the difficulty of determining with certainty that a fossil has retained some evidence of its original aluminosilicate association (Butterfield, Balthasar and Wilson, 2007). Clay minerals can precipitate in many different sedimentary

environments and under many diagenetic conditions (Odin et al, 1988), and can readily undergo alteration in response to changes in its chemical environment (Lyell, 1983). Thus, it is difficult to be certain of the origin of a fossil-clay association even in relatively unaltered material, and with excellent compositional and textural data. Although authigenic clay mineralization has a credible theoretical basis for its occurrence and preservational mechanism (Petrovich, 2001), reliable information about its commonality in BST deposits and the degree of its impact on fossil preservation is difficult to ascertain. Experimental taphonomy has discovered a strong connection between authigenic clay mineralization of bacteria and taphonomic fidelity (Ferris, Fyfe and Beveridge, 1988), but, thus far, a similar degree of success in macrofossils has only been achieved with detrital clays (Wilson and Butterfield, 2014). A positive impact on the taphonomic fidelity of macrofossils as a result of authigenic clays would only be noticeable in localities with little detrital clay (e.g. Anderson, 2010)—in most BST environments, they would be redundant.

2.3. Processes of calcium carbonates and phosphates

2.3.1 Phosphatization

While sedimentary calcium carbonates and phosphates generally form through very different processes, they are intimately related in exceptional fossil preservation. Apatite is much more structurally and chemically resistant, which not only makes it more resistant to destruction via natural processes, but also makes it easy to extract from calcareous rocks via acid maceration (Schiffbauer et al, 2014). Sedimentary phosphate deposits (phosphorite) is commonly produced by the precipitation of phosphate minerals from seawater (Pufahl, 2010). Phosphatization of soft tissues can occur in phosphorites, but also

in shales (Broce et al, 2014). Though apatite ($Ca_5(PO_4)_3(OH^-, Cl^-, F^-)$) is commonly thought of as the mineral in sedimentary phosphorites, they are most commonly composed of francolite, which is a solid solution between calcite and apatite, but can also have substitutions with sodium, magnesium and sulfate. Areas of upwelling at continental margins are excellent environments for phosphorite production. The introduction of low-oxygen, nutrient rich waters causes high rates of primary production, resulting in high rates of organic carbon accumulation (a phosphate source) and oxygen depletion. This results in authigenic phosphatization (cementation and nodule formation) of laminated sediments in distal environments, or coarse-grained peloidal phosphorites in nearshore sediments. These upwelling-related phosphorites are often interbedded with shales and cherts. Generally, periods with extensive phosphorite production, like the Permian and Miocene correspond with times of rapid ocean circulation or glacial weathering. Phosphorites can also form in restricted basins like lagoons, that could receive high quantities of terrigenous organic matter, and guano (Pufahl, 2010).

Generally, phosphatization occurs along with calcification, which aids easy extraction of fossil material, since calcite dissolves much more readily than calcium phosphate. Though they occur together, they are not thought to precipitate simultaneously. Instead, chemical conditions will either favor carbonate or phosphate precipitation, in which slight alterations to the local chemistry can abruptly cause a change from one to the other, a process compared to a "switch." Relative to calcite, apatite is favored by conditions of lower pH, lower carbonate concentrations, and higher phosphate concentrations. Decay processes are commonly invoked for producing these conditions, since respiration generally causes a decrease in pH, and organic matter has greater phosphate concentrations

than one would usually find in seawater (Briggs and Wilby, 1996). In practice, soft-tissue phosphatization occurs under low-oxygen conditions. The lack of oxygen slows decay, giving additional time for phosphatization to occur (Briggs, 2003). This cause is but another reason for the connection between anoxia and phosphatization is that organic-rich, restricted environments which favor phosphatization are usually low-oxygen (Pufahl, 2010).

There are two different microfabrics that are commonly used in descriptions of soft-tissue fossil phosphatization. The "substrate" microfabric is a result of calcium phosphate precipitating directly onto the soft tissues of an organism. This produces concentric layers of calcium phosphate. The "microbial" microfabric is a result of precipitating calcium phosphate on or inside of the bacteria which are decaying the tissues. The bacteria themselves are not usually well preserved, only showing their general shape; spherical or ellipsoidal, and there is some possibility that they are not bacterial fossils, themselves. (Wilby and Briggs, 1997) Fungal hyphae or bacterial filaments are also sometimes preserved, though they lack the granular texture characteristic of a substrate microfabric (Dong et al, 2010; Olempska, 2012). The cytoplasm of cells can be preserved in calcium phosphate as well, which appears as a groundmass of hexagonal apatite columns (Shiffbauer et al, 2012).

Embryos are preferentially preserved via phosphatization and calcification pathways. In the Ediacaran Doushantuo Formation, numerous putative animal embryos are preserved, some bearing features that resemble organelles. These represent the oldest probable animal fossils, and are preserved in several stages of cell division. During the Cambrian and lowest Ordovician, numerous animal embryos are preserved, including

Markuelia (Dong et al, 2010) and *Pseudooides* (Donoghue et al, 2006). In some of these, it is only the cuticular outer envelope of the egg that is preserved in phosphate, though the interior is calcite-infilled (Broce et al, 2014). No phosphate is necessary to preserve an egg, as evidenced by some calcified gastropod eggs from the Cretaceous, though they exhibit poor preservation (Zaton et al, 2017).

In BST deposits, gut tracts of organisms are commonly phosphatized. In this case, the gut forms an enclosed region where conditions conducive to phosphatization form and persist in isolation from the surrounding seawater. Microbial decay often has an early start in the digestive tracts of organisms, and digestive fluids are commonly rich in phosphate. Some arthropods form granules of phosphate in their digestive tract *in vivo* to serve as temporary storage of calcium for use in forming a new exoskeleton after molting. Instances of gut-tract phosphatization are most common among Cambrian arthropods, possibly due to their moulting tendencies (Lerosey-Aubril, 2012). Hyoliths are also known for their tendency for gut-tract phosphatization (Devaere et al, 2014). Gut tract phosphatization can preserve fossils of the gut microbiota (Zhu et al, 2004)

2.3.2 Calcification

Calcite association with soft tissues is not usually described in BST preservation, but it is capable of preserving some very remarkable fossils. For instance, stromatolites are often preserved in calcite due to the "alkalinity engine" processes resulting from the decay of organic carbon by sulfur-reducing microbes within the sediment, which increase carbonate concentrations with only circumstantial pH drawdown (Gallagher et al, 2012).

The same process produces carbonate concretions around decaying organisms, sometimes preserving soft-bodied organisms within.

One of the best examples of exceptionally calcitized fossils is the Herefordshire lagerstätte, in which microfossils are preserved as calcite within calcite nodules. The different coloration of the fossil vs. host rock allows the fossils to be distinguished. The fossils are casts of the original organisms (Orr et al, 2000). “Coal balls” are another example of concretionary calcite preservation. They are calcite concretions which occur in coal beds, and can exceed 1 meter in diameter, or 4 meters for agglomerations of coal balls. Plants are preserved with cellular resolution within coal balls, and some show little evidence of decay. One explanation for how coal balls might form is via erosion of a semi-impermeable layer of shale overlying the peat. If decay-related carbon dioxide had accumulated, and was pressurized by the overlying shale, then a sudden release of pressure could prompt the rapid precipitation of calcite, thus forming large carbonate concretions over a short timescale (Demaris, 2000).

Early calcite cementation might play an important role in BST preservation in most localities. Some BST lagerstätten, like the Wheeler Shale, contain a significant fraction of detrital carbonate particles. This detrital carbonate could dissolve during a stage of decay, then reprecipitate around a fossil as decay increases alkalinity (like in Fig 2.1), thus limiting the access of oxygen and sulfate to decay-related microbes. Authigenic carbonate cement is an abundant component of some fossiliferous sections of the Wheeler Shale (Gaines et al, 2005). Some BST deposits, including the Burgess Shale itself exhibit calcite cementation on the surface of bed tops that thoroughly cemented the upper ~ 1 cm of the event beds which interred exceptionally preserved fossils. Though not fossil-associated

calcite, such extensive bed-top calcite cementation could serve to restrict the diffusion of oxygen and sulfate to the site of decay (Gaines et al, 2012a). Weathering results in the dissolution of the bed tops, necessitating unweathered material for their identification (Gaines et al, 2012b). Under experimental conditions, pure carbonate sediment is not advantageous for the inhibition of decay (Wilson and Butterfield, 2014), but BST preservation has occurred in carbonate settings without aluminosilicates (Anderson, 2010).

REFERENCES

Amores, Derek R. and Lesley A. Warren (2007) "Identifying when microbes biosilicify: The interconnected requirements of acidic pH, colloidal SiO_2 and exposed microbial surface" *Chemical Geology* 240:298-312

Anderson, Evan Pelzner (2010) "*Chuaria, Vendotaenia,* and the taphonomy of the carbonaceous compression" M. S. thesis, Department of Geosciences, Virginia Polytechnic Institute and State University

Andrews, Julian E., Peter Brimblecombe, Tim D. Jickells, Peter S. Liss and Brian Reid (2005) *An Introduction to Environmental Chemistry 2nd Edition* Blackwell Publishing, Malden, MA.

Bailey, Jake V., Timothy D. Raub, A. Nele Meckler, Benjamin K. Harrison, Theresa M. D. Raub, Abigail M. Green and Victoria J. Orphan (2010) "Pseudofossils in relict methane seep carbonates resemble endemic microbial consortia" *Palaeogeography, Palaeoclimatology, Palaeoecology* 285:131-142

Ballhaus, Chris, Carole T. Gee, Conny Bockrath, Karin Geef, Tim Mansfeldt and Dieter Rhede (2012) "The silicification of trees in volcanic ash – An experimental study" *Geochimica et Cosmochimica Acta* 84:62-74

Barghoorn, Elso S. and Stanley A. Tyler (1965) "Microorganisms from the Gunflint Chert" *Science* 147:563-577

Beveridge, T. J. and R. G. E. Murray (1980) "Sites of Metal Deposition in the Cell Wall of *Bacillus subtilis*" *Journal of Bacteriology* 141:876-887

Beveridge, T. J., J. D. Meloche, W. S. Fyfe and R. G. E. Murray (1983) "Diagenesis of Metals Chemically Complexed to Bacteria: Laboratory Formation of Metal Phosphates, Sulfides, and Organic Condensates in Artificial Sediments" *Applied and Environmental Microbiology* 45:1194-1108

Bossellmann, Katja (2007) *Sulfate reduction and iron-manganese cycling in intertidal surface sediments in the southern North Sea*. PhD dissertation from Carl von Ossietzky Universität Oldenburg

Böttcher, Michael E., Andrea M. Smock and Heribert Cypionka (1998) "Sulfur isotope fractionation during experimental precipitation of iron(II) and manganese(II) sulfide at room temperature" *Chemical Geology* 146:127-134

Botting, Joseph P., Lucy A. Muir, Mark D. Sutton and Talfan Barnie (2011) "Welsh gold: A new exceptionally preserved pyritized Ordovician biota" *Geology* 39:879-882

Briggs, Derek E. G., Simon H. Bottrell, Robert Raiswell (1991) "Pyritization of soft-bodied fossils: Beecher's Trilobite Bed, Upper Ordovician, New York State" *Geology* 19:1221-1224

Briggs, Derek E. G., R. Raiswell, S. H. Bottrell, D. Hatfield and C. Bartels (1996) "Controls on the pyritization of exceptionally preserved fossils:an analyisis of the lower Devonian Hunsrück Slate of Germany" *American Journal of Science* 296:633-663

Briggs, Derek E. G. and Philip R. Wilby (1996) "The role of the calcium-carbonate-calcium phosphate switch in the mineralization of soft-bodied fossils" *Journal of the Geological Society, London* 153:665-668

Briggs, Derek E. G., (2003) "The Role of Decay and Mineralization in the Preservation of Soft Bodies" *Annual Review of Earth and Planetary Science* 31:275-301

Broce, Jesse, James D. Schiffbauer, Kriti Sen Sharma, Ge Wang and Shuhai Xiao (2014) "Possible animal embryos from the Lower Cambrian (Stage 3) Shuijingtuo Formation, Hubei Province, South China" *Journal of Paleontology* 88:385-394

Butterfield, Nicholas J. (1996) "Fossil preservation in the Burgess Shale: Reply" *Lethaia* 29:109-112

Butterfield, Nicholas J., Uwe Balthasar and Lucy A. Wilson (2007) "Fossil diagenesis in the Burgess Shale" *Palaeontology* 50:537-543

Butts, Susan H. (2014) "Silicification" in Reading and Writing of the Fossil Record: *Preservation Pathways to Exceptional Fossilization*. Eds. Marc Laflamme, James D. Schiffbauer and Simon A. F. Darroch. The Paleontological Society Papers v. 20.

Canfield, Donald E. and Robert Raiswell (1991) "Pyrite Formation and Fossil Preservation" *Taphonomy: Releasing the Data Locked in the Fossil Record* pp. 338-388 Eds. Peter A. Allison and Derek E. G. Briggs. Plenum Press, NY

Canfield, Donald E., Robert Raiswell and Simon Bottrell (1992) "The reactivity of sedimentary iron minerals toward sulfide" *American Journal of Science* 292:659-683

Cavalazzi, Barbara, Roberto Barbieri, Sherry L. Cady, Annette D. George, Salvatore Gennaro, Frances Westall, Alberto Lui, Roberto Canteri, Angelo Pio Rossi, Gian Gabriele Ori and Kamal Taj-Eddine (2012) "Iron-framboids in the hydrocarbon-related Middle Devonian Hollard Mound of the Anti-Atlas mountain range in Morocco: Evidence of potential microbial biosignatures. *Sedimentary Geology* 263-264:183-193

Chen, Duo Fu, Yong Yang Huang, Xun Lai Yuan, Lawrence M. Cathles III (2005) "Seep carbonates and preserved methane oxidizing archaea and sulfate reducing bacteria fossils suggest recent gas venting on the seafloor in the Northeastern South China Sea" *Marine and Petroleum Geology* 22:613-621

Chen, Duo Fu, Qian Liu, Zhangwei Zhang, Lawrence M. Cathles III and Harry H. Roberts (2007) "Biogenic fabrics in seep carbonates from an active gas vent site in Green Canyon Block 238, Gulf of Mexico" *Marine and Petroleum Geology* 24:313-320

Cotroneo, S., J.D. Schiffbauer, V.E. McCoy, U.G. Wortmann, S.A.F. Darroch, Y. Peng and M. Laflamme (2016) "A new model of the formation of Pennsylvanian iron carbonate concretions hosting exceptional soft-bodied fossils in Mazon Creek, Illinois" *Geobiology* 14:543-555

Deconinck, J. F. and H. Chamley (1995) "Diversity of smectite origins in Late Cretaceous Sediments: example of chalks from northern France" *Clay Minerals* 30:365-379

Degens, E.T., H. Okada, S. Honjo and J. C. Hathaway (1972) "Microcrystalline Sphalerite in Resin Globules Suspended in Lake Kivu, East Africa" *Mineralium Deposita* 7:1-12

DeMaris, Philip J. (2000) "Formation and distribution of coal balls in the Herrin Coal (Pennsylvanian) Franklin County, Illinois Basin, USA" *Journal of the Geological Society, London* 157:221-228

Devaere, Léa, Sébastien Clausen, J. Javier Álvaro, John S. Peel and Daniel Vachard (2014) "Terreneuvian Orthothecid (Hyolitha) Digestive Tracts from Northern Montagne Noire, France; Taphonomic, Ontogenetic and Phylogenetic Implications" *PloS ONE* 9:e88583

Dong, Xi-Ping, Stefan Bengtson, Neil J. Gostling, John A. Cunningham, Thomas H. P. Harvey, Artem Kouchinsky, Anatoly K. Val'kov, John E. Repetski, Marco Stampanoni, Federica Marone and Philip C. J. Donoghue (2010) "The anatomy, taphonomy, taxonomy and systematic affinity of *Markuelia*: Early Cambrian to Early Ordovician scalidophorans" *Palaeontology* 53:1291-1314

Donoghue, Philip C. J., Stefan Bengtson, Xi-ping Dong, Neil J. Gostling, Therese Huldtgren, John A. Cunningham, Chongyu Yin, Zhao Yue, Fan Peng and Marco Stampanoni (2006) "Synchrotron X-ray tomographic microscopy of fossil embryos" *Nature* 442:680-683

Eby, G. Nelson (2004) *Principles of Environmental Chemistry* Brooks/Cole, Belmont, CA

Farrell, Úna C., Markus J. Martin, James W. Hagadorn, Thomas Whiteley and Derek E. G. Briggs (2009) "Beyond Beecher's Trilobite Bed: Widespread pyritization of soft tissues in the Late Ordovician Taconic foreland basin" *Geology* 37:907-910

Farrell, Úna C., Derek E. G. Briggs, Emma U. Hammarlund, Erik A. Sperling and Robert R. Gaines (2013) "Paleoredox and pyritization of soft-bodied fossils in the Ordovician Frankfort Shale of New York" *American Journal of Science* 313:452-489

Farrell, Úna C. (2014) "Pyritization of soft tissues in the fossil record: An overview" *Reading and Writing of the Fossil Record: Preservation Pathways to Exceptional Fossilization*. pp. 147-162 Eds. Marc Laflamme, James D. Schiffbauer and Simon A. F. Darroch. The Paleontological Society Papers v. 20.

Faure, Gunter (1998) "Principles and applications of geochemistry: a comprehensive textbook for geology students" 2nd ed. Prentice Hall, NJ.

Ferris, F. G., W. S. Fyfe and T. J. Beveridge (1987) "Bacteria as nucleation sites for authigenic minerals in a metal-contaminated lake sediment" *Chemical Geology* 63:225-232

Ferris, F. G., W. S. Fyfe and T. J. Beveridge (1988) "Metallic ion binding by *Bacillus subtilis:* Implications for the fossilization of microorganisms" *Geology* 16:149-152

Gaines, Robert R. (2005) "A new hypothesis for organic preservation of Burgess Shale taxa in the middle Cambrian Wheeler Formation, House Range, Utah" *Palaeogeography, Palaeoclimatology, Palaeoecology* 220:193-205

Gaines, Robert R., Emma Hammarlund, Xianguang Hou, Changshi Qi, Sarah E. Gabbot, Yuanlong Zhou, Jin Peng and Donald E. Canfield (2012a) "Mechanism for Burgess Shale-type preservation" *Proceedings of the National Academy of Sciences of the United States of America* 109:5180-5184

Gaines, Robert R., Emma Hammarlund, Xianguang Hou, Changshi Qi, Sarah E. Gabbot, Yuanlong Zhou, Jin Peng and Donald E. Canfield (2012b) "Reply to Butterfield: Low-sulfate and early cements inhibit decay and promote Burgess Shale-type preservation" *Proceedings of the National Academy of Sciences of the United States of America* 109:5180-5184

Gardner, James H. (1908) "The physical origin of certain concretions" *The Journal of Geology* 16:452-458

Gaudin, A., M. D. Buatier, D. Beaufort, S. Petit, O. Grauby and A. Decarreau (2005) "Characterization and Origin of Fe3+-montmorillonite in deep-water calcareous sediments (Pacific Ocean, Costa Rica Margin)" *Clays and Clay Minerals* 53:452, 465

Gehling, James G. (1999) "Microbial mats in terminal Proterozoic siliciclastics; Ediacaran death masks" *Palaios* 14:40-57

Gallagher, K. L., T. J. Kading, O. Braissant, C. Dupraz and P. T. Visscher (2012) "Inside the alkalinity engine: the role of electron donors in the organomineralization potential of sulfate-reducing bacteria" *Geobiology* 10:518-530

Giresse, P. and A. Wiewióra (2001) "Stratigraphic condensed deposition and diagenetic evolution of green clay minerals in deep water sediments on the Ivory Coast-Ghana Ridge" *Marine Geology* 179:51-70

Gong, Yi-Ming (2007) "Pyrite framboids interpreted as microbial colonies within the Permian *Zoophycos* spreiten from southeastern Australia" *Geological Magazine* 145:95-103

Hegna, Thomas A., Markus J. Martin and Simon A. F. Darroch (2017) "Pyritized *in situ* trilobite eggs from the Ordovician of New York (Lorraine Group): Implications for trilobite reproductive biology" *Geology* 45:199-202

Helfferich, F. and A. Katchalsky (1970) "A Simple Model of Interdiffusion with Precipitation" *The Journal of Physical Chemistry* 74:308-314

Iler, Ralph K. (1979) *The Chemistry of Silica: Solubility, Polymerization, Colloid and Surface Properties and Biochemistry of Silica.* John Wiley & Sons

Johnson, Ralph Gordon (1964) "The Community Approach to Paleoecology" *Approaches to Paleoecology* (Eds. John Imbrie and Normal Newell) 107-134

Jones, Brian (2010) "Warm-water neritic carbonates" *Facies Models 4* pp. 341-370 Eds. Noel P. James and Robert W. Dalrymple. Geological Association of Canada, Canada.

Kenchington, Charlotte G. and Philip R. Wilby (2014) "Of time and taphonomy: Preservation in the Ediacaran" *Reading and Writing of the Fossil Record: Preservation Pathways to Exceptional Fossilization*. pp. 163-216 Eds. Marc Laflamme, James D. Schiffbauer and Simon A. F. Darroch. The Paleontological Society Papers v. 20.

Köhler, Birgit, Arieh Singer and Peter Stoffers (1994) "Biogenic Nontronite from Marine White Smoker Chimneys" *Clays and Clay Minerals* 42:689-701

Konhauser, Kurt O., Brian Jones, Vernon R. Phoenix, Grant Ferris and Robin W. Renaut (2004) "The Microbial Role in Hot Spring Silicification" *AMBIO: A Journal of the Human Environment* 33:552-558

Kremer, Barbara and Józef Kaźmierczak (2005) "Cyanobacterial mats from Silurian black radiolarian cherts: Phototrophic life at the edge of darkness?" *Journal of Sedimentary Research* 75:897-906

Lerosey-Aubril, Rudy, Thomas Hegna, Carlo Kier, Enrico Bonino, Jörg Habersetzer, Matthieu Carré (2012) "Controls on Gut Phosphatization: The Trilobites from the Weeks Formation Lagerstätte (Cambrian; Utah)" *PloS ONE* 7:e32934

Locatelli, Emma R., Sean McMahon and Hans Bilger (2017) "Biofilms mediate the preservation of leaf adpression fossils by clays" *Palaios* 32:708-724
Love, Leonard Gregory (1957) "Micro-organisms and the presence of syngenetic pyrite" *Quarterly Journal of the Geological Society* 113:429-440
Lyell, Mitchell (1983) "The brown-green color transition in marine sediments: A marker of the Fe(III)-Fe(II) redox boundary" *Limnology and Oceanography* 28:1026-1033
Maclean, L. C. W., T. Tyliszczak, P. U. P. A. Gilbert, D. Zhou, T. J. Pray, T. C. Onstott and G. Southam (2008) "A high-resolution chemical and structural study of framboidal pyrite formed within a low-temperature bacterial biofilm" *Geobiology* 6:471-480
Martin, Derek, Derek E. G. Briggs and R. John Parkes (2004) "Experimental attachment of sediment particles to invertebrate eggs and the preservation of soft-bodied fossils" *Journal of the Geological Society, London* 161:735-738
Mera, Matilde Urrutia and Terrance J. Beveridge (1993) "Mechanism of Silicate Binding to the Bacterial Cell Wall in *Bacillus subtilis*" *Journal of Bacteriology* 175:1936-1945
Murray, H. H. (1999) "Applied clay mineralogy today and tomorrow" *Clay Minerals* 34:39-49
Naughton, Julie, Gina Duggan, Billy Bourke and Marguerite Clyne (2014) "Interaction of microbes with mucus and mucins: Recent developments" *Gut Microbes* 5:48-52
Nordstrom, D. Kirk and Charles N. Alpers (1999) "Negative pH, efflorescent mineralogy, and consequences for environmental restoration at the Iron Mountain Superfund site, California" *Proceedings of the National Academy of Science* 96:3455-3462
Odin, G. S. and B. Sen Gupta (1988) "Geological Significance of the Verdine Facies" *Green Marine Clays* (Ed. G. S. Odin) *Developments in Sedimentology 45* Elsevier, Netherlands
Odin, G.S. and P. D. Fullagar (1988) "Geological Significance of the Glaucony Facies" *Green Marine Clays* (Ed. G. S. Odin) *Developments in Sedimentology 45* Elsevier, Netherlands
Odin, G.S., R. W. O'B. Knox, R. A. Gygi and S. Guerrak (1988) "Green Marine Clays from the Oolitic Ironstone Facies: Habit, Mineralogy, Environment" *Green Marine Clays* (Ed. G. S. Odin) *Developments in Sedimentology 45* Elsevier, Netherlands
Orr, Patrick J., Derek E. G. Briggs, Stuart L. Kearns (1998) "Cambrian Burgess Shale Animals Replicated in Clay Minerals" *Science* 281:1173-1175
Orr, Partick J., Derek E. G. Briggs, David J. Siveter and Derek J. Siveter (2000) "Three-dimensional preservation of a non-biomineralized arthropod in concretions in Silurian volcanoclastic rocks from Herefordshire, England" *Journal of the Geological Society, London* 157:173-186
Orr, Patrick J. (2014) "Late Proterozoic-Early Phanerozoic 'taphonomic windows': The environmental and temporal distribution of recurrent modes of exceptional preservation" *Reading and Writing of the Fossil Record: Preservation Pathways to Exceptional Fossilization.* Eds. Marc Laflamme, James D. Schiffbauer and Simon A. F. Darroch. The Paleontological Society Papers v. 20.
Perry, Karen A. and Thomas F. Pedersen (1993) "Sulphur speciation and pyrite formation in meromictic ex-fjords" *Geochimica et Cosmochimica Acta* 57:4405-4418
Petrovich, Radomir (2001) "Mechanisms of fossilization of the soft-bodied and lightly armored faunas of the Burgess Shale and some other classical localities" *American Journal of Science* 30:683-726
Phoenix, Vernon R., Dave G. Adams and Kurt O. Konhauser (2000) "Cyanobacterial viability during hydrothermal biomineralization" *Chemical Geology* 169:329-338
Postgate, John Raymond (1984) *The Sulphate-reducing Bacteria* Cambridge University Press, NY
Pufahl, Peir K. (2010) "Bioelemental Sediments" *Facies Models 4* Eds. Noel P. James and Robert W. Dalrymple. Geological Association of Canada, St. Johns, Canada.
Reddy, Gopal, Md. Altaf, B. J. Naveena, M. Venkateshwar, E. Vijay Kumar "Amylolytic bacterial lactic acid fermentation – A review" *Biotechnology Advances* 26:22-34
Rickard, David (2012) "Sulfidic Sediments and Sedimentary Rocks" Developments in Sedimentology 65. NLD:Elsevier Science and Technology, Amsterdam
Rust, George W. (1930) "Colloidal primary copper ores at Cornwall Mines, Southeastern Missouri" *The Journal of Geology* 43:398-426
Schieber, Jürgen (2002a) "Sedimentary pyrite: A window into the microbial past" *Geology* 30:531-534
Schieber, Jürgen (2002b) "The Role of an Organic Slime Matrix in the Formation of Pyritized Burrow Trails and Pyrite Concretions" *Palaios* 17:104-109
Schiffbauer, James D., Shuhai Xiao, Kriti Sen Sharma and Ge Wang (2012) "The origin of intracellular structures in Ediacaran metazoan embryos" *Geology* 40:223-226

Schiffbauer, James D., Adam F. Wallace, Jesse Broce and Shuhai Xiao (2014) "Exceptional fossil conservation through phosphatization" in Reading and Writing of the Fossil Record: *Preservation Pathways to Exceptional Fossilization*. Eds. Marc Laflamme, James D. Schiffbauer and Simon A. F. Darroch. The Paleontological Society Papers v. 20.

Schmidt-Rhaesa, Andreas (2013) "Priapulida" In Ed. Schmidt-Rhaesa *Handbook of Zoology: Gastrotricha, Cycloneuralia and Gnathifera: Volume 1: Nematomorpha, Priapulida, Kinorhyncha, Lorcifera*, DeGruyter, Germany. 147-180

Schoonen, Martin A. A. (2004) "Mechanisms of sedimentary pyrite formation" *Mechanisms of sedimentary pyrite formation* Eds. Jan P. Amend, Katrina J. Edwards and Timothy W. Lyons. Geological Society of America, Boulder, CO

Schopf, J. William (1968) "Microflora of the Bitter Springs Formation, Late Precambrian, Central Australia" *Journal of Paleontology* 42:651-688

Shapiro Russell and Henry Fricke (2002) "Teepee Buttes: fossilized methane-seep ecosystems" *Field Trip Guidebook* Geological Society of America, Boulder, CO. 94-101

Środoń, J. (1999) "Use of clay minerals in reconstructing geological processes: recent advances and some perspectives" *Clay Minerals* 34:27-37

Stabili, Loredana, Roberto Schirosi, Margherita Licciano and Adriana Giangrande (2009) "The mucus of *Sabella spallanzanii* (Annelida, Polychaeta): Its involvement in chemical defence and fertilization success" *Journal of Experimental Marine Biology and Ecology* 374:144-149

Sutherland, Bruce R., Kai J. Barrett and Murray K. Gingras (2014) "Clay settling in fresh and salt water" *Environmental Fluid Mechanics* 15:147-160

Sweeny, R. E. and I. R. Kaplan (1973) "Pyrite Framboid Formation: Laboratory Synthesis and Marine Sediments" *Economic Geology* 68:618-634

Tarhan, Lidya G., Ashleigh v.S. Hood, Mary L. Droser, James G. Gehling and Derek E. G. Briggs (2016) "Exceptional preservation of soft-bodied Ediacara Biota promoted by silica-rich oceans" *Geology* 44:951-954

Thiessen, Reinhardt (1920) "Occurrence and Origin of Finely Disseminated Sulfur Compoundsin Coal" *Transactions of the American Institute of Mining, Metallurgical and Petroleum Engineers* 63:913-931

Tomescu, Alexandru M. F., Gar W. Rothwell, and Rosmarie Honegger (2006) "Cyanobacterial macrophytes in an Early Silurian (Llandovery) continental biota: Passage Creek, lower Massanutten Sandstone, Virginia, USA" *Lethaia* 39:329-338

Vallentyne, J. R. (1963) "Isolation of pyrite spherules from recent sediments" *Limnology and Oceanography* 8:16-29

Virtasalo, Joonas J., Ludvig Löwemark, Heikki Papunen, Aarno T. Kotilainen and Martin J. Whitehouse (2010) "Pyritic and baritic burrows and microbial filaments in postglacial lacustrine clays in the northern Baltic Sea" *Journal of the Geological Society, London* 146:1185-1198

Wacey, David, Matt R. Kilburn, Martin Saunders, John Cliff and Martin D. Brasier (2011) "Microfossils of Sulphur-metabolizing cells in 3.4-billion-year-old rocks of Western Australia" *Nature Geoscience* 4:698-702

Wilby, Philip R. and Derek E. G. Briggs (1997) "Taxonomic trends in the resolution of detail preserved in fossil phosphatized soft tissues" *Geobios* 30:493-502

Wilkin R. T., H. L. Barnes and S. L. Brantley (1996) "The size distribution of framboidal pyrite in modern sediments: An indicator of redox conditions" *Geochimica et Cosmochimica Acta* 60:3897-3912

Wilkin, Richard T. and Michael A. Arthur (2001) "Variations in pyrite texture, sulfur isotope composition and iron systematics in the Black Sea: Evidence for Late Pleistocene to Holocene excursions of the O_2-H_2S redox transition" *Geochimica et Cosmochimica Acta* 65:1399-1416

Wilson, Lucy A. and Nicholas J. Butterfield (2014) "Sediment effects on the preservation of Burgess Shale-type compression fossils" *Palaios* 29:145-153

Wilson, Mark A. and Paul D. Taylor (2017) "Exceptional pyritized cyanobacterial mats encrusting brachiopod shells from the upper Ordovician (Katian) of the Cincinnati, Ohio, region" *Palaios* 32:673-677

Zaton, Michał, Alexandr A. Mironenko and Kamila Banasik (2017) "Gastropod egg capsules from the Lower Cretaceous of Russia preserved by calcitization" *Palaeogeography, Palaeoclimatology, Palaeoecology* 466:326-333

Zhu, M.-Y., J. Vannier, H. Van Iten and Y.-L.Zhao (2004) "Direct evidence for predation on trilobites in the Cambrian" *Proceedings of the Royal Society of London B* 271:S277-S280

Zorn, M. E., M. K. Gingras and S. G. Pemberton (2010) "Variation in burrow-wall micromorphologies of select intertidal invertebrates along the Pacific Northwest coast, USA: Behavioral and diagenetic implications" *Palaios* 25:59-72

CHAPTER 3: ANALYSIS OF TAPHONOMIC CHARACTERISTICS OF SOFT-BODIED FOSSILS FROM IN THE CAMBRIAN HOUSE RANGE EMBAYMENT OF THE AMERICAN WEST

3.1. Introduction

3.1.1 Objectives/Significance

The primary means of investigating taphonomic processes is through the examination of fossil material. Macro-scale examination alone is insufficient in today's world of taphonomic research. Visual examination of fossil material can be misleading, and cannot provide fine-scale compositional and textural information. Electron microscopy is especially useful for this end (for an overview of electron microscopy methodology, 1.1.2).

Since the nature of relationships between clay minerals and Burgess-Shale-type (BST) fossils has not been conclusively determined, it is an important avenue of investigation (see 2.2). There are abundant BST fossils from the Cambrian (Muscente et al, 2017), but since the Cambrian was so long ago (541-485 Ma, Cohen, Harper and Gibbard, 2017), Cambrian rocks have been subjected to extensive alteration, including weathering. Consequently, when studying Cambrian fossils, it is of utmost importance to distinguish between mineralization that is *detrital, authigenic, diagenetic, metamorphic* and *weathering-related*. Even if a fossil has a different clay composition associated with different morphological features (Orr, 1998), it cannot be assumed to be authigenic (pre-lithification) clay, since the timing of clay replacement varies between different histologies (Butterfield, Balthasar and Wilson, 2007). Thus, not only are the generalized differences

between fossil and host-rock clay compositions important, but also an examination of the mineralogical qualities of the fossil-associated clays and general alteration history.

3.1.2 Organisms

The BST fossil localities which were deposited in the House Range Embayment (HRE) are a convenient choice for the investigation of BST processes, partly because of the extensive collections housed in the University of Kansas Biodiversity Institute. The twenty fossils examined (Tab 3.1) include three specimens of *Ottoia prolifica* and two specimens of *Eldonia ludwigii*, but the majority of the samples are *incertae sedis*.

Priapulid worms are abundant fossils in the Burgess Shale (~505-509 Ma, Muscente et al, 2017), as well as many other Cambrian BST localities. They are notable from the Sirius Passet lagerstätte of Greenland, and the Chengjiang lagerstätte of China, which are among the oldest BST localities with animal fossils (514-521 Ma, Muscente et al, 2017). Phosphatized priapulid body-fossils have recently been recovered from the Kuanchuanpu Formation (~535 Ma). These, like the majority of modern priapulids, are meiofaunal (Liu et al, 2014). The Kuanchuanpu also contains putative kinorhynchs (Zhang et al, 2015), making the divergence date for scalidophora (and ecdysozoa) older than 535 Ma. The oldest fossil evidence for priapulid worms is the trace fossil *Treptichnus pedum*, the first occurrence of which is defined as the base of the Cambrian. Experimental studies show that modern priapulids can make traces very similar to *Treptichnus pedum* with their probing behaviours (Vannier et al, 2010). Priapulids exhibit annulations, due to the spacing between the circular muscles that they use for locomotion. Though priapulids are considered soft-bodied, they are partially chitinous. Larval priapulids are protected by a

Sample	Preservation	Probable identification	Figures and tables
204770	Thinly kerogenized, thickly kerogenized surficial features	*Ottoia prolifica*	Fig. 3.4, 3.5, 3.11
293598	Pyrite association, with euhedral pyrite filling	vermiform	Fig. 3.9
293608	Pyrite filling	vermiform	-
293611	Aluminosilicified, some Fe and Mn oxides	vermiform	Fig. 3.10, 3.16, Tab. 3.2
298531	Kerogenized, pyrite-associated surficial features	*Ottoia prolifica*	Fig. 3.4, 3.5
314051	Aluminosilicified	*Eldonia ludwigi*	Fig. 3.2, 3.11, Tab. 3.3
314096	Thinly kerogenized, some pyrite, barite	*Ottoia prolifica*	Fig. 3.4, 3.5, 3.12
314106	Mouldic. Kerogenized gut contents	*Eldonia ludwigi*	Fig. 3.15, Tab. 3.4
314107	Phosphatized, ropy texture	coprolite	Fig. 3.14
314111	Kerogenization, pyrite-association, aluminosilicification, bladed barite	vermiform	Fig. 3.12
314112	Pyrite-associated outline, annulations	vermiform	-
314114	Pyrite and monazite associations	vermiform	Fig. 3.13, 3.15, 3.16, Tab. 3.6
314147	Bladed monazite, some pyrite	vermiform	Fig. 3.6
314159	Pyrite-association, intermittent gut pyrite filling	vermiform	Fig. 3.8, 3.16, Tab. 3.5
314186	Kerogenization, pyrite-association, aluminosilicification, monazite, calcite	vermiform	Fig. 3.6, 3.10, 3.13, 3.17, Tab. 3.2
314191	Pyrite and barite association	vermiform	-
314202	Pyrite-associated outline and surficial features, pyrite-associated gut	vermiform	-
314215	Intermittent pyrite and barite	vermiform	Fig. 3.12
314253	Extensive pyrite framboids, microcryst groundmass	*Belorhaphe*	Fig. 3.9
377069	Pyrite-associated outline and surficial features, intermittent gut encrustation	vermiform	Fig. 3.7

Table 3.1 The fossils examined in this study, with their KUMIP specimen number, preservation style, best-guess of identity and the figures in which they appear

chitinous lorica, which they lose as they mature. The cuticle is adorned with specialized chitinous elements (scalids, setae, anal hooks and tubuli). Though the cuticle (skin) of priapulids is very proteinaceous, it is 4-15% comprised of chitin, though not in the form of

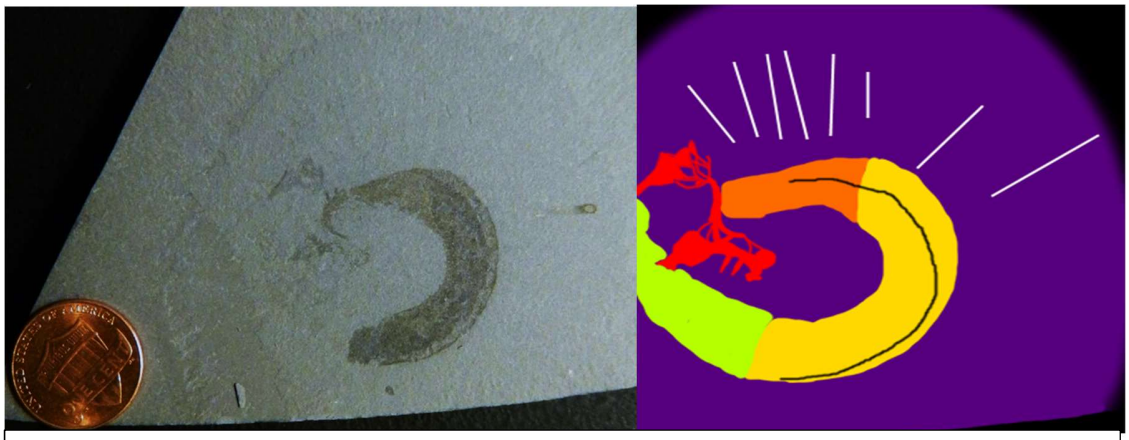

Figure 3.1 KUMIP 314051, (left) optical and (right) schematic. Red=oral tentacles, orange=foregut, yellow=midgut, green=hindgut, black=alimentary canal, purple=outer membrane, white=radial canals.

an exoskeleton (Schmidt-Rhaesa, 2013). The cuticle and gut are commonly preserved via carbonaceous compression (Morris and Robison, 1986).

One of the most peculiar organisms discovered in the Burgess Shale is *Eldonia ludwigi* (Fig. 3.1). Be advised that much of the terminology used to describe *Eldonia* morphology is interpretive. The organism consists of a thin, flexible outer envelope, with a large, coiled sac (originally described as the "alimentary canal," but the true alimentary canal is a thin feature that runs through the coiled sac, which is better interpreted as the coelum) encircling the centre of the envelope. One end of the coelum exhibits paired, branching tentacles (for feeding, presumably). A section of the coiled sac close to the feeding tentacles is much wider and more prominently preserved than the rest of the coiled sac, and is sometimes referred to as the "midgut." The outer envelope contains a series of "canals," which radiate from the centre of the envelope, and sometimes branch, possibly serving some vascular function. (Van Roy, 2006). The membrane also contains what looks like concentric muscles. It was discovered by Charles D. Walcott in 1910, who initially assumed it was a medusiform cnidarian (jellyfish), and considered the coelum to be an annelid in a commensal relationship with the medusa. At a Geological Society of America

meeting later that year, the medusa+annelid hypothesis was rejected in favor of a holothurian (sea cucumber) interpretation, since echinoderms often have a coiled alimentary canal. It was still considered to be medusiform, though known pelagic holothurians are not truly medusiform (Walcott, 1911).

Though *Eldonia ludwigi* does not have any modern relatives, it does have affinities to fossil taxa that have been discovered since, and, actually, prior to *Eldonia ludwigi*, forming the unranked category of "eldonioids." The first eldonioid to be discovered (in 1822) was *Discophyllum peltatum* from the Ordovician of New York (Hall, 1847), and was classified under Zoophyta. *Paropsonema cryptophya* (Silurian of Australia; Clarke, 1900) was discovered in 1895 in the Silurian of New York, and was originally classified as an echinoid. These taxa, discovered prior to *Eldonia ludwigii*, and both belong to the paropsonemids. Paropsonemids are the only group of eldonioids that are found beyond the Cambrian. Unlike *Eldonia*, they are rigidly sclerotized, concavo-convex, lack concentric muscles, and are ornamented on the convex side. Paropsonemids persisted into the Devonian (Van Roy, 2006).

A new probable relative of eldonioids was reported in 2010 by Caron, Morris and Shu (Fig. 3.2). Found only in the Burgess Shale, *Herpetogaster* bears a striking resemblance to the coiled sac that is common to all eldonioids, including the paired, branching feeding tentacles, however *Herpetogaster* lacks the outer membrane entirely, and is attached to the seafloor by a stalk and holdfast. The authors suggest that *Herpetogaster,* the eldonioids and *Phlogites* are stem group ambulacrarians (Caron, Morris and Shu, 2010).

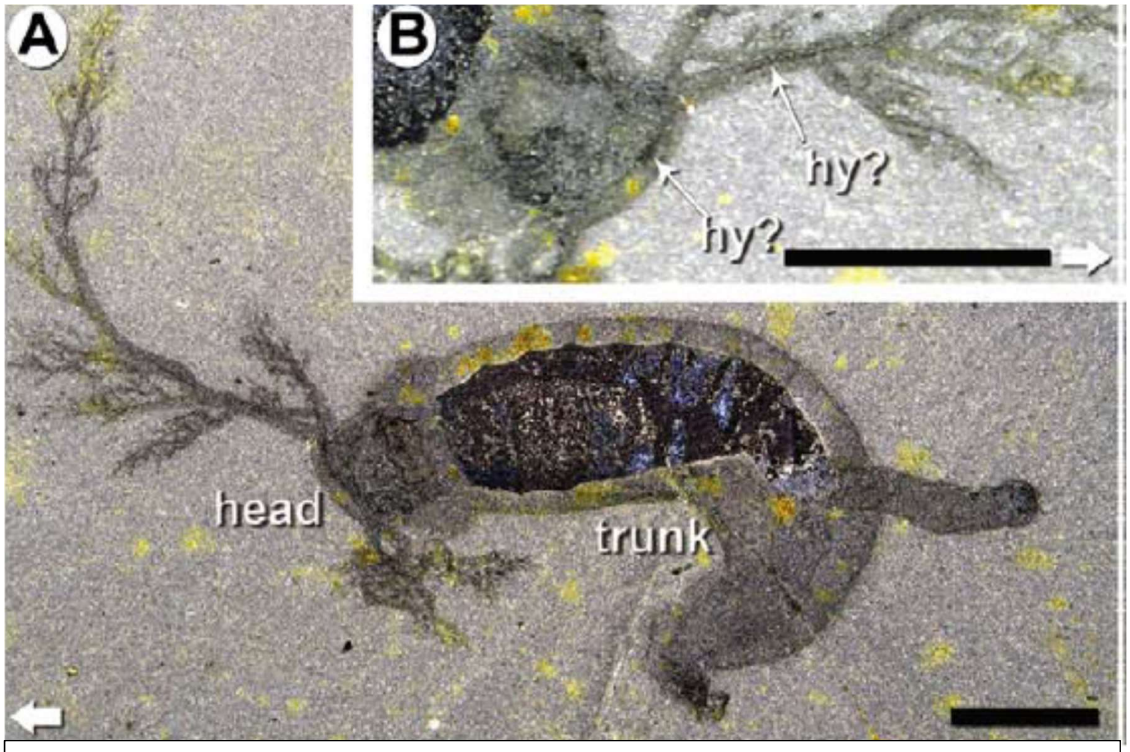

Figure 3.2 *Herpetogaster* of the Burgess Shale. hy? = putative hydraulic system and/or vascular canal. Scale bar is 5 mm. From Caron, Morris and Shu, 2010.

Various forms of species interactions have been suggested for eldonioids, which does little to clarify its life mode, in addition to Walcott's (1911) initial worm+medusa hypothesis, eldonioids have been suggested to be associated with onychophorans (velvet worms). *Microdictyon* and *Paucipodia are* commonly associated with *Eldonia*, but it is unclear whether this is scavenging or symbiotic or what (Jun-Yuan, Mao-Yan and Gui-Qing, 1995). Onychophoran commensalism seems to be very taxon-specific, since *Aysheaia* is found associating only with sponges (Bergström and Hou, 2001). *Rotadiscus,* a heavily sclerotized eldonioid, has records of several species interactions. At least one specimen has apparent repaired damage of the disc, possibly due to predation. Epibionts associate with *Rotadiscus*, including filamentous algae and putative bradoriids. These epibionts associate very strongly with the outer margin of *Rotadiscus*, which suggests that

its life position was concave-up, on the sediment-water interface (Dzik, Yuanlong and Maoyan, 1997).

The life position of eldonioids has been hotly contested. Generally speaking, turbulently transported medusaiform organisms are most likely to settle concave-up, but a significant proportion will settle concave-down (Van Roy, 2006). Rigid objects, like brachiopod or bivalve shells, almost always settle concave-up, but easily flip over in response to currents on the seafloor (Simões et al, 2005). In the Burgess Shale, *Eldonia* are randomly oriented and are often folded, which is to be expected, considering that they were likely transported and buried in turbidites (Van Roy, 2006). In the Chengjiang lagerstätten, the vast majority of *Eldonia* individuals are concave-down, which Chen Zhu and Zhou (1995) consider to be support for a pelagic, concave-down life mode, though most of them are deposited within an event-bed, and some are imbricated. *Discophyllum* from the Ordovician of Morocco show the opposite trend, with all individuals preserved concave-up. If they were transported, then it is almost certain that at least some would be preserved in the opposite orientation (Van Roy, 2006).

Attempting to find a singular life-mode for all eldonioids may not be appropriate, since different taxa have different properties. A series of concentric ridges exist on the outer surface of paropsonemids, which resemble growth lamellae, but consistent placement of these features on specimens of different sizes makes an accretionary growth mode unlikely. They more likely grew via inflation (MacGabhann, 2012). It is unclear whether these concentric ridges are related to the purported muscles in *Eldonia*. The rigid, robust paropsonemids have no obvious means of locomotion, and, as Van Roy (2006) observed, are only found concave-up when *in-situ*. *Eldonia*, on the other hand, is an organism with a

thin, flexible membrane and concentric muscles. Such an organism could exhibit locomotion, and could be fully nektonic in any orientation, or be intermittently sessile and concave-up, like upside-down jellyfish. The conflicting information on eldonioid life position may be resolved by taking morphological differences into account (MacGabhann, 2012).

Paropsonemids are commonly preserved as molds, but *Eldonia* is preserved as a carbonaceous compression. While most morphological features of *Eldonia* are preserved as run-of -the mill carbon residues, the midgut is much thicker, and is often reflective. Butterfield (1996) observed that it is only the interior of the midgut that is reflective. It is often coated by a nonreflective black or brown layer. While the interior can be more than 97 atomic % carbon, the exterior contains substantial (e.g. 6 at..%) silicon and aluminum (Butterfield, 1996). Considering the alteration history of the Burgess Shale (Butterfield, Balthasar and Wilson, 2007), the clay association with the exterior of the midgut could be either authigenic or metamorphic, except that the midgut is usually thought to be on the interior of the eldonioids, not part of the exterior of the organism.

By and large, the *incertae sedis* specimens in this study are too poorly preserved to classify or describe. In some cases, it is uncertain whether they are body fossils, burrows or coprolites. Though these poorly-preserved specimens have indistinct *morphology*, they exhibit highly diverse *taphonomy*. Many poorly-preserved specimens were selected on the basis that they looked unique, in some way different than the other specimens. In spite of the tremendous diversity of these poorly-preserved specimens, they have largely been neglected in the literature, with most research revolving around the best specimens only. It may seem counterintuitive to pursue specimens that exhibit poor preservation, and, in fact,

one reviewer of my paper on the subject (Broce and Schiffbauer, 2017) asked why I did not analyze higher-quality specimens. For the record: I did not intentionally select *bad* specimens… I intentionally selected *diverse* specimens, most of which *are* bad specimens in the usual way samples are judged, but good samples for studying regional trends in taphonomy. In fact, the unique qualities of the specimens resulted in the discovery of some novel taphonomic phenomena. The differences between the specimens exist despite having been deposited in broadly the same environment, and altered by the same processes. The data provided by the poorly-preserved specimens were useful for understanding the taphonomy of the well-preserved specimens because they are produced by a common suite of processes.

3.1.3 Paleoenvironment

The House Range suite of sedimentary units are a Middle Cambrian succession of units that were deposited in the HRE (Rees, 1986) from ~519-497 (Muscente et al, 2017). What is now Utah once contained the West coast of North America, including a broad continental shelf (Rees, 1986; Fig. 3.3). Some local subsidence, likely the result of a NW-SE trending normal fault to the South, produced the HRE, which contains much deeper facies than the surrounding area. Generally, carbonates were deposited when the supply of clastic sediment was locally interrupted (Elrick and Snider, 2002), like during transgessions (Brett et al., 2009). The clastic sediment appears to have originated in the North and were likely transported by geostrophic currents (Elrick and Snider, 2002), except for the quartzose silt grains, which are undoutedly aeolian (Gaines, Kennedy and Droser, 2005). The clastic deposits within the embayment are largely shales that appear to have been

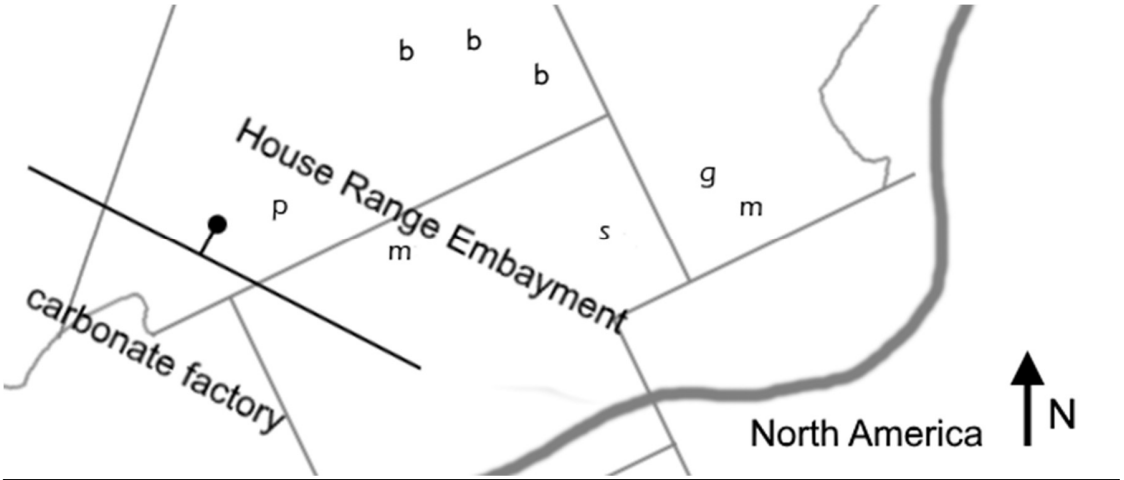

Figure 3.3 Map showing House Range Embayment and approximate Cambrian coastline with modern state lines. Also marked: where fossils were collected from the (p) Pioche Fm, (m) Marjum Fm, (s) Spence Shale, (g) Gibson Jack Formation, and the locations of (b) barite mines (From Perry and Visher, 2015) and (m) monazite-bearing phosphorites (From Jackson and Christiansen, 1993).

deposited by turbidity currents travelling in a SW direction (Elrick and Snider, 2002). BST preservation corresponds with shales that are low in bioturbation, indicating dysoxic conditions (Gaines and Droser, 2003), although V and Ni redox proxies suggest oxic bottom waters throughout the Wheeler and Spence Shales (Kloss et al., 2015).

The Pioche Formation is the earliest BST-fossil bearing unit in this succession (Delamaran) (Brett et al., 2009), and likely predates the HRE. The Grassy Springs Member of the Pioche Formation contains some fissile shale (Eddy and McCollum, 1998). The Combined Metals Member is mostly limestone but contains some BST fossils in the shale interbeds. The overlying Comet Shale Member is mostly fissile shale, but contains some ribbon limestones (Sundberg and McCollum, 2000). One unusual property of the BST fossils of the Pioche Formation is the occasional fossil association of Monazite, a rare-earth-element phosphate mineral (Moore and Lieberman, 2009).

The Wheeler Formation, which overlies the Swasey Limestone is likely the first unit deposited in the embayment, since the Swasey-Wheeler contact is a pronounced

drowning surface (Rees, 1986). The shales of the Wheeler Formation are the first expression of BST fossils in this succession, and include some priapulids (Morris and Robison, 1986). The BST-fossil bearing shales of the Wheeler consist of grey to black couplets (Gaines and Droser, 2003). The overlying Marjum Formation (Brett et al., 2009) is predominantly limestone, but contains some shale (Elrick and Snider, 2002). The priapulid worms of the Marjum are located in a blue-grey finely-laminated calcareous shale that weathers to a yellowish brown (Morris and Robison, 1986). The Weeks Formation overlies the Marjum Formation (Brett et al., 2009).

In the Spence shale, fossil priapulids are located in a blue-grey micaceous shale (Morris and Robison, 1986). The Spence Shale was deposited to the North of the embayment, in a detrital belt distal from a carbonate belt. The Miner's Hollow locality of the Spence Shale is more distal than the Antimony Canyon locality (Lyon, 2011) and likely had highly variable bottom-water redox conditions (Garson et al., 2011). The fossil priapulids are thought to be allochthonous because none of the local trace fossils match priapulid origins (Morris and Robison, 1986), and BST fossils only occur on bedding planes devoid of burrows. They and other soft-bodied organisms likely washed in with a storm turbidite (Gaines and Droser, 2010).

3.2 Results

3.2.1 Kerogenization

Most samples resemble a carbonaceous compression, but, under microanalysis, areas of organic carbon are not apparent. The specimens typically contain higher carbon concentrations in the fossil than the host rock (see discriminant analysis from Broce and

Schiffbauer, 2017). Even in KUMIP 298531, specimens with a visible carbon film, areas of the fossil that are without visible organic carbon also have higher carbon concentrations than the host rock. It is possible that the carbon that was originally in the organisms (1) migrated into nearby interstices, (2) adsorbed onto clay minerals, or (3) invaded the interlayers of clay minerals. Alternately, (4) the carbon could exist as calcite, since fossils also generally exhibit higher calcium concentrations (Broce and Schiffbauer, 2017). This cryptic carbon appears to affect the coloration of the fossil.

The three specimens that show morphological details via kerogenization are the three *Ottoia* specimens (KUMIP 298531, 204770 and 314096; Fig. 3.4), whereas most of the rest are not preserved well enough to facilitate classification. In the *Ottoia* specimens, only the cuticle and gut tract are preserved. Since the majority of the samples are not preserved well enough to retain external morphology, it is possible that at least some of them are *Ottoia* or other recognizable organisms from the HRE, but could not be identified (taphonomic bias). Alternately, *Ottoia* and *Eldonia* could have higher preservation potential than other organisms, which are impossible to identify due to consistently poor preservation (taxonomic bias). Though the cuticle of priapulids is beautifully kerogenized in BST deposits, the only part of annelid integument that seems to become kerogenized is the chaeta, e.g. the chitinous “bristles” of polychaetes. Annelids without prominent chaeta are virtually unknown in BST deposits. There is a major histological difference between priapulid and anne lid cuticle in terms of chitin-content: though priapulids contain a significant portion of c hitin in their digestive tract and cuticle (Schmidt-Rhaesa, 2013), annelids do not (Richards, 1978). Since chitin is highly resistant to microbial decay (Butterfield, 1990) and thermal maturation processes (Briggs, 1999), annelids without

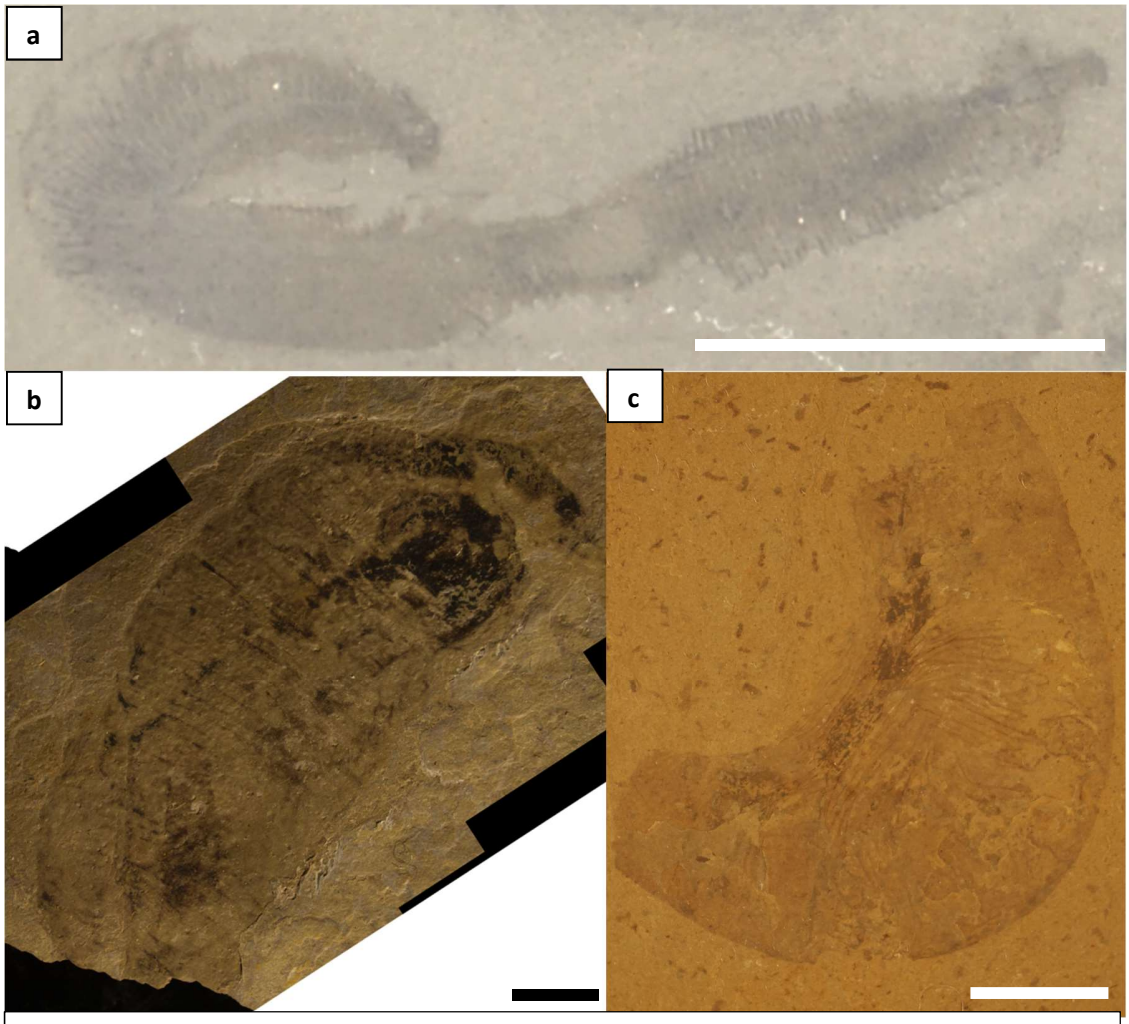

Figure 3.4 Optical images of *Ottoia* specimens (a) KUMIP 204770 (b) KUMIP 314096 (c) KUMIP 298531. All scale bars 1 cm.

chaeta or other resistant parts may be poorly-preserved, even in BST localities. Unidentifiable vermiform objects in BST localities may represent missing diversity in soft-bodied worm taxa, like *Annelida*.

The *Ottoia* specimens appear to have the annular features and gut tract visibly kerogenized. The kerogen in KUMIP 204770 consists of irregular blebs of carbon (Fig 3.5 a), whereas those in 298531 occur in narrow but prominent bands (Fig 3.5 c) and in 314096 they are more continuous (Fig 3.5). The annular features are very thin (Fig. 3.4), indicating

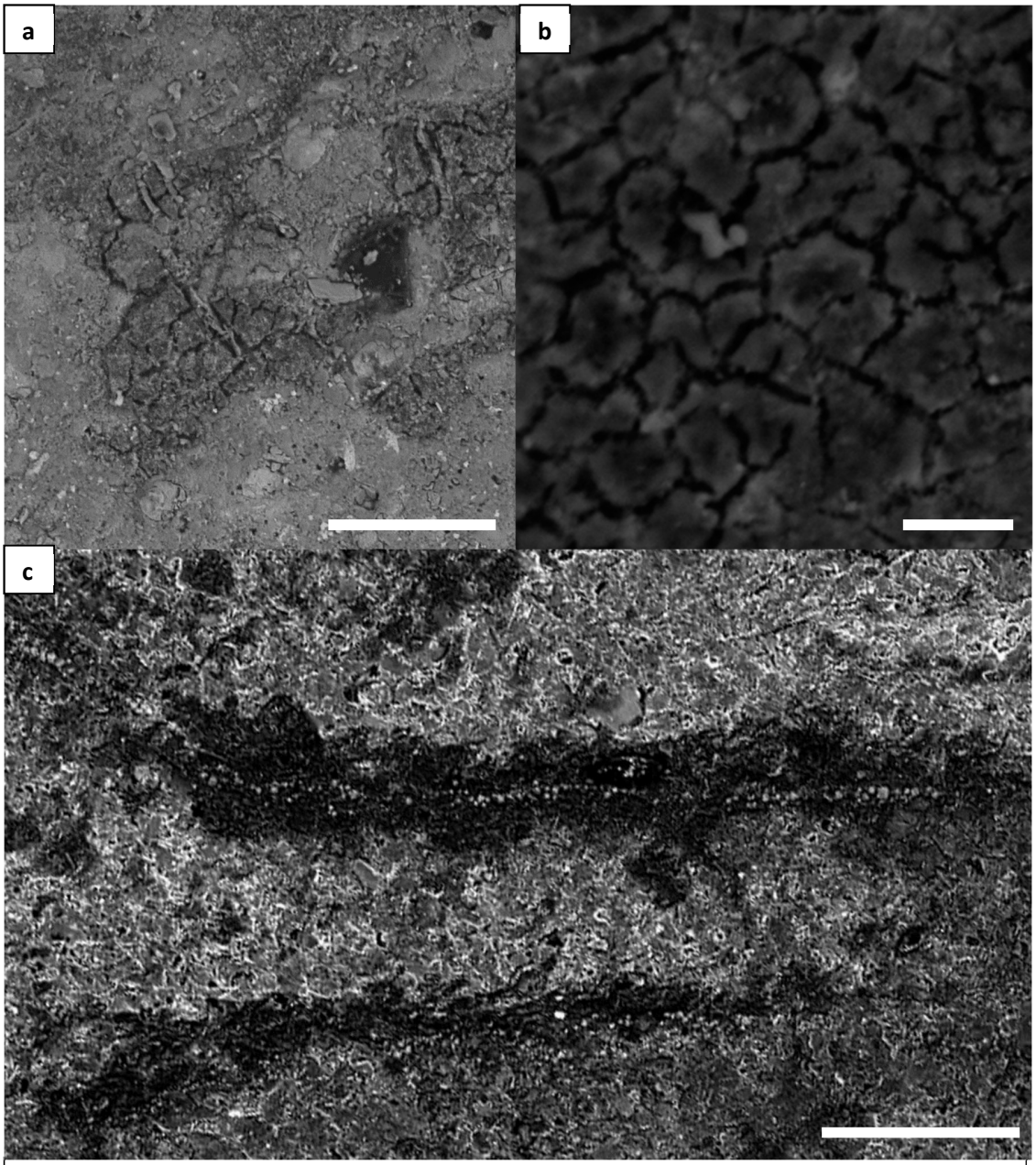

Figure 3.5 BSE images of *Ottoia* specimens (a) Carbon bleb from KUMIP 204770. (b) Polygonally cracked carbon film from KUMIP 298531 (c) Interannuli from KUMIP 314096 with included pyrite. Scale bars: a=40 μm, b=20 μm, c=100 μm.

that these are not the annuli themselves, but the areas between the annuli (interannuli) that are preserved. This is further supported by the existence of a thin line of pyrite that runs down the center of the carbonaceous lines in KUMIP 298531 (Fig 3.5 c). My model for the preservation of interannuli, is as follows: in priapulids, annuli are the surficial expression

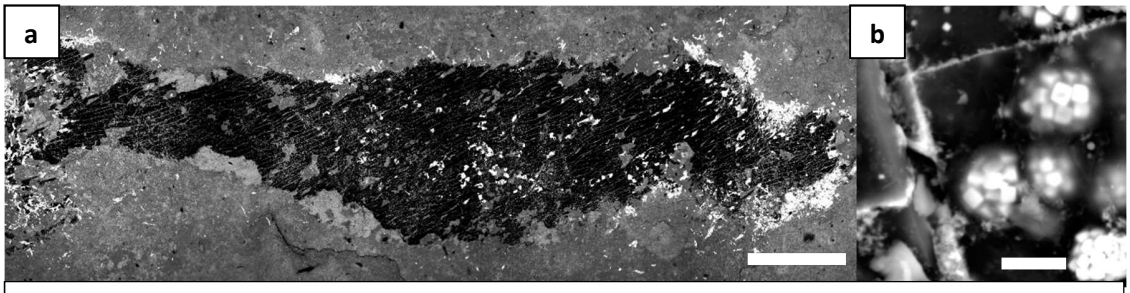

Figure 3.6 BSE images of KUMIP 314186 (a) Carbon film showing cracking pattern. (b) Pyrite framboids trapped within the carbon film. Note that, due to the low backscatter coefficient of carbon the framboids are still visible at depth within the film. Scale bars: a=100 μm, b=5 μm

of ring-shaped muscles that run down the body of the worm (Schmidt-Rhaesa, 2013), but muscles are labile tissues and are unlikely to be preserved. The cuticle contains chitin (Schmidt-Rhaesa, 2013), and will be preserved. A disproportionate amount of cuticle will exist in the crevices between annulations, since it is folded there. Enclosed spaces like interannuli are favorable environments for sulfide to accumulate, thus producing pyrite.

Carbonaceous compression is commonly thought of as preservation of fossils as a carbon film, but the very well-preserved *Ottoia* fossils are instead comprised of discrete carbonaceous blebs. Texturally, these blebs exhibit polygonal cracking (Fig. 3.5 a, b), which may a result of volumetric reduction during diagenesis. True carbon films are only exhibited in KUMIP 314111 and 314186. The carbon film in KUMIP 314186 exhibits two orientations of fractures, one direction exhibiting much longer fractures than the other (Fig. 3.6 a). The directionality of these fractures do not follow the bends in the fossil, which indicates that they are unrelated to primary morphology. KUMIP 314186 also exhibits pyrite framboids which are “trapped” within the carbon film (Fig. 3.6 b). Since KUMIP 314186 does not exhibit pyrite outside of the carbon film, the pyrite was either (1) restricted to particular morphology or (2) removed by weathering reactions, except for those protected by the carbon film (See 3.2.4).

3.2.2 Pyritization

Very little pyrite remains in the sample material. Oxidative weathering has long since converted the pyrite into iron oxides, but many of these retain their original crystal form, like framboids. For the sake of ease of communication, I will be referring to iron oxides as pyrite, since that is their inferred origin.

The most common form of pyritization in these BST fossil localities is an elevated concentration of framboidal pyrite. These pyrite framboids are most common in annular bands (interannuli?), along the borders of the fossil, and around the borders of the gut. Interannuli (KUMIP 297531, Fig. 3.5 c) are a probable site for pyrite precipitation, since forms an environment where the sulfide produced via the decay of the organism can become concentrated. Since many of these fossils could potentially also be trace fossil burrows, an alternate explanation for the annular pyrite association is as difference in sediment porosity in backfill structures (see KUMIP 377069, 314112, Fig. 3.7 a). Without additional morphological or taphonomic data, it is difficult to distinguish between a lightly-pyritized worm and a lightly-pyritized burrow.

The presence of pyrite on the boundary of the fossil and gut (KUMIP 377069, 314202, Fig. 3.7 b) can be explained by the geometry of compression. If one considers a cylindrical organism covered in pyrite particles prior to compaction, then a disproportionate amount of pyrite will be present where the slope of the body wall is the highest—that is, the sides. Thus, if the specimen is compressed vertically, with volume-loss of the carbonaceous body, the majority of the pyrite will remain at the sides. The same phenomenon will apply to pyrite precipitation in the gut. It stands to note that, if the gut

wall were not preserved, KUMIP 377069 and 314202 would be indistinguishable from trace fossils.

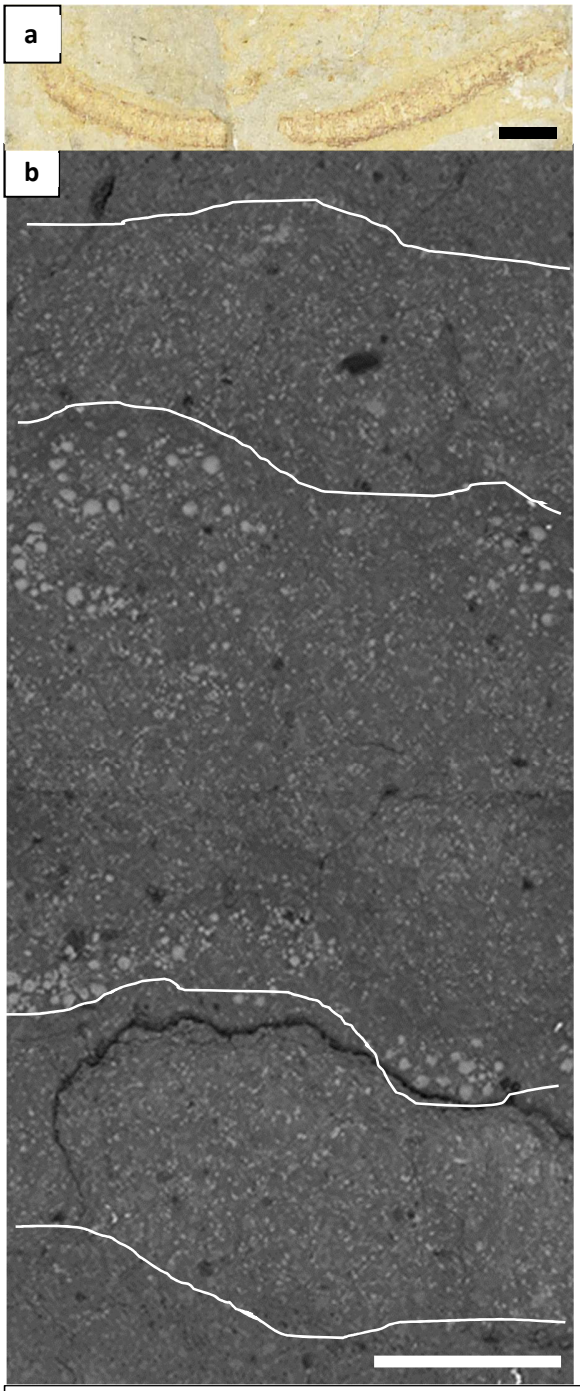

Three-dimensional pyritization is visible in KUMIP 314159 and 293598. In the case of KUMIP 314159, the three-dimensional pyritization occurs intermittently on the length of the organism (Fig. 3.8 a). It is considered to be a gut tract, since these areas are much narrower than the total fossil. Areas outside of the inferred gut are preserved as an elevated occurrence of pyrite framboids and euhedra. These are areas which exhibit large pyrite euhedra are overgrown by acicular pyrite crystals (Fig. 3.8 b). KUMP 293598 is the other case of three-dimensional pyritization. The pyrite in KUMIP 293598 is comprised of large, partly intergrowing pyrite euhedra (Fig. 3.9 b). Three-dimensional pyritization like

Figure 2.3.2.1 KUMIP 377069 (a) Optical image. Note annular features and prominent fossil boundary visible via red coloration. (b) BSE image. Large framboids denote boundary of gut tract, small pyrite particles are characteristic of the body. Outlined for clarity. Scale bars: a=1 cm, b=500 µm.

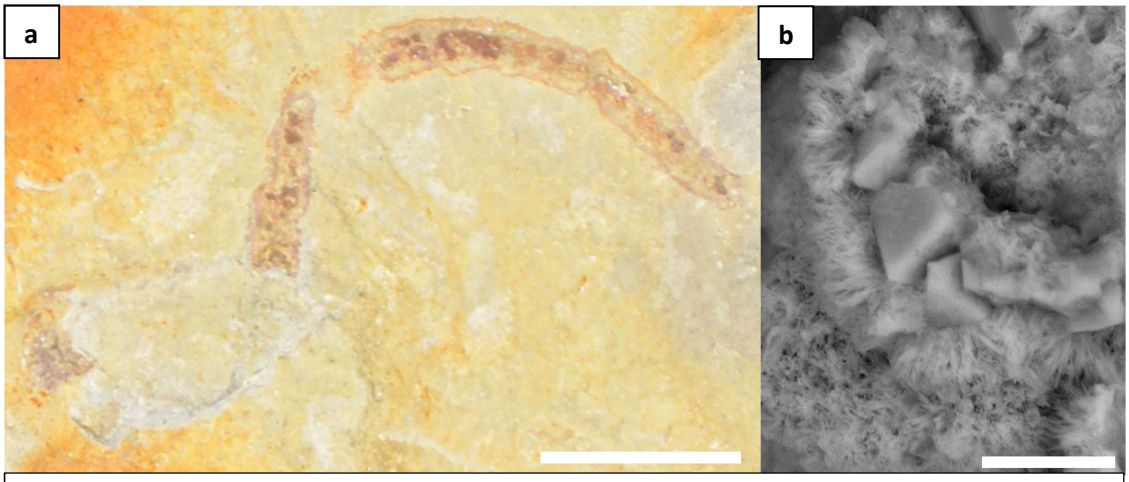

Figure 3.8 KUMIP 314159 (a) Optical image. (b) Euhedra overgrown with acicular crystals. Inset of b shown with arrow in a. Scale bars: a=1 cm, b=5 μm

this probably began when there was some void space, ideally before the collapse of the organism. The pyritization is so extensive that it requires an outside source of sulfide. It is possible that early mineralization stabilized the gut, extending the time before the gut collapses.

The most unusual kind of pyritization seen in this sample material is KUMIP 314253 (Fig. 3.9 a). It is dubiously catalogued as *Belorhaphe*, a trace fossil. The pyrite texture seen in KUMIP 314253 is pyrite framboids in and a groundmass of microcrysts. The most strikingly peculiar aspect of the pyrite framboids is that some of them appear to be overgrowing the others (Fig. 3.9 c). This texture could have ramifications for the mystery of how pyrite framboids form (See 2.2). Another unusual framboid is from KUMIP 314147. This "framboid" is an aggregate of spherical, not polygonal objects, which are coated in pyrite (Fig. 3.9 d). The framboidal object from KUMIP 314147 meets my criteria for a probable bacterial fossil (See 2.3).

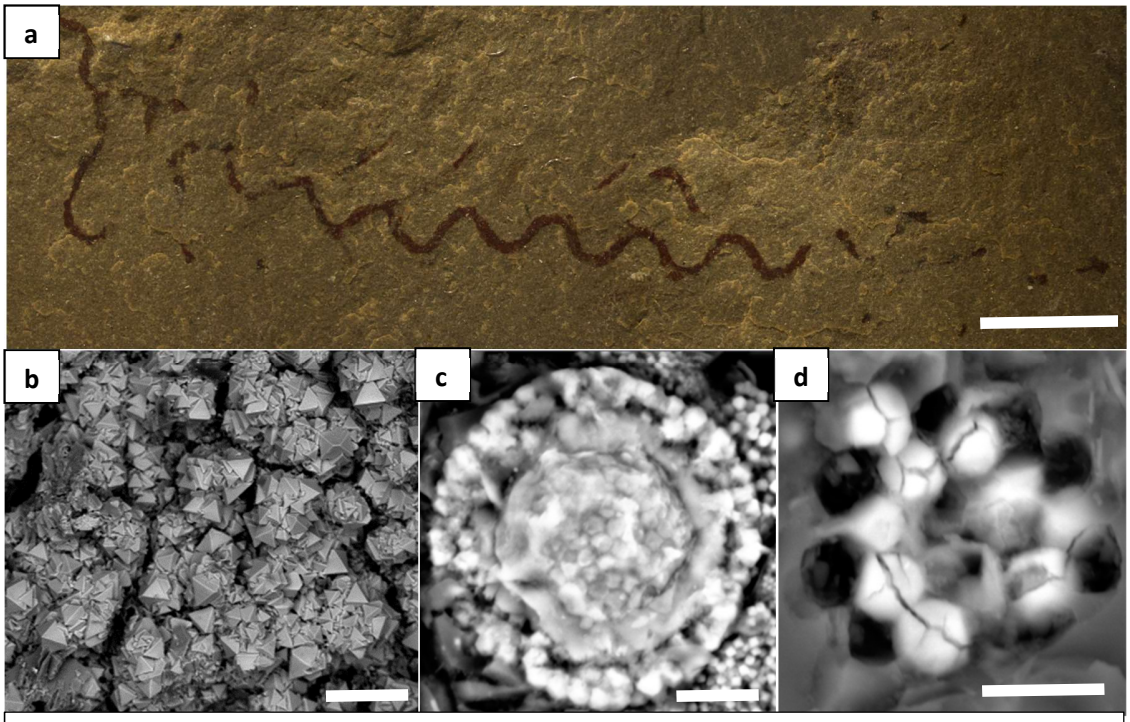

Figure 3.9 Unusual pyritization. (a) Optical image of KUMIP 314253. (b) Three-dimensional pyritization of KUMIP 293598. (c) Nested framboid from KUMIP 314253 (d) Probable bacterial fossil from 314147.Scale bars: a=5 mm, b=100 µm, c&d=5 µm.

3.2.3 Clay association

There are two conspicuous cases of clay association among the vermiform specimens, KUMIP 314186 and 293611 (Tab. 3.2). In KUMIP 314186, the clay association consists of orange clay laths (~40 µm wide and ~5 µm long) oriented perpendicular to the organic carbon film (Fig. 3.10 a). It may be void-filling, or a replacement texture. The carbon film does not bear an impression of the laths, so it is presumed that the clays grew on the carbon film, rather than the film forming on pre-existing laths. Unlike in KUMIP 293611, the fossil-associated clays are very fine-grained, even more so than the host rock (Fig. 3.16 a). Another striking thing about KUMIP 314186 is its vivid red color (Fig. 3.10 b).

Though eldonid KUMIP 314051 looks exceptionally kerogenized to the naked eye (Fig.3.2), only clay minerals are apparent in microanalysis. The morphological features in

		O	C	Si	Al	Fe	P	Ca	Mg	Ti	Na
KUMIP 314186	HR	59.788	13.88	14.318	7.414	2.026	2.224	0	0.254	0.062	0.032
	Fossil Clays	58.77	15.74	10.78	9.41	2.06	2.77		0.21		0.26
		52.28	21.94	9.5	8.06	5.03	2.71		0.48		
		58.01	15.98	9.42	7.91	5.98	2.53		0.17		
KUMIP 293611	HR	56.078	19.406	14.244	6.562	1.024	1.624	0.072	0.642	0.304	0.044
	Fossil Clays	59.21	15.79	13.45	6.77	2.29	1.89		0.52	0.07	
		52.27	27.32	11.9	3.18	4.07	0.71	0.16	0.4		
		56.35	23.71	8.83	7.29	1.31	1.93		0.3	0.06	0.21

Table 3.2 EDS fossil-clay compositions compared to the average host rock composition for specimens with prominent fossil clays. Values in atomic percentage.

the fossil appear to consist of an elevated concentration of clay flakes or tabulae which are distinguishable in backscatter due to their elevated iron concentration (Fig. 3.11 a, b, Tab 3.3). These clays replicate both internal and external features, whereas authigenic clays would be expected to replicate only external features. The iron-clays in the gut are unlikely to be ingested clays, since they are so different than the clays of the host rock. It is more likely that these clays replaced some precursor that was present in initial fossilization, such as kerogen or organic carbon. One problem with the replacive interpretation is that the carbon in no other specimen exhibits this kind of replacement.

Some samples (like KUMIP 204770) exhibit a textural difference between the clays of the fossil and host-rock (Fig. 3.11). Fossils are generally smooth, and rocks are generally rough. Since the host rock of these fossils is argillaceous, and variable across micron-scale distances, it is difficult to disentangle potential compositional fossil/host rock compositional differences, especially considering the micron-scale interaction volume for EDS signal generation. To identify generalized differences between fossil and host rock, a discriminant analysis was run on the most abundant elements (8 elements, accounting for

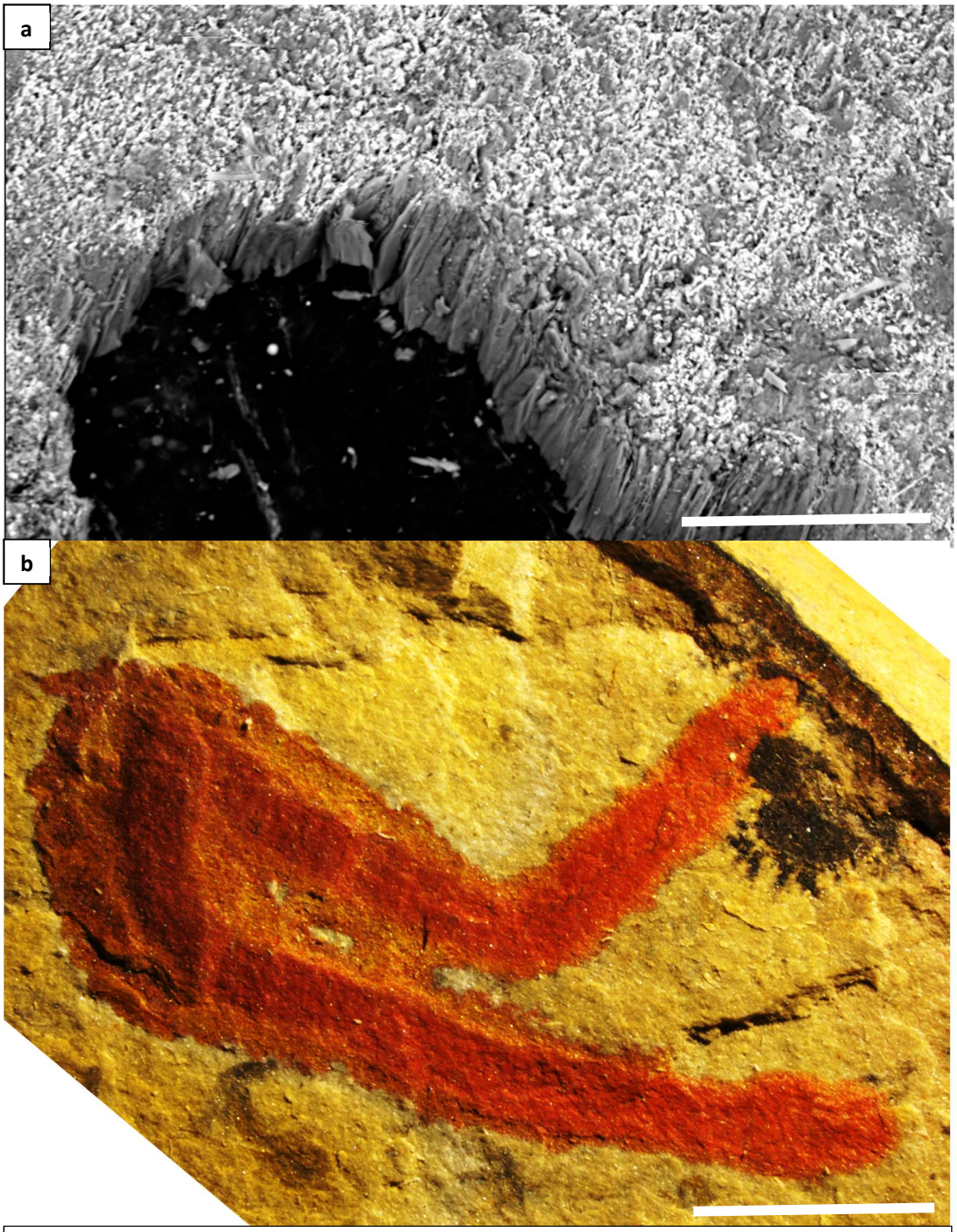

Figure 3.10 Fossils with unusual clay association. (a) BSE image of the clay association of KUMIP 314186, adjacent to the carbon film (b) Optical image of KUMIP 293611. Scale bars: a=100 µm & b=5 mm

more than 99% of the composition of the specimens) from a set of 319 EDS points collected from the argillaceous parts of fifteen vermiform fossils and their rocks. The values were

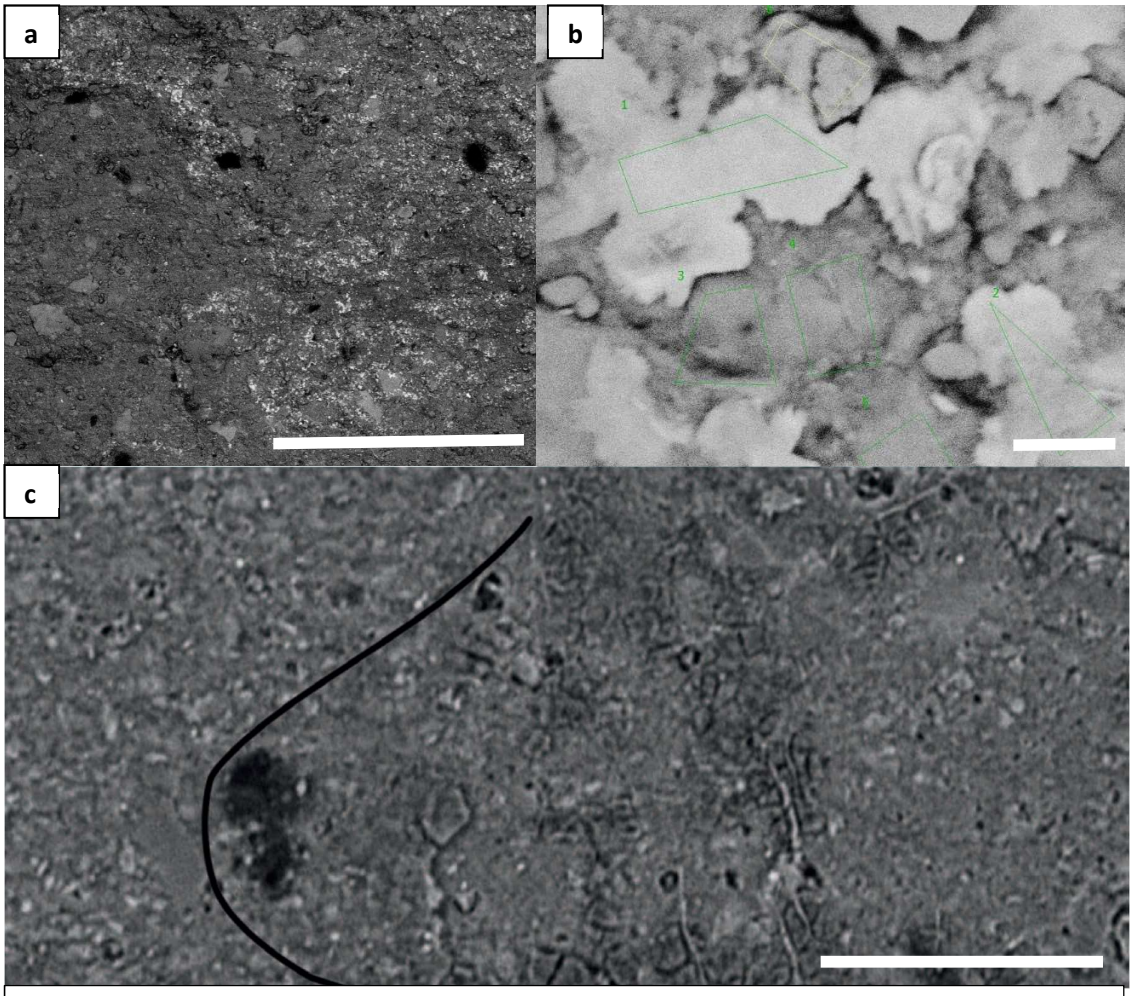

Figure 3.11 BSE image of clay associations (a) BSE image of the tip of the oral tentacles. Due to the high iron content, the clays exhibit bright signal in BSE (b) Clays in the alimentary canal near the boundary between the mid- and hindgut. Shows zones of table 3.3 (c) Textural difference in clays of KUMIP 204770. Fossil (right) and host-rock (left). Boundary in black. Scale bars: a=300 µm, b=3 µm, c=100 µm.

arcsine transformed to prevent highly abundant elements like oxygen from dominating the variation. The discriminant analysis works first by transforming the data to minimize within-group variation, then finding the multivariate direction of maximum between-group variation (Hammer, Harper and Ryan, 2001).

	Zone1 Fe	Zone2 Fe	Zone3 Blank	Zone4 Ca	Zone5 Mg	Zone6 CO_3	Mean
Carbon	10.33	10.96	10.43	11.33	9.93	15.86	11.47
Oxygen	63.82	64.59	63.29	63.52	64.37	63.21	63.80
Sodium	0.46	0.37	0.25	0.47	0.48	0.28	0.39
Magnesium	1.26	0.99	1.23	1.86	2.39	0.81	1.42
Aluminium	5.79	5.72	6.45	6.17	6.23	4.24	5.77
Silicon	11.02	11.13	14.26	11.74	11.90	8.47	11.42
Potassium	1.11	1.13	1.35	1.33	1.03	0.81	1.12
Calcium	1.47	1.41	1.35	2.09	1.21	5.04	2.10
Iron	4.73	3.71	1.39	1.48	2.47	1.27	2.51

Table 3.3 EDS fossil-clay compositions from Fig. 3.11. (KUMIP 314051) Atomic percentages.

The discriminant analysis produced the following discriminant function:

$$-8.957*\mathrm{Mg} + 6.999*\mathrm{Fe} - 6.943*\mathrm{K} +$$

$$3.494*\mathrm{Si} + 2.163*\mathrm{Al} + 1.345*\mathrm{Ca} - 0.826*\mathrm{O} + 0.080*\mathrm{C}$$

If the EDS compositional data of a point were entered into this discriminant function (as an atomic percentage), the result would be the discriminant value (DV) of that point. Fossil-like compositions will plot as positive values, and host-rock-like compositions will plot as negative. For more information on the methodology, and an archive of the points used, see Broce and Schiffbauer, 2017. The discriminant analysis worked as advertised, and all of the specimens showed higher average discriminant values than their host lithologies, except for KUMIP 314111, due to its high magnesium and potassium concentrations. A Hotelling's T^2 test showed a significant ($p = 0.0026$) overlap between the mean fossil and host-rock compositions. The reclassification percentage of the points was fairly poor at 58.42%, which is unsurprising considering how much overlap exists between the points.

One potentially confounding factor with this discriminant analysis is the dependence of the discriminant function on iron. Since framboidal pyrite association is a common form of fossil preservation in these specimens, it is possible that the preferential iron association is a result of pyrite. Though I was careful to choose only points that appeared to be devoid of pyrite, I based these decisions on BSE images. The interaction volume (signal generation depth) is higher for EDS than BSE, so the electron beam could have been interacting with hidden pyrite. Rerunning the discriminant analysis without iron produced a Hotellings T^2 difference of means was insignificant ($p = 0.361$). This means that without iron, the fossil clay compositions are not significantly different from the host-rock compositions. Magnesium is the largest contributor to the discriminant value, but when magnesium was excluded, the Hotelling's T^2 and reclassification percentage wasn't much worse. The difference in composition, whether pyrite, clay or iron staining, is an important component that separates these fossils from their host-rocks. Even if it is an association of iron-bearing clay, it does not necessarily mean it is authigenic. The near-ubiquity of pyrite in these specimens means that alteration of clays from the oxidation of pyrite (as in Gaudin et al, 2005) could have produced a fossil-associated iron-clay signal.

The discriminant analysis used here was modeled after that of Selly, 2015, who ran a similar analysis on a number of fossils, mostly from anomalocaridid mouth-part exuviae from the Cambrian HRE (mostly Pioche Formation). The discriminant functions generated using different fossils are not necessarily comparable, but due to the similar locality, Selly's (2015) discriminant analysis could be a useful comparison. It's possible that the majority of the differences would be a result of taxonomic differences. The use of weight percent rather than atomic percent makes direct comparison different between Selly's (2015)

discriminant analysis and that of Broce and Schiffbauer (2017), but, generally, lighter elements like carbon and magnesium would have a larger coefficient in the weight percent discriminant function, and heavier elements would have a smaller coefficient. The two functions are largely similar, but silicon is negative in the Selly (2015) function, indicating that it associates more commonly with the host-rock than the fossil.

3.2.4 Other mineral associations

Stoichiometrically, for a point that contains clays, calcite and kerogen, the problem of distinguishing between clay-hosted and calcite-hosted calcium using only EDS data is unsolvable. Nevertheless, this sample material contains clear-cut instances of taphonomic calcite association. KUMIP 314186 exhibits a calcite crust. Since this sample is buried in calcite silts, it is possible that this calcite could have been mobilized to the fossil area at any time in its history, but probably a time when there was void space to fill. Calcite was found to be generally fossil associated in the discriminant analysis (see 3.2.3). One potential mechanism for calcite precipitation in the vicinity of fossils is the production of bicarbonate via sulfate reduction, like in microbial mats (Gallagher et al, 2012).

Some samples exhibit barite. In KUMIP 314111, the barite is bladed and mostly found around the exterior of the fossil (Fig. 3.12 a). Barite needles are found in KUMIP 314191. The barite in KUMIP 314215 is located in the gut tract (Fig 3.12 b). KUMIP 314096 exhibits large (> 1mm) patches of barite, probably void-filling late-stage barite (Fig. 3.12 c). The mechanism proposed in Broce and Schiffbauer, 2017 to explain barite association with soft-bodied fossils is as follows: Barium is a redox-sensitive metal, but its solubility is not determined by oxygen concentrations. Rather, barium requires sulfate to

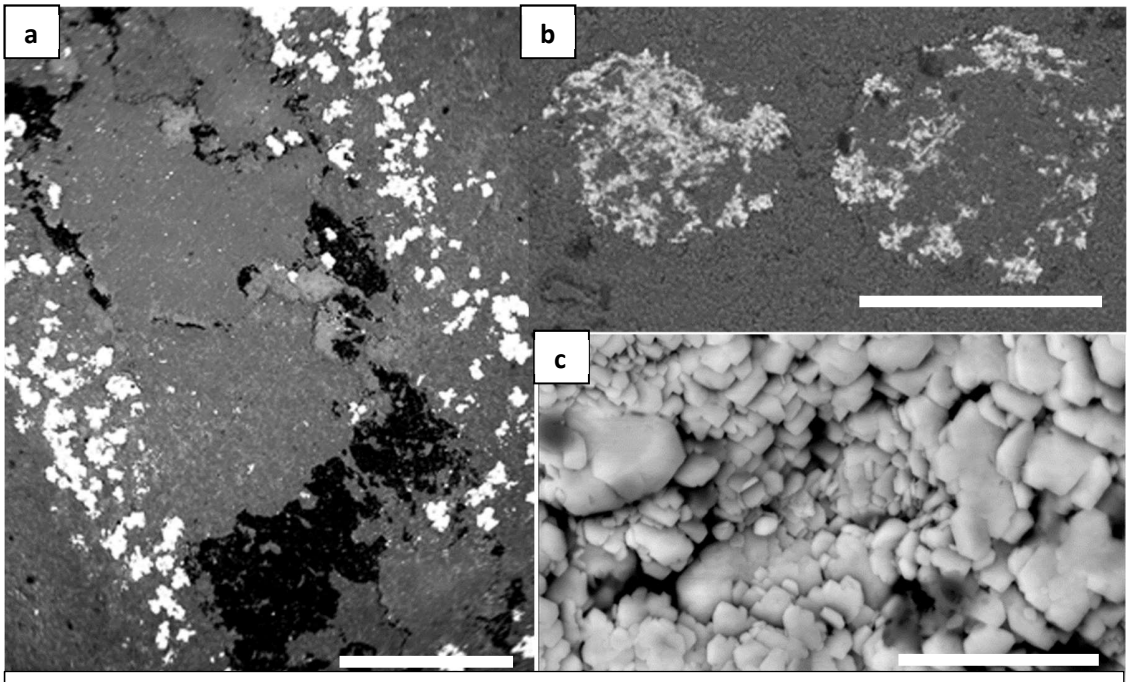

Figure 3.12 Barite-fossil association. (a) KUMIP 314111, showing carbon (black) and barite (white). (b) KUMIP 314215. (c) Texture of barite from KUMIP 314096. Scale bars: a=1 mm, b=300 μm, c=10 μm.

precipitate out of solution. Thus, an oxygen rich, barium-bearing fluid can exist as long as no sulfate is present. The oxidative weathering of pyrite produces sulfate ions, which will cause barium to precipitate out. This process has been proposed, but not for fossil-associated barite (Hanor, 2000). Supporting evidence for this mechanism includes the pyrite in KUMIP 314186. The only pyrite present in KUMIP 314186 is pyrite framboids trapped within a carbon film. The barite in KUMIP 314186 occurs as needles and stellae. Some of these barite crystals are surrounded by clay minerals that have a displacement texture (Fig. 3.13 a), illustrating that the barite must have grown *in situ*.

Monazite is a mineral which has previously only been found in fossil association in the HRE (Moore and Lieberman, 2009), but no previous mechanism had been proposed.

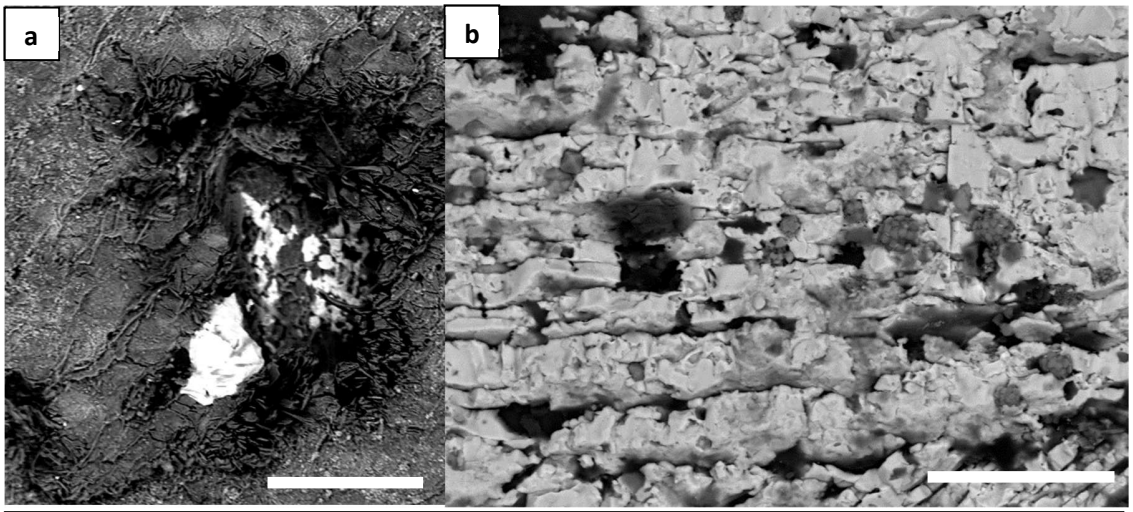

Figure 3.13 Unusual mineral associations. (a) KUMIP 314186, showing clay textures around barite grain. (b) Section of monazite from KUMIP 314114. Note that the pyrite framboids have a lower backscatter coefficient than monazite. (c) Scale bars: a=100 μm, b=40 μm, c=10 μm.

In this study, it is present in KUMIP 314114 and 314186 (Fig. 3.13 b). Monazite is a light rare-earth-element (cerium, lanthanum, neodymium, thorium) phosphate mineral. It is commonly precipitated during dissolution of apatite (Spear and Pyle, 2002). Since calcium phosphate minerals are commonly found in association with fossils, including the gut tracts of arthropods in BST lagerstätten (See 2.3.1), alteration of phosphate to monazite is a plausible mechanism for fossil association of monazite. Alternately, the monazite could have grown authigenically (Čopjakováab, Novákb and Franců, 2011), but it is uncertain whether this could have produced a fossil-association. Calcium phosphate comprises the vast majority of KUMIP 314107 (Fig. 3.14). Some parts of KUMIP 314107 contain clay minerals. Due to its composition and ropy appearance, it is likely to be a coprolite, though, at almost 2 cm wide, it must have been excreted by one of the largest Cambrian animals in the sea.

Figure 3.14 KUMIP 314107. Scale bar=1 cm

3.2.5 Gut contents

The most conspicuous gut contents in these samples is located in the eldonid KUMIP 314106. Within the midgut, this fossil contains a triangular object of roughly the same size and shape as a hyolith (Cambrian enigmatic organism, usu. interpreted as a primitive mollusk), as well as some dark, carbonaceous dots (Fig. 3.15 a). A hyolith shell within an eldonioid gut would suggest a hunting or scavenging lifestyle for *Eldonia*. Via microanalysis, the supposed hyolith was found to be no be lacking any differential texture. The only compositional difference was slightly elevated carbon concentrations. (Tab. 3.4). The feature seems to be strictly topographic. The location of the "hyolith" shows that it is merely an artifact of the alimentary canal forming a low angle with the boundary of the midgut (Fig. 3.15 b). The dots had compositions comparable to kerogenized organic carbon, and thus may be true gut contents (Tab. 3.4).

On one end of KUMIP 314114, a small, reflective object is present (Fig. 3.15 c & d). It appears to be a ~1mm linguilid brachiopod shell. An organic carbon film is present. The surface of the shell is strongly etched (Fig. 2.3.5 c). The etching could be indicative of having spent time in an acidic digestive tract. KUMIP 314114 may have had a predatory life mode.

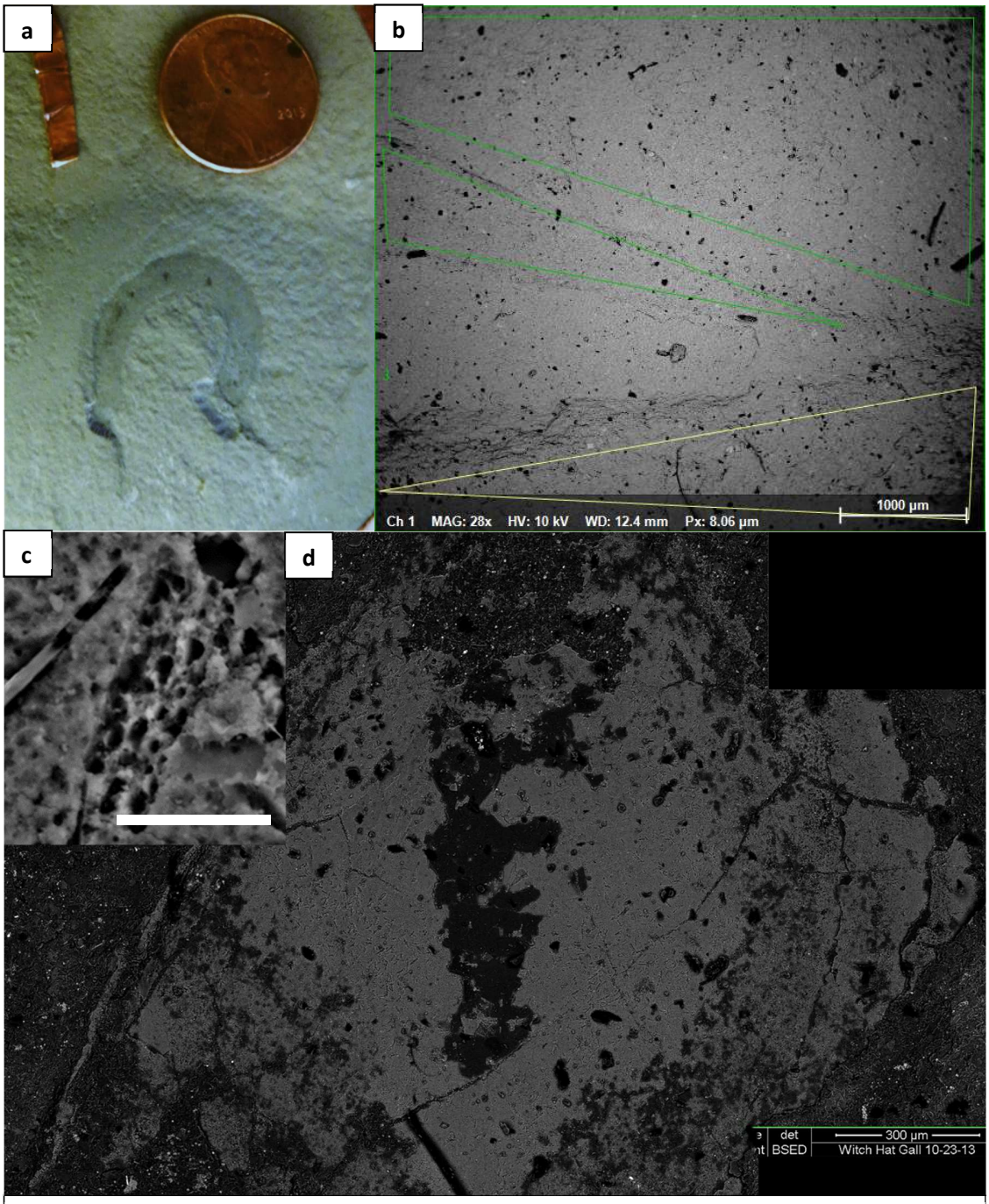

Figure 3.15 Unusual gut contents. a & b are KUMIP 314106. b &c are KUMIP 314114. (a) Optical image. Arrow indicates putative hyolith. (b) BSE image of putative hyolith, corresponding to zone 2. (c) Etching of lingulid shell. Scale bar=10 µm (d) Lingulid shell.

Small carbonaceous objects are kerogenized within KUMIP 293611 (Fig. 3.1 a).

The aluminosilicified medial region is dotted with small, roughly circular organic carbon

	Bkgrnd	Hyolith	Dot 1	Dot 2
Al	7.6	7.2	5.8	7
Ca	1.4	1.5	0.7	0.8
C	9.2	11.2	19.5	13.6
Fe	0.8	0.8	0	0
Mg	1.6	1.6	1.2	1.2
N	0	0	2.5	1.8
O	62.2	60.1	58.5	61.4
K	1.7	1.6	1	1.3
Si	15	15	10.2	12.4
Na	0.5	0.5	0.5	0.5

Table 3.4 EDS data from KUMIP 314106 as atomic percent. "Bkgrnd" and "Hyolith" correspond to zones 1 and 2 from Figure 2.5.3.1b.

blobs. These resemble acritarchs. It is unclear whether these objects are gut contents, gut microbiota, contamination or what.

In some parts of the pyritized gut tract of KUMIP 314159 the pyrite encrusts clay minerals (Fig 3.16 b). These clay particles must have been in the gut prior to pyritization, and are inferred to be ingested particles. On this basis, KUMIP 314159 may be an infaunal worm. The clay particles exhibit lower organic carbon than the host rock (Table 3.5). It's possible that digestive processes removed organic carbon and/or carbonate from these particles, resulting in lower carbonate concentration.

3.2.6 Spatial relationships between mineral modes in complex specimens

The minerals in KUMIP 314114 seems erratic, but there are some visible patterns. Monazite occurs as isolated blades, some of which exhibit twinning. Some areas show very extensive monazite mineralization, in association with pyrite framboids. In addition to isolated pyrite framboids, there are pockets of concentrated pyrite framboids, and microcryst groundmass (Fig. 3.16 c). Barite and clay particles are also present, as well as one unidentified calcium-rich mineral (Fig. 3.16 d & e, Tab. 3.6). The pattern of mineral

	O	C	Si	Al	Fe	K	Ca	Mg	Ti	Na	P	Cl	Cu
Mean Fossil	58.3	12.2	13.4	8.79	3.39	2.66	0.47	0.34	0.06	0.17	0.06	0.02	0.02
Gut-hosted	62.5	8.86	12.2	10.3	2.66	3.19		0.19					
	70.3		13.7	11.5	1.35	2.87		0.12					
	54.5		34.8	3.85	4.56	0.23		1.53					
	53.9		19.7	16.3	2.19	7.91							

Table 3.5 EDS data from KUMIP 314159 as atomic percent. Compares composition of pyrite-encrusted clay particles within the gut tract (like Fig. 2.3.6.1b to the average clay composition elsewhere on the fossil.

association in KUMIP 314111 is concentric (Fig. 3.12 a). It has a prominent carbon film on the interior, surrounded by clay minerals, which are surrounded by barite.

The most complex mineral relationships in this study are contained in KUMIP 314186. There are two concentric regions, presumed to be gut and body of KUMIP 314186 (Fig. 3.6 a). The interior is a prominent carbon film, which contains pyrite framboids (Fig. 3.6 b). The underside of the carbon film is intermittently encrusted with calcite and orange, iron-rich clay laths (Fig. 3.10 a). Barite needles and stellae occur around all sides of the fossil, but most abundantly on the lateral boundaries of the carbon film. Some of these show displacement textures. The fossil is directly overlain by fining-upward calcite silts (Fig. 3.17), indicating that it was on the surface of the sediment when it was buried by a calcareous turbidite.

3.3 Conclusions

3.3.1 Advancements

In the analysis of the fossils of the HRE, the fossils were found to exhibit characteristics which have previously been observed in other specimens. Some bore new characteristics, which have not been described before. New explanations for existing phenomena were also proposed.

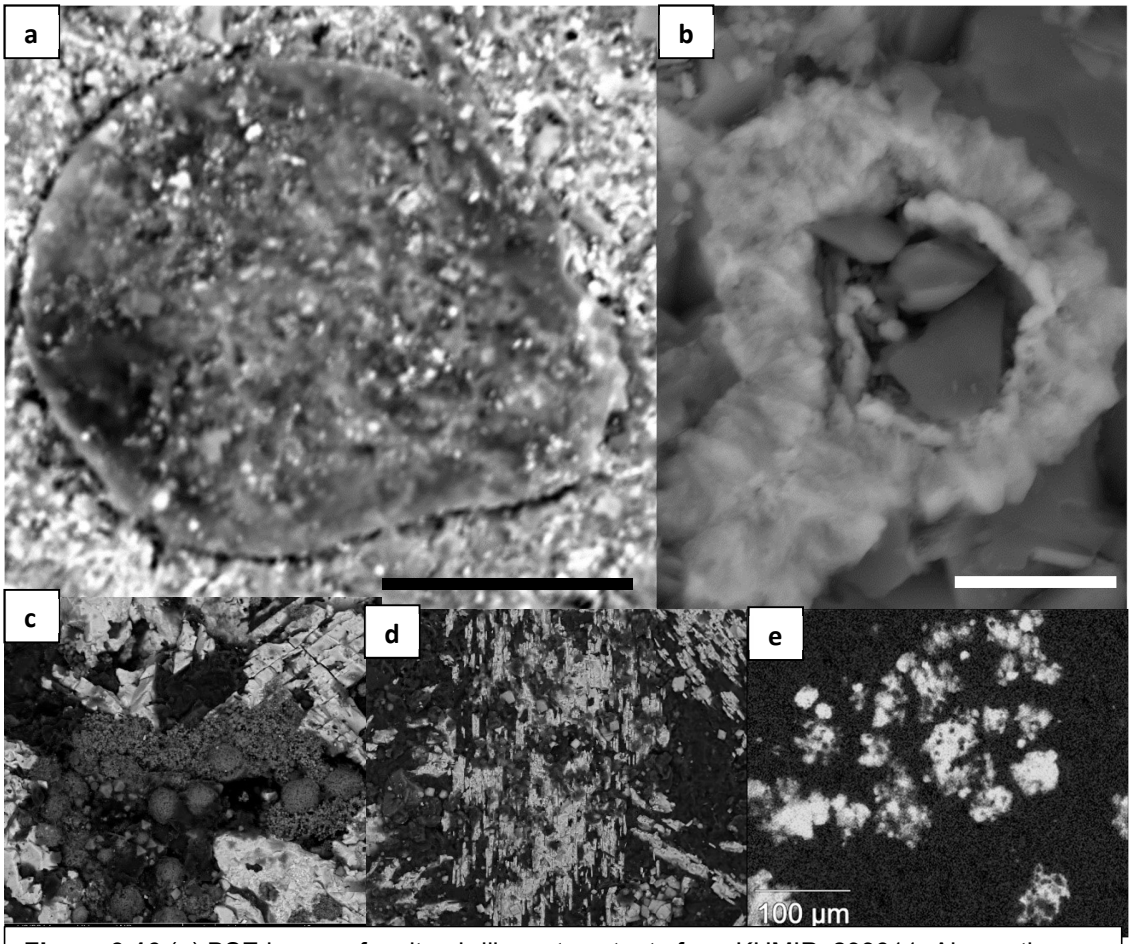

Figure 3.16 (a) BSE image of acritarch-like gut contents from KUMIP 293611. Also notice fine-scale clay texture. (b) BSE image of clay particle encrusted with pyrite from KUMIP 314159. See compositional information in Tab. 2.3.5.2. (c) BSE image of pyrite-rick pocket inside of a monazite zone in KUMIP 314114. (d) BSE image of location of the KUMIP 314114 calcium anomaly. Bright areas are monazite, but area also includes clay minerals, pyrite, and barite. (e) EDS Calcium element map of d. For more detailed compositional information, see Tab. 2.3.6. Scale bars are a=50 µm, b=5 µm and c=40 µm

Certain spatial relationships are explained as compression artifacts, such as the presence of elevated concentrations of pyrite around the borders of fossils and the borders of gut tracts, and the preferential kerogenization of interannuli. The preferential association of pyrite with interannuli is a result of each interannulus acting as a region where sulfide can accumulate. The greater detail of *Ottoia* fossils relative to the *incertae sedis* was suggested to be a result of the chitin content of priapulid integument. Two instances of three-dimensional gut tract pyritization are identified, and are suggested to be a result of

C	O	Mg	Al	Si	P	S	K	Ca	Ti	Mn	Fe
											2.70
	43.33		2.07	11.88	1.90	0.73	1.10	35.92	0.38		
				3.04							0.83
	43.77		3.22			1.24	0.19	47.73			
8.35				0.42							1.06
	41.27	0.24	0.53			0.63	0.40	46.78		0.31	
				3.17							
17.65	46.22	0.19	2.24		0.54	0.31	0.47	12.93			16.28
				1.38							
23.67	39.51	0.15	0.83		0.12	0.47	0.18	17.56			16.14

Table 3.6 EDS data of the calcium anomaly of KUMIP 314114 in atomic percent.

early stabilization and later overgrowth. Framboids overgrowing framboids are reported. One instance of a probable fossilized bacterial colony is identified.

Replacive clay textures were identified in one worm and one *Eldonia* fossil. The latter exhibited excellent anatomical detail. Fossil barite association is identified with several modes of growth, and suggested to be a result of oxidative pyrite weathering. Monazite associations are also identified, and suggested to be altered from fossil-associated apatite, which could have occurred at any stage of authigenesis or diagenesis. A brachiopod was found to be probable worm gut contents. Spherical carbonaceous objects are possible gut contents. Hyolith gut contents for *Eldonia* was refuted.

3.3.2 General taphonomy and alteration model of BST HRE fossils

Although the vermiform fossils of the HRE display wildly different styles of preservation, they can be understood in a common framework of preservation and alteration. The fossil material was buried by turbidites. Most of the fossil material was either rapidly buried after death, or already in the subsurface at the time of obrution. Infaunal organisms could suffocate as a result of rapid sedimentation, and the establishment

of anoxic sediment conditions. Once anoxia became established, SRBs went to work, providing the sulfide for pyrite precipitation.

Figure 3.17 BSE image of the cacitic turbidite which overlies KUMIP 314186.Scale bar is 100 µm.

Organic tissues are favorable sites for pyrite precipitation, and the potential for pyrite precipitation would have been vastly improved in areas that had favorable geometric conditions for sulfide concentration, such as annulations and digestive tracts. Whatever objects were located in the gut tracts (e.g. detrital clays) became trapped within the minerals that precipitate in the gut, whether they be pyrite or apatite. The bicarbonate produced by SRBs could have prompted the precipitation of early calcite cements (Reid et al, 2000), helping to seal the fossil and inhibit further decay. Some methanogenesis and fermentation may occur after sulfate reduction becomes unfeasible. Chitin, like that found in priapulid integument, has a greater potential to survive decay (Briggs, Evershed and Lockheart, 2000). If oxic conditions resumed when decay slowed, pyrite oxidation could have produced iron-smectites (Gaudin et al, 2005).

Further pyritization may occur after decay ceased, causing pyrite overgrowth. If initial pyritization was sufficient to stabilize the gut, the gut may infill with pyrite entirely. Thermal alteration of kerogen would cause volumetric reduction of remaining kerogen, and

the remnants may form polygonal cracks, or envelop pyrite particles. Kerogen maturation progressed until only inert kerogen remained. Chitin, like that found in priapulid cuticle, preferentially converted to inert kerogen. Fluids rich in rare-earth elements permeated the region, replacing the calcium in apatite with cerium, lanthanum, neodymium and thorium.

Oxidative weathering converted pyrite to iron oxides. In cases where barium-rich oxic fluids interacted with the rock, the pyrite oxidation produced local barite precipitation. Pyrite that was interred within a carbon film was protected from oxidation and baritization. Any void spaces still extant during oxidative weathering could have been filled by iron oxides, calcite, barite or clay minerals. For more information, please refer to Broce and Schiffbauer, 2017.

REFERENCES

Broce, Jesse S. and James D. Schiffbauer (2017) "Taphonomic analysis of Cambrian vermiform fossils of Utah and Nevada, and implications for the chemistry of Burgess Shale-type preservation" *Palaios* 32:600-619

Brett, Carlton E., Peter A Allison, Michael K. DeSantis, W. David Liddell and Anthony Kramer (2009) "Sequence stratigraphy, cyclic facies, and *lagerstätten* in the Middle Cambrian Wheeler and Marjum Formations, Great Basin, Utah" *Palaeogeography, Palaeoclimatology, Palaeoecology* 277:9-33

Briggs, Derek E. G., (1999) "Molecular taphonomy of animal and plant cuticles: selective preservation and diagenesis" *Philosophical Transactions of the Royal Society of London B* 354:7-17

Briggs, D. E. G., R. P. Evershed and M. J. Lockheart (2000) "The biomolecular paleontology of continental fossils" *Paleobiology* 26:169-193

Butterfield, Nicholas J. (1990) "Organic preservation of non-mineralizing organisms and the taphonomy of the Burgess Shale" *Paleobiology* 16:272-286

Butterfield, Nicholas J. (1996) "Fossil preservation in the Burgess Shale: Reply" *Lethaia* 29:109-112

Butterfield, Nicholas J., Uwe Balthasar and Lucy A. Wilson (2007) "Fossil diagenesis in the Burgess Shale" *Palaeontology* 50:537-543

Caron, Jean-Bernard, Simon Conway Morris and Degan Shu (2010) "Tentaculate Fossils from the Cambrian of Canada (British Columbia) and China (Yunnan) Interpreted as Primitive Deuterostomes" *PLoS ONE* 5:e9586

Chen Jun-yuan, Zhu Mao-Yan and Zhou Gui-Qing (1995) "The Early Cambian medusiform metazoan *Eldonia* from the Chengjiang Lagerstätte" *Acta Palaeontologica Polonica* 40:213-244

Clarke, John M. (1900) "Paropsonema cryptophyta; a peculiar echinoderm from the Intumescens-zone (Portage beds) of western New York" *Bulletin of the New York State Museum* 39:172-186

Cohen, K.M., D. A. T. Harper, P. L. Gibbard (2017) ICS International Chronostratigraphic Chart 2017/02. International Commission on Stratigraphy, IUGS. www.stratigraphy.org

Čopjaková, Renata, Milan Novák and Eva Franců (2011) "Formation of authigenic monazite-(Ce) to monazite-(Nd) from Upper Carboniferous graywackes of the Drahany Upland: Roles of the chemical composition of host rock and burial temperature" *Lithos* 127:373-385

Dzik, Jerzy, Zhao Yuanlong and Zhu Maoyan (1997)"Mode of life of the Middle Cambrian eldonioid lophophorate *Rotadiscus*" *Palaeontology* 40:385-396

Eddy, Julie D. and Linda B. McCollum (1998) "Early Middle Cambrian *Albertella* Biozone Trilobites of the Pioche Shale, Southeastern Nevada" *Journal of Paleontology* 72:864-887

Elrick, Maya and Anna C. Snider (2002) "Deep-water stratigraphic cyclicity and carbonate mud mound development in the Middle Cambrian Marjum Formation, House Range, Utah, USA" *Sedimentology* 49:1021-1047

Kloss, Tristan J., Stephen Q. Dornbos, Jun-Yuan Chen, Lindsay J. McHenry, Pedro J. Marenco (2015) "High-resolution geochemical evidence for oxic bottom waters in three Cambrian Burgess Shale-type deposits" *Palaeogeography, Palaeoclimatology, Palaeoecology* 440:90-95

Gaines, Robert R. and Mary L. Droser (2003) "Palaeoecology of the familiar trilobite *Elratia kingii*: An early exaerobic zone inhabitant" *Geology* 31:941-944

Gaines, Robert R., Martin J. Kennedy and Mary L. Droser (2005) "A new hypothesis for organic preservation of Burgess Shale taxa in the middle Cambrian Wheeler Formation, House Range, Utah" *Palaeogeography, Palaeoclimatology, Palaeoecology* 220:193-205

Gaines, Robert R. and Mary L. Droser (2010) "The paleoredox setting of Burgess Shale-type deposits" *Palaeogeography, Palaeoclimatology, Palaeoecology* 297:649-661

Gallagher, K. L, T. J. Kading, O. Braissant, C. Dupraz and P. T. Visscher (2012) "Inside the alkalinity engine: the role of electron donors in the organomineralization potential of sulfate-reducing bacteria" Geobiology 10:518-530

Garson, Daniel E., Robert R. Gaines, Mary L. Droser, W. David Liddell and Aaron Sappenfield (2011) "Dynamic paeaeoredox and exceptional preservation in the Cambrian Spence Shale of Utah" *Lethaia* 45:164-177

Gaudin, A., M. D. Buatier, D. Beaufort, S. Petit, O. Grauby and A. Decarreau (2005) "Characterization and Origin of Fe3+-montmorillonite in deep-water calcareous sediments (Pacific Ocean, Costa Rica Margin)" *Clays and Clay Minerals* 53:452,465

Hall, James (1847) "Paleontology of New York" vol. 1 Caroll & Cook Printers, NY

Hammer, Ø., D. A. T. Harper, and P. D. Ryan (2001) PAST. Paleontological Statistics Software Package for Education and Data Analysis: Palaeontologia Electronica, v. 4. http://palaeo-electronica.org/2001_1/past/issue1_01.htm

Hanor, Jeffrey S. (2000) "Barite-Celestine Geochemistry and Environments of Formation" *Reviews in Mineralogy and Geochemistry* 40:193-275

Jackson, Wayne D. and Grey Christiansen (1993) "International Strategic Minerals Inventory Summary Report—Rare-Earth Oxides" *U.S. Geological Survey Circular* 930-N

Liu, Yunhuan, Shuhai Xiao, Tiequan Shao, Jesse Broce and Huaqiao Zhang (2014) "The oldest known priapulid-like scalidophoran animal and its implications for the early evolution of cycloneuralians and ecdysozoans" *Evolution & Development* 16:155-165

Lyon, Eva (2011) *The interrelationship between the bio- and sequence stratigraphy of the Middle Cambrian Spence Shale of northern Utah and southern Idaho.* MS Thesis, Utah State University. ProQuest LLC. Ann Arbor, MI

MacGabhan, Breandán Anraoi (2012) "A Solution to Darwin's Dilemma: Differential Taphonomy of Ediacaran and Paleozoic Non-Mineralised Discoidal Fossils" PhD dissertation. National University of Ireland

Moore, Rachel A. and Bruce S. Lieberman (2009) "Preservation of early and Middle Cambrian soft-bodied arthropods from the Pioche Shale, Nevada, USA" *Palaeogeography, Palaeoclimatology, Palaeoecology* 277:57-62

Morris, S. Conway and R. A. Robison (1986) "Middle Cambrian priapulids and other soft-bodied fossils from Utah and Spain" *The University of Kansas Paleontological Contributions* 117:1-22

Muscente, A. D., James D. Schiffbauer, Jesse Broce, Marc Laflamme, Kenneth O' Donnell, Thomas H. Boag, Michael Meyer, Andrew D. Hawkins, John Warren Huntley, Maria McNamara, Lindsay A. MacKenzie, George D. Stanley Jr., Nancy W. Hinman, Michael H. Hofmann, and Shuhai Xiao (2017) "Exceptionally preserved fossil assemblages through geologic time and space" *Gondwana Research* 48:164-188

Orr, Patrick J., Derek E. G. Briggs, Stuart L. Kearns (1998) "Cambrian Burgess Shale Animals Replicated in Clay Minerals" *Science* 281:1173-1175

Perry, Rich and Mike Visher (2014) "Major Mines of Nevada 2014" *Nevada Bureau of Mines and Geology Speical Publication* P-26

Rees, M. N. (1986) "A fault-controlled trough through a carbonate platform: The Middle Cambrian House Range Embayment" *Geological Society of America Bulletin* 97:1054-1067

Richards, K. Sylvia (1978) "Epidermis and Cuticle" In Physiology of Annelids Ed. P. J. Mill. Academic Press, UK

Reid, R. P., P. T. Visscher, A. W. Decho, J. F. Stolz, B. M. Bebout, C. Dupraz, I. G. Macintyre, H. W. Paerl, J. L. Pinckney, L. Prufert-Bebout, T. F. Steppe and D. J. DesMarais (2000) "The role of microbes in accretion, lamination and early lithification of modern marine stromatolites" *Nature* 406:989-992

Schmidt-Rhaesa, A., 2013 "Priapulida" *Handbook of Zoology, Gastrotricha, Cycloneuralia and Gnathifera* Ed. Schmidt-Rhaesa. De Gruyter, Germany. 147-180

Selly, Tara Lee (2015) *Predators and predation in the Cambrian Period: Quantitative methods in taphonomy and paleoecology* M.S. thesis. University of Missouri

Simões, Marcello G., Sabrina Coelho Rodrigues, Juliana de Moraes Leme and Marcos Cesar Bissaro Júnior (2005) "The settling pattern of brachiopod shells: Stratigraphic and taphonomic implications to shell bed formation and Paleoecology" *Revista Brasileira de Geociências* 35:383-391

Spear, Frank S. and Joseph M. Pyle (2002) "Apatite, monazite and xenotime in metamorphic rocks" *Reviews in Mineralogy and Geochemistry* 48:293-335

Sundberg, Frederick A. and Linda B. McCollum (2000) "Ptychopariid Trilobites of the lower-middle Cambrian boundary interval, Pioche Shale, Southeastern Nevada" *Journal of Paleontology* 74:604-630

Vannier, Jean, Ivan Calandra, Christian Gaillard and Anna Żylińska (2010) "Priapulid worms: Pioneer horizontal burrowers at the Precambrian-Cambrian boundary" *Geology* 38:711-714

Van Roy, Peter (2006) "Non-trilobite arthropods from the Ordovician of Morocco" PhD dissertation, Ghent University.

Walcott, Charles D. (1911) "Middle Cambrian Holothurians and Medusae" *Smithsonian miscellaneous collections* 57:41-68

Zhang, Huaqiao, Shuhai Xiao, Yunhuan Liu, Xunlai Yuan, Bin Wan, A. D. Muscente, Tiequan Shao, Hao Gong and Guohua Cao (2015) "Armored kinorhynch-like scalidophoran animals from the early Cambrian" *Scientific Reports* 5:16521

CHAPTER 4: PROBLEMATIC DISCOIDAL FOSSILS FROM THE GIBSON JACK FORMATION OF SOUTHERN IDAHO

4.1 Introduction

The Gibson Jack Formation is a small shale formation that crops out in Southeastern Idaho. The only reported fossil occurrences from the Gibson Jack formation are two specimens of Naraoia, a stem-group arthropod from the. These naroiids exhibit goethite bumps, which were likely pyrites, originally (Robison, 1984). I collected samples from the locality described in Robison, 1984, which is a short ways up Gibson Jack Creek (marked g on Fig. 3.3). The Middle Cambrian Gibson Jack Formation at this locality consists of olive-to-tan metasomatized shales overlying a thick Precambrian quartzite. While no additional samples of Naroia were recovered, numerous macroalgae fragments and a discoidal fossil were discovered.

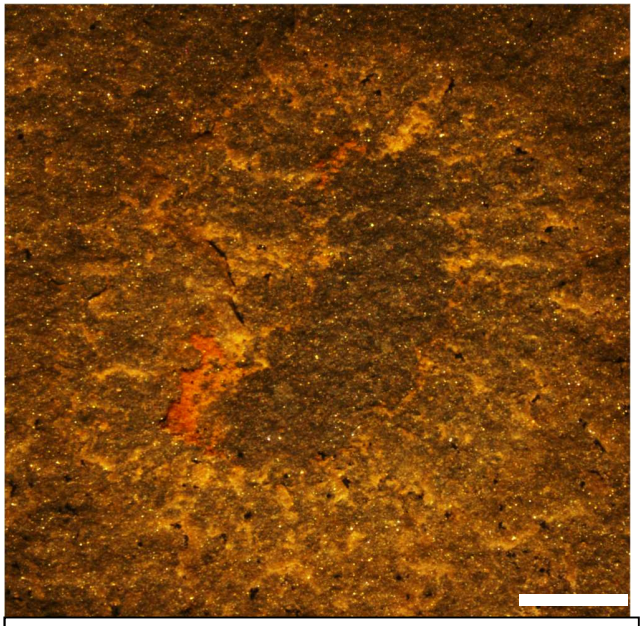

Figure 4.1 Optical image of discoidal fossil from Gibson Jack Creek. Scale bar= 1 mm

The discoidal fossil (Fig. 4.1) is five mm in diameter, consisting of a dark, crescent shape which resembles an eldonioid midgut. Both ends of the crescent shape are a light orange, but one end exhibits much more orange material than the other. Orange linear features radiate from the organism towards the outer boundary of the fossil. Outwardly,

Figure 4.2 Optical images of discoidal fossils from the Slate Mountain locality.

this combination of features matches that of a common member of Cambrian BST faunas, the eldonioid (See 3.1.2).

The sample was intriguing, but was the only one found. A second excursion was made to Slate Mountain (~2.5 mi South of Gibson Jack Creek), at which, according to the USGS geologic map of the area (Rodgers and Othberg, 1999), the Gibson Jack Formation had extensive exposure. Two localities were visited. Not only was there vastly greater exposure (especially at the outcrop just north of the peak), but the discoidal fossils were found in tremendous abundance (Figure 4.2). These showed some inconsistency with the specimen from the Gibson Jack Creek locality. The dark, crescent shape was present in the Slate Mountain discoids, but was straight in many specimens. The Slate Mountain discoids had a wider range of sizes. One very poorly-preserved specimen was larger than two cm in diameter.

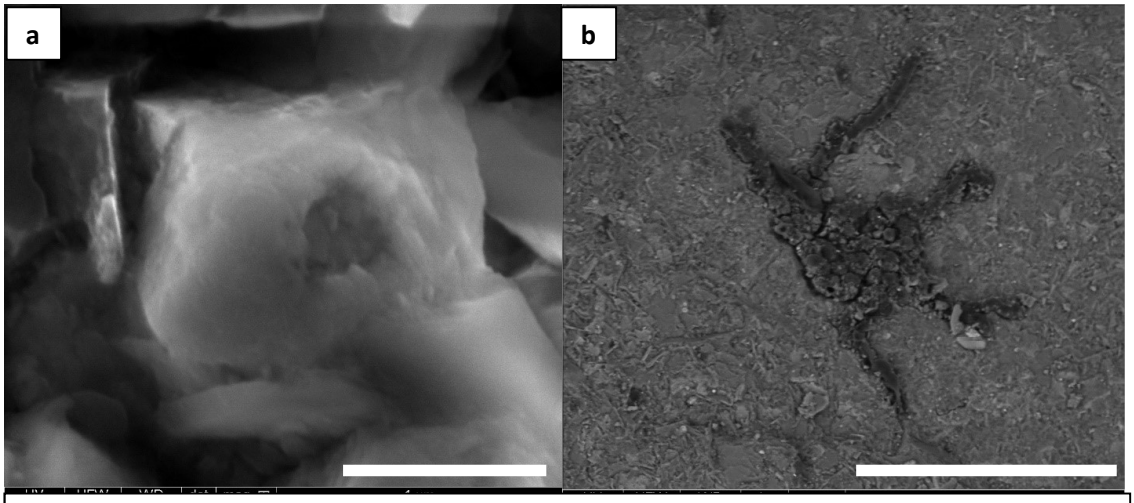

Figure 4.3 SEM images of the Gibson Jack Creek locality fossil. (a) ETD image of hollow microcryst. (b) BSE image of alaga from proximity to the Gibson Jack Creek discoid. Scale bars: a=1 μm b=100 μm

4.2 Results

The discoid of Gibson Jack Creek exhibited higher iron content on the fossil than the host rock. The dark crescent exhibits elevated carbon and potassium concentrations, indicative of kerogenization and aluminosilicification (whether authigenic or secondary). The orange sections on the ends of the gut tract are microcrystalline iron oxides. orange, radial features consist of framboidal iron oxides, presumably after pyrite. One of these pyrite framboids exhibits hollow microcrysts, in which the interior of the microcryst is visible (Fig. 4.3 a). The algae preserved near the discoid is preserved as a carbon film, with what looks like original morphology (Fig. 4.3 b). The preservation of these alage indicates that the burial environment was capable of exceptional kerogenization without clay-replacement, at least for some histologies.

From the standpoint of an eldonioid interpretation, these mineral associations make sense. Aluminosilicification is known from the *Eldonia* KUMIP 314051 (see 3.2.3). The

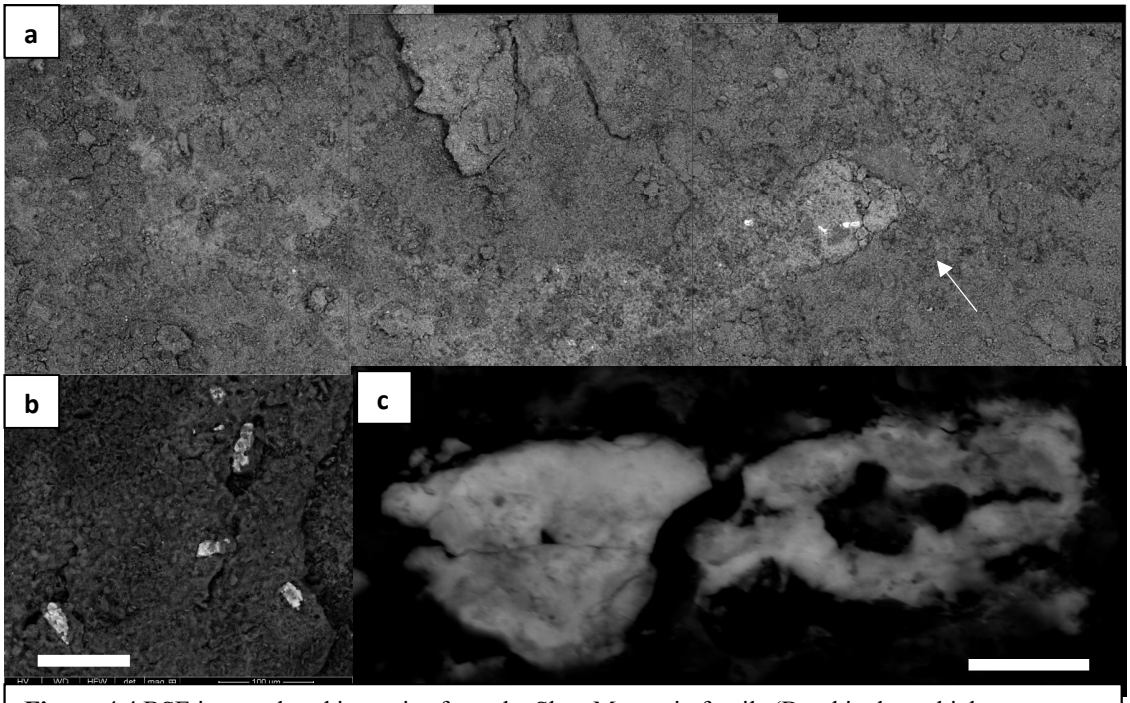

Figure 4.4 BSE images brockite grains from the Slate Mountain fossils (Brockite has a high backscatter coefficient, and will appear bright in BSE images. (a) Crescent of a well-preserved specimen. Brockite is indicated with an arrow (b) BSE image of more crescent-hosted brockite. (c) closeup of brockite grain. Scale bars: a=500 μm, b=100 μm, c=10 μm

radial canals of eldonioids (see 3.1.2) are enclosed environments which could produce pyrite. It is possible that the anterior and posterior end of the midgut could be an interface where sulfide generated in the midgut could have reacted with iron in the porewater, producing preferential pyritization on the ends of the crescent.

Instead of only exhibiting an iron oxide groundmass on the ends of the crescent shape, the Slate Mountain discoids exhibit a crescent shape that is entirely coated in a fine-grained iron oxide crust. The crescent is also elevated in potassium concentration. Unlike the outer, discoidal region is carbon-rich relative to the host rock. The most peculiar trait exhibited by the Slate Mountain discoids is the presence of brockite grains in the crescent (Fig. 4.4). These rectangular crystals of brockite can be over 70 μm in length and appear randomly oriented in most specimens. Brockite, a calcium, thorium phosphate has never been reported in association with fossils, however it was likely produced by a similar

mechanism to the monazite (cerium, lanthanum, neodymium, thorium phosphate) in the HRE fossils (see 3.2.4). Apatite is commonly associated with the gut tracts of arthropods and hyoliths (see 2.3.1), and can be altered by LREE-bearing fluids, replacing the calcium.

Some brockite grains exhibit a small lead EDS peak, which opens the possibility of radiometric dating of the alteration event, but there is far too much error in the EDS quantification for a useful age determination. Idaho is known for its world-class thorium deposits due to an alteration event. It is possible that this same alteration event caused fossil-bearing apatite to become brockite. During the Early Permian (299-273 Ma), this region of Idaho was a "phosphorite giant," (Pufahl, 2010, Wardlaw and Collinston, 1986) a basin that produced a tremendous quantity of phosphorite, the Phosphoria Formation. Some monazite occurs in the Phosphoria (Jackson and Christiansen, 1993), but the brockite grains only exhibit thorium, and no other REEs. Any relationship between the Phosphoria monazite and the brockite grains is unclear.

4.3 Conclusions

The morphology of the discoids are a strong indication that the fossils are biological in origin. The crescent shape exhibits a number of shapes and curves, which seems unlikely for an abiologically mineralized feature. The peculiar arrangement of different minerals in such an ordered structure does not have an apparent abiotic association.

Though I am confident that these are fossils, the identity of the fossilized organism is difficult to approach. These fossils do resemble eldonioids, but the crescent has a variable shape, and is not found in consistent placement within the circular region. The same could be said of the *Eldonia* from the Burgess Shale, since they are often folded and deformed

(Walcott, 1911), but the circular region of the discoids do not show evidence of such deformation. The explanation for the thorium-rich grains is that fossil apatite had been altered to brockite, but apatite is not known in association with eldonioids. Pyritization is known from eldonioids, but not this extensively (MacGabhann, 2012). Aluminosilicification is known from *Eldonia*, but with iron-rich clays, not potassium (see 3.2.3). The discoids are a plausible size for *Eldonia*, but would be among the smallest. Since *Eldonia* is typically found in assemblages with *Eldonia* of different sizes, and its growth is somewhat isometric (MacGabhann, 2012) it would be highly unusual to find an assemblage exclusively of abundant *Eldonia* juveniles. Though eldonioids are the most likely affinity, the evidence in favor is still too weak to take a position.

What we *can* tell about these organisms, is the taphonomic history. The shales of the Gibson Jack formation are the distal extent of turbidites. The discoids were likely transported and buried by these turbidites. The turbidites were argillaceous, which served to inhibit autolysis (see 1.3.3). Anoxic conditions must have been established locally, in order to facilitate the production of pyrite. The pyrite precipitation was localized around the radial features and crescent shape, which was rich source of labile organic carbon for SRBs to decay.

REFERENCES

Jackson, Wayne D. and Grey Christiansen (1993) “International Strategic Minerals Inventory Summary Report—Rare-Earth Oxides” *U.S. Geological Survey Circular* 930-N

MacGabhan, Breandán Anraoi (2012) “A Solution to Darwin’s Dilemma: Differential Taphonomy of Ediacaran and Paleozoic Non-Mineralised Discoidal Fossils” PhD dissertation. National University of Ireland

Pufahl, Peir K. (2010) “Bioelemental Sediments” *Facies Models 4* Eds. Noel P. James and Robert W. Dalrymple. Geological Association of Canada, St. Johns, Canada.

Robison, R. A. (1984) "New occurrences of the unusual trilobite Naraoia from the Cambrian of Idaho and Utah" *The University of Kansas Paleontological Contributions*. Paper 112.

Rodgers, D.W., and Othberg, K.L. (1999) "Geologic map of the Pocatello South quadrangle, Bannock and Power Counties, Idaho" Idaho Geological Survey Geologic Map GM-26, scale 1:24,000.
Walcott, Charles D. (1911) "Middle Cambrian Holothurians and Medusae" *Smithsonian miscellaneous collections* 57:41-68
Wardlaw, Bruce R. and James W. Collinston (1986) "Paleontology and deposition of the Phosphoria Formation" *Contributions to Geology, University of Wyoming* 24:107-142

CHAPTER 5: ACTUALISTIC TAPHONOMY UNDER CHEMOSTAT CONDITIONS

5.1 Introduction

5.1.1 Experimental taphonomy

Though it is possible to interpret the taphonomic history of a fossil based on its mineralogical characteristics alone, there is always some risk of proposing a non-viable taphonomic pathway. Since the biology and chemistry of a decaying corpse is complex, unseen factors can defy even an expert's predictions. Thus, taphonomic interpretations must be tested experimentally. Some actualistic experiments are conducted in real environments, and others in the laboratory. Lab experiments offer greater control over the experimental conditions, but are not similar to natural environments.

One important way that lab experiments differ from those in natural environments is that where most natural waters are connected to a near-infinite reservoir of dissolved constituents, lab taphonomy experiments are typically conducted in containers of fluid. Some are closed containers (Briggs and Kear, 1993), and others are open to the atmosphere (Iniesto et al, 2015). This is a serious issue, especially for small containers, since they will rapidly run out of the dissolved ions that are necessary for decay. When attempting an experiment in anoxic conditions, this is convenient, since aerobes will rapidly consume the available oxygen (Sansom, 2014). The trouble is that sulfate will also become limited, which will inhibit the amount of sulfide that can be produced for pyrite. Of course, sulfide cannot diffuse out of the system, but closed conditions will rapidly bring all decay other than fermentation to a grinding halt.

5.1.2 Methodology

Cl:	13.176
Na:	7.363
SO4:	1.817
Mg:	0.902
K:	0.287
Ca:	0.273
HCO3:	0.137
Br:	0.038
Sr:	0.006
F:	0.001

Table 5.1 Concentration of ions in artificial seawater in g/L, without iron.

To circumvent the problem of sulfate depletion, I discarded some fluid from sample containers each day, replacing it with fresh artificial seawater. We hypothesized that this technique would generate more pyrite. The microorganisms would be provided with more of the constituents they need for decay. All experiments were run in seawater with 24 g/L Instant Ocean® Carribean sea salt (Tab. 5.1). The experiments were run in an anoxic chamber with a N_2 and H_2 atmosphere, though oxygen concentrations did fluctuate over the course of the experimental runs. During the six runs (Tab. 5.2), numerous variables were used, including (1) iron concentration (2) type of iron salt used to increase iron concentration (3) presence of a calcite buffer (4) sediment type (5) decay organism (6) bacterial inoculate (7) container size (8) rate of fluid cycling and (9) length of experiment.

1) The seawater was doped with dissolved iron (II), up to 8 mM. This is considerably higher than the modern ocean iron concentrations (~5 nM, Rickard, 2012).

2) The salts used to increase iron concentrations was originally Sigma Aldrich® iron chloride tetrahydrate ($FeCl_2 \bullet 4H_2O$), but we switched to ammonium iron sulfate hexahydrate ($(NH_4)_2Fe(SO_4)_2 \bullet 6H_2O$) because it may have a less severe impact on the fluid chemistry.

3) In some runs the iron-doped seawater was buffered with calcite, to counter the tendency for the artificial seawater to spontaneously become acidic.

SN	[Fe]	Fe salt	Calc	Sed	Org	Strain	Size	Cycle	Dur
1BN	1.07	Cl	No	None	Shrimp	Ds	1000	Batch	15
1BS	1.07			Sand			1000	Batch	
1BC	1.07			Fine Si			1000	Batch	
1CN	1.07			None			150	50	
1CS	1.07			Sand			150	50	
1CC	1.07			Fine Si			150	50	
2BN	0.42	Cl	No	None	Shrimp	Dvh	1000	Batch	18
2BS	0.42			Sand			1000	Batch	
2BC	0.42			Fine Si			1000	Batch	
2CN	0.42			None			150	50	
2CS	0.42			Sand			150	50	
2CC	0.42			Fine Si			150	50	
3BN	0.42	Cl	No	None	Shrimp	Dvh	1000	Batch	7
3BS	0.42			Sand			1000	Batch	
3BC	0.42			Fine Si			1000	Batch	
3CN	0.42			None			150	100	
3CS	0.42			Sand			150	100	
3CC	0.42			Fine Si			150	100	
4AlS	0.42	SO_4	No	Kaolinite	Worm	Dv	250	60	30
4SS	0.42			Sand			250	60	
4SF	0.42			Sand			250	200	
5AlS	0.42	SO_4	No	Kaolinite	Worm	Dv	250	Batch	30
5AlF	0.42			Kaolinite			250	100	
5CaS	0.42			Chalk			250	Batch	
5CaF	0.42			Chalk			250	100	
5SiS	0.42			Fine Si			250	Batch	
5SiF	0.42			Fine Si			250	100	
6AlS	0.42	SO_4	Yes	Kaolinite	Worm	Ds	250	Batch	29
6AlF	0.42			Kaolinite			250	100	
6CaS	0.42			Chalk			250	Batch	
6CaF	0.42			Chalk			250	100	
6SiS	0.42			Fine Si			250	Batch	
6SiF	0.42			Fine Si			250	100	

Table 5.2 Taphonomy experiments. **SN**=specimen number, **[Fe]**= iron concentration in g/L, **Fe salt**= was iron chloride (Cl) or ammonium iron sulfate (SO_4) used?, **Calc**=was a calcite buffer used?, **Sed**= type of sediment, where Fine Si= micron-scale silica powder. **Org**=was a shrimp or a waxworm decayed? Strain= what strain of Desulfovibrio was used? Ds=*salixigens*, Dv=*vulgaris*, Dvh=*vulgaris hidlenborough*, **Size**=size of the container, **Cycle**=how quickly the fluid was cycled, **Dur**=duration of the experiment in days. Specimen numbers which successfully produced iron sulfide minerals are highlighted in grey.

4) Some specimens were left unburied. Others were buried in ~2 cm of sediment. Sediment types consisted of sand, <5µm silica powder, kaolinite and chalk.

5) Shrimp and waxworms were the decay "victims." The shrimp were Great Value® Tiny Shrimp selected by weight, between 0.9 and 1.1 grams. They were soaked in dilute hydrochloric acid to remove the sodium metabisulphite preservative. The

waxworms were purchased live and decapitated immediately prior to burial. The waxworms were not sterilized, so as to permit their gut flora to begin the decay process.

6) Three strains of sulfur-reducing microbes were used for inoculation: *Desulfovibrio salixigens*, *Desulfovibrio vulgaris* and *Desulfovibrio vulgaris hildenborough*.

7) The volumes of seawater used were 150 mL, 250 mL and 1 L

8) Some specimens were decayed in batch conditions (container that has no fluid in or out, except by evaporation.) For specimens decayed under chemostat conditions 50, 60, or 100 mL/day of fluid was manually removed from the container with a syringe, and replaced with unused artificial seawater. For later test runs, a peristaltic pump was purchased to maintain a constant flow rate of 200 mL/day, but the slow rate of flow necessary for these experiments caused the pump to stall occasionally, so syringe-based fluid replacement was resumed.

9) Experimental durations were one week to one month.

pH tests were conducted daily. Fluid was regularly sampled to be measured for sulfate concentrations with the Dionex ICS 3000, and iron speciation with a 2'2 bipyridine color indicator in the Nanodrop 1000 spectrophotometer. Sediment and organism surfaces (dried in a vacuum oven) were analyzed under the SEM for texture and composition. For the conditions of each specimen, see (Tab. 5.2)

5.2 Results

5.2.1 Methodological difficulties

Utilizing the airlock to move objects in or out of the chamber results in some oxygen contamination. Though the anoxic chamber contains a platinum catalyst which can remove oxygen from the chamber, but it can still take over a week for oxygen concentrations to return to zero. The high initial oxygen was somewhat mitigated by allowing the supplies and artificial seawater to degas prior to the start of the experiment, but the victims needed to be placed in the chamber before the onset of decay, meaning that at least some oxygen would be in the chamber at the start of the experiment. At various times during the experiment, it was necessary to put additional supplies in the chamber or remove waste. This resulted in a spike in oxygen concentrations. Having some oxygen in the chamber will not necessarily invalidate the experiment, since decay is very effective at eliminating local oxygen, such that anoxic experimental decay does not require anoxic conditions (Iniesto et al, 2015). A greater concern is the effect of oxygen on the experimental fluid. The large quantity of dissolved iron (II) quickly reacted with oxygen, resulting in extensive rust precipitation. This caused the pH of the artificial seawater to become acidic. In later runs, the pH of plain artificial seawater and tap water were used as controls to monitor pH changes that are unrelated decay (Fig. 5.1), and they were found to covary. Since the control containers were not in contact with anything but the gases of the chamber, it is assumed that changes in the gas composition of the chamber drove the pH changes. Though the culprit cannot be determined with certainty, one suspect is H2S. If sulfide was being produced, then H2S could have entered the other containers, thus acidifying them via a dissociation reaction: $H_2S \rightarrow H^+ + HS^-$. Changes in the sulfide

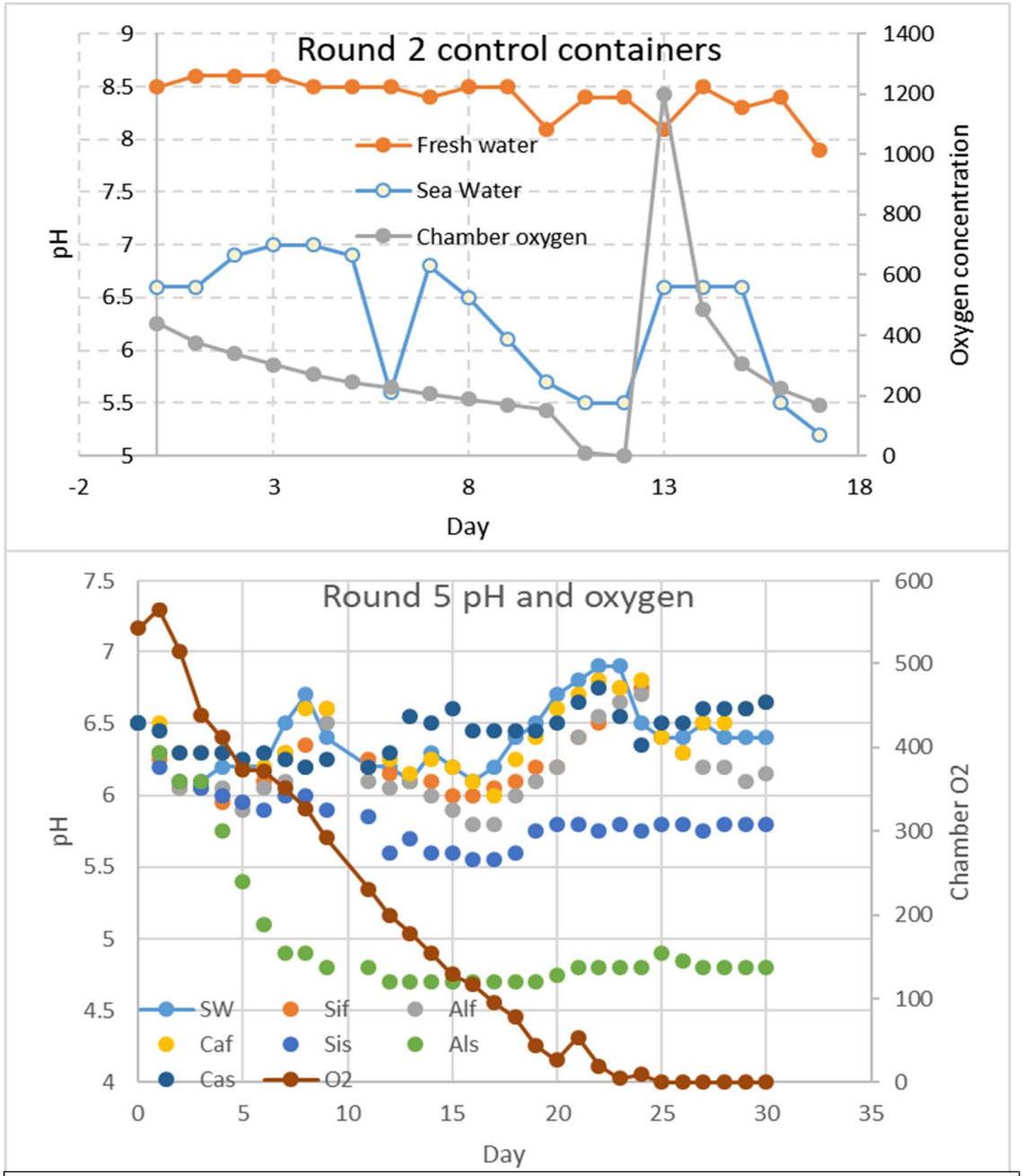

Figure 5.1 Showing changes in pH over the course of round 2 (top) and round 5 (bottom). Note the fluctuations in pH of the control seawater (which did not have any decay), which seems to be affected by perturbations in the oxygen concentration, and covaries some of the experimental fluids.

concentration of the chamber would then change the equilibrium condition of the dissolved sulfide, and consequently, pH.

The results for sulfate concentrations should be considered with skepticisim, since the sulfate standards used to build the calibration curve for the Dionex ICS 3000 exhibited fairly extreme drift. The first round of experiments produced a large quantity of evaporite minerals because the sample containers were not covered. Later experiments used closed containers.

5.2.2 Data

The SRBs were quite active, as illustrated by the development of a well-developed microbial biofilm on some of the specimens. In the samples under batch conditions, sulfate concentrations were found to decrease at an accelerating rate over the first few days, but would generally slow down by the fourth. This is consistent with the expectation that SRBs would rapidly multiply until sulfate concentrations became limiting. Since sulfate drawdown essentially ceased for batch conditions, sulfate reduction must have ceased. This confirms the necessity of using a continuous flow system for long-term decay experiments. Some samples developed a "decay halo," sediment discoloration common near decaying corpses. This can be caused by the precipitation of iron sulfides (Rickard, 2012), and is commonly assumed to be a result of iron sulfides, but there are many other factors that can cause local sediment darkening (see 2.1.1).

Iron sulfides were actually very rare in the experimental runs. Sediment and organism samples were very thoroughly searched for iron sulfides. Though iron sulfides were very common in some samples, other samples only yielded single, tiny fragments of iron sulfide. Thus, exhaustive searching was necessary. One such individual fragment (Fig. 5.2 a, b) was the only true pyrite found in any sample run. The experimental conditions

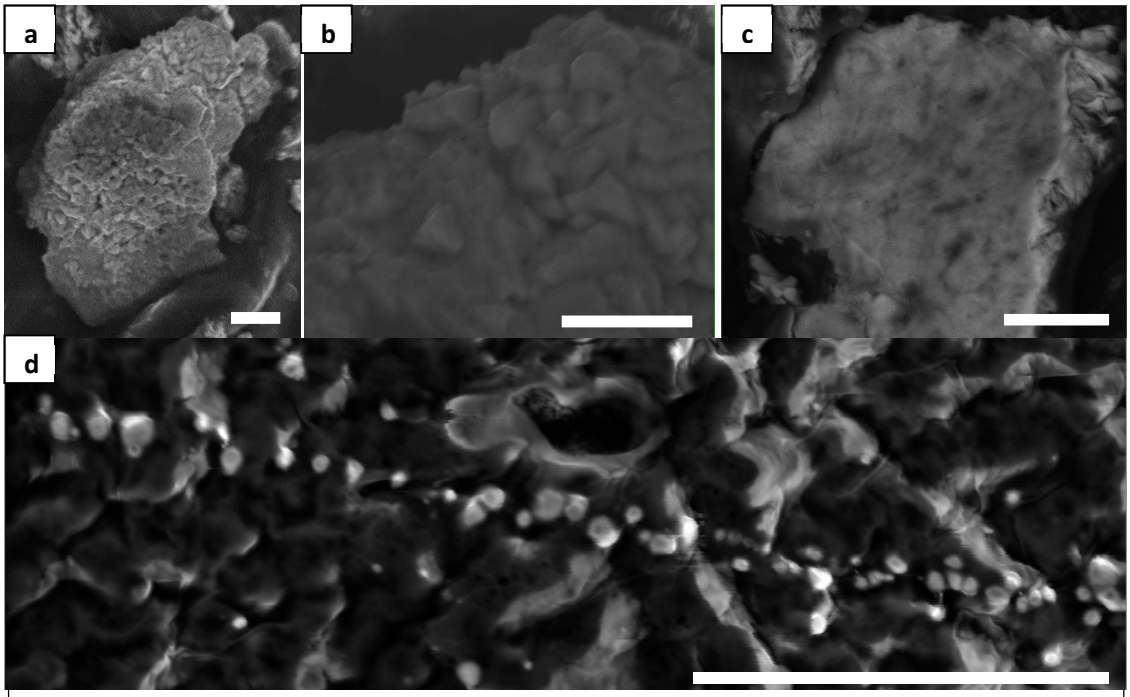

Figure 5.2 (a & b) BSE images of pyrite flake from 3CS (c) BSE image of iron monosulfide flake from 5SiS. (d) Line of Fe/Cu particles from 4AlS. Scale bars are a=10 µm, b=5 µm, c=10 µm, d=50 µm

that produced it was 3CS: sand substrate, 100 mL/d fluid replacement in a 250 mL container. It is a flake of pyrite 30 µm long, consisting of intergrowing pyrite euhedra with a maximum size of ~ 1 µm. It was found on the organism, but was not attached. In the same sample, a filament-shaped aggregate of similar iron sulfide euhedra was spotted, but when the microscope was focused on it, the electron beam caused it to skip off of the sample. It was never recovered. Such pyrite aggregates indicate an environment where many nucleation sites appeared almost simultaneously, and grew, encrusting a surface.

A lone iron monosulfide flake (Fig. 5.2 c) was recovered from a different sample (5SiS): silica powder substrate, batch conditions. This flake was found in the sediment, but the surface that was exposed to the SEM was smooth. Acicular crystals radiated away from the smooth side. This indicates that it had grown on a smooth surface, but later fell off. The nucleation conditions must have been similar to the pyrite flake.

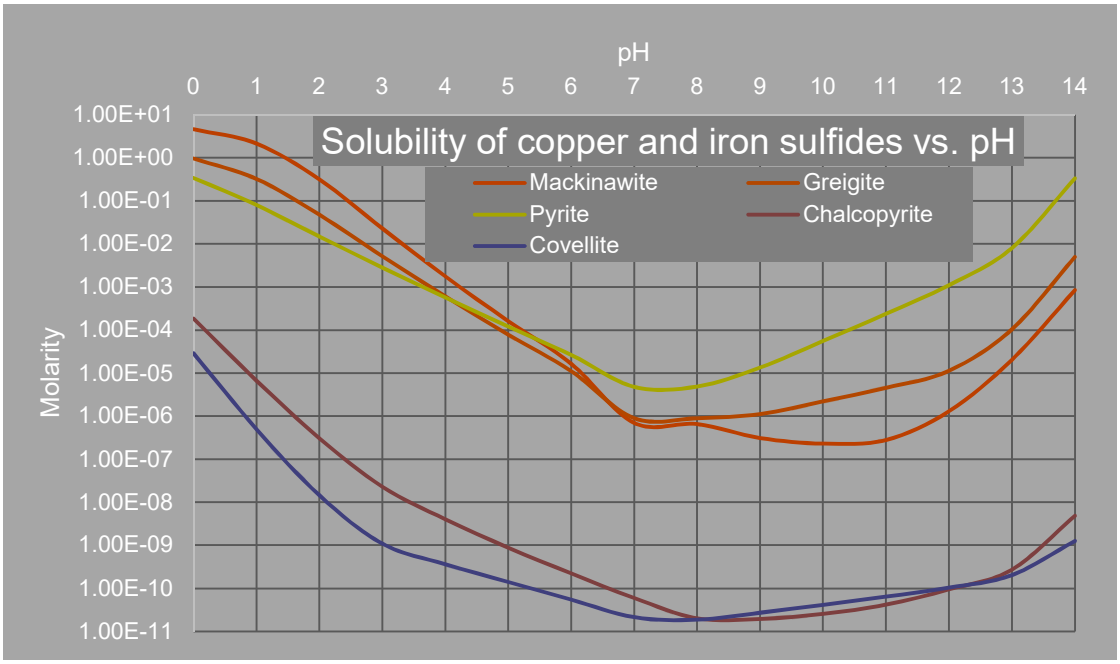

Figure 5.3 Solubility of various iron and copper sulfides modeled using PHREEQC at 20°C

Iron/copper sulfides and pure copper sulfides appeared in some samples. Undoubtedly, this is a result of copper contamination in the sample fluid, which would normally be absent in natural seawater. Copper sulfides are less soluble than iron sulfides (Fig. 5.3), so their precipitation would be favored. In one sample (4AlS: 60 mL/d cycling, kaolinite substrate), the copper sulfides appeared as highly abundant particles of 4 µm or less (Fig. 5.2d). These particles were attached to the organism. In some places, they formed linear features, reminiscent of the lines of pyrite framboids in KUMIP 298531 (Fig. 3.5 c), but these formed without any interannulation-like crease, which casts doubt on the interpretation of pyrite framboid lines as evidence of a former invagination. The composition of the particles were between that of a typical bornite, covellite and villamaninite (Fig. 5.4 a).

Aggregates of tiny chalcopyrite grains were found in two runs (6AlS and 6AlF: calcite buffered solution, kaolinite substrate, Fig. 5.4 b). These were ~5 µm across, but

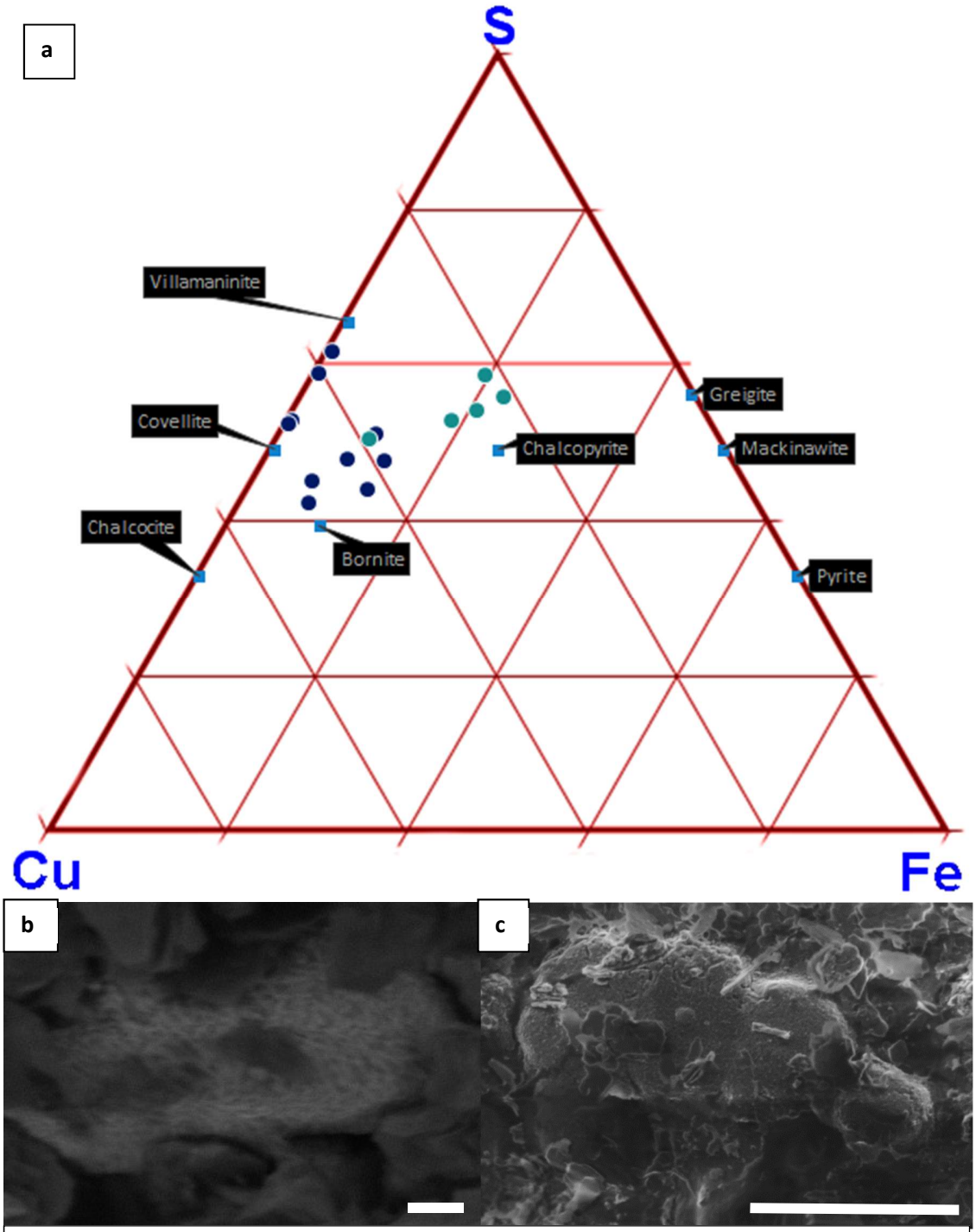

Figure 5.4 (a) Ternary diagram comparing compositions of iron and copper sulfide minerals from the 4AlS (teal dots) and 6AlF (navy dots) to known iron and copper sulfides. (b) Fe/Cu aggregate from 6AlF. (c) chalcopyrite flake from 6AlS. Arrow points to etching. Scale bars b=1 µm, c=10 µm.

comprised of blades 200-500 nm long and 50-100 nm wide or sp herules appx. 150-250

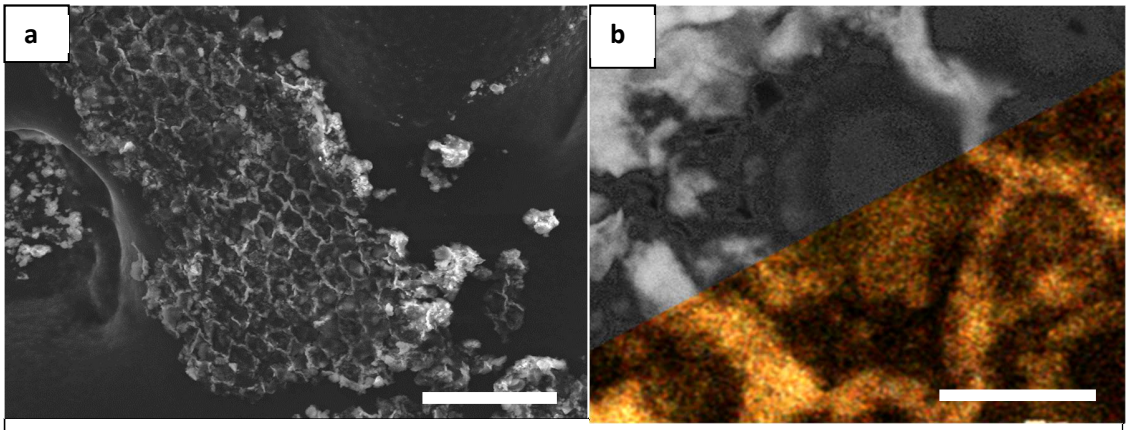

Figure 5.5 (a) ETD image of a mold of the exoskeleton of a waxworm. (b) BSE and element map of one of the areas of raised, hexagonal ridges. Iron is depicted as red and sulfur is depicted as yellow. Scale bars: a=50 µm, b=5 µm

nm in diameter. Again, these must be the result of rapid nucleation and growth in a spatially-restricted area. The largest of these (from 6AlS) chalcopyrite flakes, at 30 µm across, is covered in twisting cavities (Fig.5.4 c), appx.100-250 µm wide. The cavities appear to be etch marks. It is possible that the chalcopyrite was undergoing dissolution. If so, it opens the possibility that metal sulfides that had precipitated began to dissolve, making them impossible to detect in analysis. If so, iron sulfide precipitation may be m ore prevalent in these experiments than they seem.

In samples with fine-grained sediment, the sediment commonly adhered to the surface of the "victim," and dried. When the organisms were examined with the SEM, the mold sometimes became attached to the tape that was used to adhere the organism. This sediment mold provides excellent data on the occurrence of mineral phases in close proximity to the organism's surface. The sediment examined in this manner commonly yielded iron sulfides. The exoskeleton of waxworms bears a hexagonal pattern, with crevices in between. Thus, the resulting sediment mold consisted of ridges forming hexagonal outlines (Fig. 5.5 a). These ridges were often elevated in iron and sulfur concentrations (Fig. 5.5 b). The iron sulfides precipitated interstitially in the crevices

between chitinous hexagons, likely because they form a restricted microenvironment where sulfides can accumulate. The clearest case of this phenomenon is observed in 5SiF (silica with 100 mL/d cycling, and kaolinite under batch conditions), and most EDS work of the molds shows clear iron monosulfide stoichiometry.

5.3 Conclusions

The difficulty with drawing general conclusions from these results is that each instance of pyritization exhibited unique characteristics. Compositions, mineral styles and experimental conditions differed in each case of metal sulfide precipitation. While I still consider chemostat conditions to be a superior way to run experimental taphonomy in the laboratory setting, it was shown to be unnecessary for pyrite production (5SiS and 6AlS). For the quantities of pyrite produced in these experiments, sulfate limitation is not likely to be a factor, and even small quantities of pyrite could later overgrow to form more extensive pyritization (see 2.1.7).

pH had a strong tendency to decrease over the course of the experiments. This matches models of sulfur reduction (Fig. 2.1). Unlike in the models, carbonate sediment did not result in lower pH values than inert (silica) sediment. The lowest pHs by far occurred in kaolinite sediment, which suggests that it may have been reactive.

Since copper sulfides have lower solubility than iron sulfides, it is possible that some of the cases of Fe/Cu would not have produced regular pyrite or iron monosulfides if the fluid was devoid of copper. Copper-sulfide mineral association with soft-bodied fossils is unknown from the fossil record, so the differences in mineralization that could be occurring in these experiments are unknown. The copper sulfides seemed to be

preferentially produced in kaolinite sediment. Perhaps the copper sulfides were produced because the low pH inhibited pyrite precipitation, similar to the calcite/phosphate switch phenomenon (see 2.3.1).

The patterns of mineralization in the crevices of the exoskeleton demonstrate that enclosed areas are a favorable location for the precipitation of iron sulfides (5SiF), but results from 4AlS demonstrate that crevices aren't necessary for the production of linear trends of pyrite as seen in KUMIP 298531. Even if the other iron sulfide minerals will eventually dissolve (as in 6AlS), their presence could act as a precursor to pyrite (see 2.1.3) Pyrite was produced in less than a week in 3CS, and the pyrite aggregates show a texture indicative of rapid nucleation and growth. This means that pyrite does not require long timescales to occur, if conditions are right for its production.

REFERENCES

Briggs, Derek E. G. and Amanda J. Kear (1993) "Decay and preservation of polychaetes: taphonomic thresholds in soft-bodied organism. *Paleobiology* 19:107-135

Iniesto, Miguel, Celia Laguna, Maximo Florín, M. Carmen Guerrero, Alvaro Chicote, Angela D. Buscalioni and Ana I López-Archilla (2015) "The impact of microbial mats and their microenvironmental conditions in early decay of fish" *Palaios* 30:792-801

Rickard, David (2012) "Sulfidic Sediments and Sedimentary Rocks" Developments in Sedimentology 65. NLD:Elsevier Science and Technology, Amsterdam

Sansom, Robert S. (2014) "Experimental Decay of Soft Tissues" in *Reading and Writing of the Fossil Record: Preservation Pathways to Exceptional Fossilization*. Eds. Marc Laflamme, James D. Schiffbauer and Simon A. F. Darroch. *The Paleontological Society Papers* v. 20.

VITA

Jesse Storm Broce grew up in scenic Idaho, which is a convenient place for geologists due to the mountainous terrain, and sparse vegetation. His parents were a schoolteacher and a cadastral surveyor, both nature-lovers. He worked as a lifeguard during the summers, until he graduated from Salmon High School in 2007. He studied Geology at University of Idaho, where he worked as a resident assistant until 2011. For his master's degree, he attended Virginia Tech, studying under Dr. Shuhai Xiao. There, his main project was studying phosphatized fossil embryos which he fortuitously recovered from some limestones he had collected in China. After he was awarded his M.S. in Geosciences, Jesse began his PhD research under one of his collaborators, Dr. James D. Schiffbauer, the results of which are presented here. Jesse aspires to continue working in academia on exceptionally preserved fossil material.